AFRL-RV-PS-
TR-2012-0226

AFRL-RV-PS-
TR-2012-0226

DETERMINATION OF LOVE- AND RAYLEIGH-WAVE MAGNITUTDES FOR EARTHQUAKES AND EXPLOSIONS AND OTHER STUDIES

Jessie L. Bonner, et al.

Weston Geophysical Corp
181 Bedford Street, Suite 1
Lexington, MA 02420

30 December 2012

Final Report

AIR FORCE RESEARCH LABORATORY
Space Vehicles Directorate
3550 Aberdeen Ave SE
AIR FORCE MATERIEL COMMAND
KIRTLAND AIR FORCE BASE, NM 87117-5776

DTIC COPY

NOTICE AND SIGNATURE PAGE

Using Government drawings, specifications, or other data included in this document for any purpose other than Government procurement does not in any way obligate the U.S. Government. The fact that the Government formulated or supplied the drawings, specifications, or other data does not license the holder or any other person or corporation; or convey any rights or permission to manufacture, use, or sell any patented invention that may relate to them.

This report was cleared for public release by the 377 ABW Public Affairs Office and is available to the general public, including foreign nationals. Copies may be obtained from the Defense Technical Information Center (DTIC) (http://www.dtic.mil).

AFRL-RV-PS-TR-2012-0226 HAS BEEN REVIEWED AND IS APPROVED FOR PUBLICATION IN ACCORDANCE WITH ASSIGNED DISTRIBUTION STATEMENT.

/ / SIGNED / /	/ / SIGNED / /
Robert Raistrick	Edward J. Masterson, Colonel, USAF
Project Manager, AFRL/RVBYE	Chief, Battlespace Environment Division

This report is published in the interest of scientific and technical information exchange, and its publication does not constitute the Government's approval or disapproval of its ideas or findings.

REPORT DOCUMENTATION PAGE

Form Approved
OMB No. 0704-0188

1. REPORT DATE *(DD-MM-YYYY)*	**2. REPORT TYPE**	**3. DATES COVERED** *(From - To)*
30-12-2012	Final Report	12 Jun 2009 – 30 Sep 2012

4. TITLE AND SUBTITLE
Determination of Love- and Rayleigh-Wave Magnitudes for Earthquakes and Explosions and Other Studies

5a. CONTRACT NUMBER
FA8718-09-C-0012

5b. GRANT NUMBER

5c. PROGRAM ELEMENT NUMBER
62601F

6. AUTHOR(S)
Jessie L. Bonner, Anastasia Stroujkova, Dale Anderson, Jonathan McCarthy, Robert Herrmann, and David Russell

5d. PROJECT NUMBER
1010

5e. TASK NUMBER
PPM00004767

5f. WORK UNIT NUMBER
EF004236

7. PERFORMING ORGANIZATION NAME(S) AND ADDRESS(ES)

Weston Geophysical Corp.
181 Bedford Street, Suite 1
Lexington, MA 02420

8. PERFORMING ORGANIZATION REPORT NUMBER

9. SPONSORING / MONITORING AGENCY NAME(S) AND ADDRESS(ES)
Air Force Research Laboratory
Space Vehicles Directorate
3550 Aberdeen Ave SE
Kirtland AFB, NM 87117-5776

10. SPONSOR/MONITOR'S ACRONYM(S)
AFRL/RVBYE

11. SPONSOR/MONITOR'S REPORT NUMBER(S)
AFRL-RV-PS-TR-2012-0226

12. DISTRIBUTION / AVAILABILITY STATEMENT
Approved for public release; distribution is unlimited. (377ABW-2013-0074 dtd 22 Jan 2013)

13. SUPPLEMENTARY NOTES

14. ABSTRACT

Since the 1960s, comparing a Rayleigh-wave magnitude, M_s, to the body-wave magnitude, m_b, (e.g., M_s:m_b) has been a robust tool for the discrimination of earthquakes and explosions. In this report, we apply a Rayleigh-wave formula *as is* to Love waves and examine the possibilities for discrimination using only surface wave magnitudes (e.g., M_s:M_s). To calculate the magnitudes we apply the time-domain magnitude technique called M_s*(VMAX)* developed by Russell (2006) to Rayleigh and Love waves from explosions and earthquakes. Our results indicate that for the majority of the earthquakes studied (>75%), the M_s*(VMAX)* obtained from Love waves is greater than the estimate from Rayleigh waves. Conversely, 79 of 82 nuclear explosions analyzed (96%) had network-averaged M_s*(VMAX)*-Rayleigh equal to or greater than the M_s*(VMAX)*-Love. We used logistic regression to examine an M_s(Rayleigh):M_s(Love) discriminant. Cross-validation analysis of the new discriminant correctly identifies 57 of 82 explosions and 246 of 264 earthquakes while misidentifying 22 explosions as earthquakes and 11 earthquakes as explosions. This report provides additional studies that supplement these findings as well as comparative research for M_s(Rayleigh):M_s(Love) versus M_s:m_b using common data.

15. SUBJECT TERMS
Explosions, surface waves, magnitudes

16. SECURITY CLASSIFICATION OF:			**17. LIMITATION OF ABSTRACT**	**18. NUMBER OF PAGES**	**19a. NAME OF RESPONSIBLE PERSON**
a. REPORT	**b. ABSTRACT**	**c. THIS PAGE**			Robert Raistrick
Unclassified	Unclassified	Unclassified	Unlimited	96	**19b. TELEPHONE NUMBER** *(include area code)*

This page is intentionally left blank.

TABLE OF CONTENTS

LIST OF FIGURES

LIST OF TABLES

This page is intentionally left blank.

CHAPTER 1: DETERMINATION OF LOVE- AND RAYLEIGH-WAVE MAGNITUDES FOR EARTHQUAKES AND EXPLOSIONS

Jessie L. Bonner, Anastasia Stroujkova, and Dale Anderson

INTRODUCTION

Since the 1960s, comparing a Rayleigh-wave magnitude, M_s, to the body-wave magnitude, m_b, (e.g., M_s:m_b) has been a robust tool for the discrimination of earthquakes and explosions. In this article, we apply a Rayleigh-wave formula *as is* to Love waves and examine the possibilities for discrimination using only surface wave magnitudes (e.g., M_s:M_s). To calculate the magnitudes we apply the time-domain magnitude technique called M_s*(VMAX)* developed by Russell (2006) to Rayleigh and Love waves from explosions and earthquakes. Our results indicate that for the majority of the earthquakes studied (>75%), the M_s*(VMAX)* obtained from Love waves is greater than the estimate from Rayleigh waves. Conversely, 79 of 82 nuclear explosions analyzed (96%) had network-averaged M_s*(VMAX)*-Rayleigh equal to or greater than the M_s*(VMAX)*-Love. We used logistic regression to examine an M_s(Rayleigh):M_s(Love) discriminant. Cross-validation analysis of the new discriminant correctly identifies 57 of 82 explosions and 246 of 264 earthquakes while misidentifying 22 explosions as earthquakes and 11 earthquakes as explosions. Further comparative research is planned for M_s(Rayleigh):M_s(Love) versus M_s:m_b using common data. We fully expect that M_s(Rayleigh):M_s(Love) will contribute significantly to multivariate event identification.

The discrimination of small nuclear explosions and earthquakes remains a difficult, but very important problem for the nuclear explosion monitoring community. The relative difference between the body-wave (m_b) and surface-wave (M_s) magnitudes for a seismic event is one of the most effective discriminant techniques available at teleseismic and regional distances. The discriminant is based on the fact that shallow earthquakes usually generate substantially more surface-wave energy than explosions at a given m_b, and thus are characterized by a larger surface-wave magnitude. Differences in focal mechanisms and the near-source material velocity also help to improve the discriminant performance (Stevens and Day, 1985). The 2006 and 2009 North Korean announced explosions have puzzled scientists due to their large M_s estimates compared to the m_b (Bonner et al., 2008). Although mechanisms for the large Rayleigh waves have been proposed (e.g., Patton and Taylor, 2008), the issue has yet to be resolved conclusively. As a result of these events, major changes have been suggested (Selby et al., 2012) in the event screening procedures using M_s:m_b estimates.

Many surface wave magnitude scales have been based on empirical (Gutenberg, 1945; Vaněk et al., 1962; Marshall and Basham, 1972) or theoretical (Rezapour and Pearce, 1998; Stevens and McLaughlin, 2001; Russell, 2006) aspects of surface wave propagation. While formulas such as Vaněk et al., (1962) were originally developed for horizontal component data and variable periods, most earthquake monitoring organizations have settled on estimating M_s using ~20 seconds period Rayleigh waves. For the nuclear explosion monitoring community, this makes perfect sense considering that an isotropic explosion should not generate Love waves. However, tectonic release (Toksöz and Kehrer, 1972) near the explosion source often results in Love

waves being radiated and recorded from explosions with amplitudes usually—but not always—smaller than the Rayleigh waves.

For earthquakes, the amplitude of Love and Rayleigh waves are dependent upon focal mechanism. The analysis of the theoretical radiation pattern of Rayleigh and Love waves for shallow sources and few simple focal mechanisms is available as Appendix 1-A to this chapter (*e.g.*. Aki and Richards, 2002). For example it follows from Equations A5 and A7 that the Love wave amplitudes for the strike-slip focal mechanism are greater than those for a dip-slip mechanism for a given seismic moment. Notice that the factor of 2 introduced by the differences in focal mechanism translates into a magnitude difference of $log_{10}2 \approx 0.3$. It is also possible that a dip-slip earthquake can produce Rayleigh waves with greater amplitudes than Love waves.

The purpose of this effort is to assess the application of an M_s formula, originally developed and applied to Rayleigh-waves, to both Love and Rayleigh waves. We apply the method *in the same manner* to both phases for three different earthquake datasets as well as a global dataset of nuclear explosions. We examine whether improved discrimination is possible by combining the Love and Rayleigh wave magnitudes. Finally, we discuss possible methods for improving the analysis (e.g., using longer surface wave periods, different attenuation corrections, etc) based on results of this study.

LOVE WAVE MAGNITUDE ESTIMATION

We evaluate applicability of $M_s(VMAX)$ (Variable-period, MAXimum amplitude surface wave magnitude estimation) to Love waves. The formula for $M_s(VMAX)$ was developed by Russell (2006) while the measurement technique, which is currently in use at the United States Geological Survey as Ms_VX, was developed by Bonner et al. (2006). $M_s(VMAX)$ was developed for Rayleigh waves measured at variable periods between 8 and 25 seconds. It is defined as follows:

$$M_s(VMAX) = \log(A) + \frac{1}{2}\log(sin\,\Delta) + 0.0031\left(\frac{T_0}{T}\right)^{1.8}\Delta - \log(f_c) - 0.43 - 0.66\log\left(\frac{T_0}{T}\right) \quad , \quad (1)$$

where T_0 = 20 s is the reference period, Δ is the great circle distance in degrees, f_c is the corner frequency of the filter, the constant (0.43) was obtained for a zero-phase, third order Butterworth filter. The second term of Equation 1-1, $(\frac{1}{2}\log(sin\,\Delta))$ is a correction for the geometrical spreading, the third term, $0.0031\left(\frac{T_0}{T}\right)^{1.8}\Delta$, is a period-dependent attenuation correction and the fifth term, $-0.66\log\left(\frac{T_0}{T}\right)$, is a period-dependent excitation correction.

For this report, we apply Equation 1 *as is* to Love waves. We use the same processing for the Love waves as Bonner et al. (2006) designed for Rayleigh except that we filter the transverse components, rotated from the horizontals, for the Love-wave magnitude estimates. Examples of Butterworth filtering for Rayleigh and Love waves are shown in Figure 1a,b.

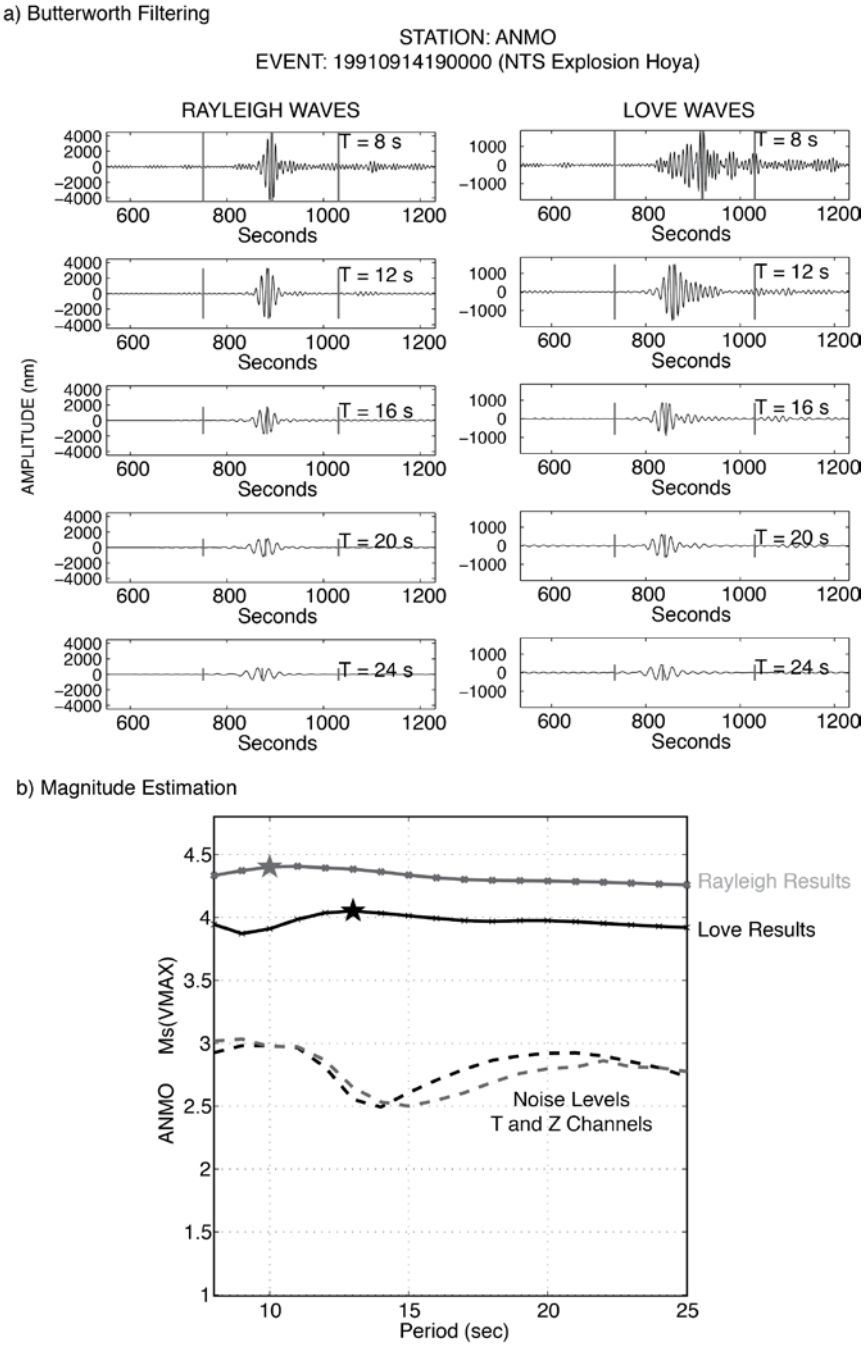

Figure 1. Examples of the $M_s(VMAX)$ technique applied to a) Rayleigh and b) Love waves from a Nevada Test Site explosion (Hoya). The Butterworth filters are computed at center periods between 8 and 25 seconds (not all filter panels are shown in this figure). The maximum amplitude in each filter band in a Rayleigh and Love wave group velocity window (small vertical lines) is input into Equation 1-1 and 18 different magnitudes c) are estimated. The magnitude at the period of maximum amplitude (shown as a star) is used as the final $M_s(VMAX)$ for a station and combined with others for a network average.

The data are filtered at center periods of 8, 9, 10,…25 seconds, the maximum amplitude at each period is measured, and Equation 1 is used to form 18 different magnitude estimates for each station (Figure 1b). The magnitude at the period of the maximum amplitude is assigned as the $M_s(VMAX)$ for a particular station, and combined with other stations to form a network average for an event. For this study, analysts (the first two co-authors) identified all Rayleigh- and Love-wave phases; however, we are currently working on automated methods to identify the phases and measure the amplitudes.

RESULTS AND DISCUSSION

Earthquakes

Equation 1 was applied to estimate $M_s(VMAX)$ for both Rayleigh and Love waves for three separate earthquake datasets (Figure 2). The first dataset (Table 1) included 109 events located in the Middle East with the body wave magnitudes ranging between 3.8 and 6.1. The database samples a variety of different focal mechanisms. The stations used to estimate surface wave magnitudes are distributed throughout Eurasia with distances ranging from approximately 83 to over 10000 km. The data for these stations were obtained from the Incorporated Research Institutions (IRIS) in Seismology Data Management Center (DMC), corrected for the instrument response to displacement in nanometers, and rotated to transverse, radial, and vertical components. The Love wave magnitudes were estimated from the transverse data, while the Rayleigh wave estimates were obtained using the vertical data. The results are plotted in Figure 3a and show that $M_s(VMAX)$-Love exceeds or is equal to $M_s(VMAX)$-Rayleigh for 82 out of 109 events (75%). The dominant periods of the measurements are approximately 21-22 s for Rayleigh waves and 25 s for Love waves. The interstation standard deviation averaged 0.22 magnitude units (m.u.) for both Rayleigh and Love waves.

The second dataset (Table 2) included 31 earthquakes occurring in the Korean Peninsula and surrounding regions (Figure 2c). These events ranged in size between $3.2 < M_w < 5.1$ with the focal mechanisms (Herrmann, pers. comm. 2010) being predominantly strike-slip (www.eas.slu.edu/eqc/eqc_mt/MECH.KR, last accessed, July 2011). The distances to the three-component stations recording these events, mainly Korean Meteorological Administration (KMA) and some Global Seismographic Network (GSN) stations, ranged from 55 km to 1900 km. Similar to the Middle Eastern events, the majority of these events (25 out of 31, or 80%) had $M_s(VMAX)$-Love exceeding or equal to the $M_s(VMAX)$-Rayleigh, which is expected for a strike-slip mechanism. The dominant period of the measurements for Rayleigh waves was less than 13 s; however, the Love wave magnitudes were uniformly sampled between periods 8 and 20 s. The interstation magnitude standard deviation for the Rayleigh and Love waves averaged 0.11 and 0.22 m.u., respectively.

The third dataset (Table 3) focused on the damaging L'Aquila earthquake (6 April 2009 Mw=6.1) and its aftershocks (Figure 2c). We have estimated $M_s(VMAX)$ for 125 Italian earthquakes with $2.8 < M_w < 6.1$ using Istituto Nazionale Geofisca e Vulcanologia (INGV) stations at distances ranging from 50 to 414 km.

Table 1. Results for earthquakes located in the Middle East.

Event YYYYMMDDHHMM	Latitude, ºN	Longitude, ºE	*mb*	*Ms R*	σ_R	# R	*Ms L*	σ_L	# L
200606030715	26.759	55.843	5.4	4.57	0.16	14	4.7	0.21	15
200606031440	39.151	40.362	4.4	3.81	0.2	7	4.18	0.19	11
200606050423	37.933	28.675	4.4	3.86	0.32	13	3.92	0.25	11
200606050423	37.933	28.675	4.4	3.86	0.32	13	3.92	0.25	11
200606282102	26.925	55.866	5.8	5.57	0.15	21	5.68	0.29	22
200606291641	26.798	55.906	4.6	3.89	0.16	6	3.82	0.16	6
200606300538	26.8	55.9	4.6	3.69	0.16	17	3.74	0.18	20
200606301506	26.9	55.8	4.4	3.54	0.14	7	3.66	0.25	9
200607021939	39.274	40.96	4.7	4.24	0.09	12	4.51	0.21	17
200607172201	26.72	55.82	4.4	3.63	0.62	2	3.55	0.27	4
200609100857	27.72	54.32	4.7	4.36	0.31	11	4.36	0.24	9
200609140225	29.255	51.35	4.9	3.8	0.16	4	3.72	0.29	3
200609260814	31.909	50.653	4.5	4.2	0.08	17	4.48	0.19	15
200610131019	27.62	54.36	4.6	3.74	0.13	7	3.95	0.18	8
200611052006	37.63	48.92	4.8	4.18	0.14	13	4.42	0.21	14
200611110219	32.37	49.67	4.5	3.67	0.27	10	3.41	0.19	6
200611131059	27.646	55.088	4.5	3.78	0.05	3	3.42	0.15	4
200612291022	28.937	47.496	4.6	3.21	0.43	2			
200701071532	33.986	56.652	4.5	3.56	0.49	4	3.33	0.3	3
200701190547	32.97	48.75	4.5	3.4	0.11	2			
200701191011	31.45	49.6	4.9	3.64	0.08	3	3.54	0.08	2
200701260820	38.418	40.216	4.6	4.22	0.28	5	4.46	0.26	5
200702090222	38.39	39.043	5.1	5.08	0.21	25	5.04	0.28	25
200702121830	29.63	50.471	4.4	3.93	0.28	8	3.99	0.13	11
200702211105	38.318	39.275	5.6	5.23	0.29	21	5.39	0.2	25
200702272228	28.1	55.08	4.5	4.18	0.17	14	4.33	0.28	17
200703062232	33.49	48.93	4.7	4.02	0.13	16	4.24	0.21	18
200703171420	27.091	58.021	4.9	3.62	0.11	9	3.82	0.24	9
200703181419	28.129	51.939	4.3	3.67	0.32	3	3.78	0.4	2
200703232138	27.47	55.15	4.8	4.36	0.24	27	4.45	0.24	25
200703261100	28.65	57.49	4.6	4.07	0.33	6	4.14	0.27	3
200704092126	38.88	44.487	4.4	3.8	0.2	12	3.62	0.21	10
200704180014	30.88	50.27	4.6	3.65	0.15	9	3.65	0.17	12
200704250419	28.19	56.22	5.1	4.6	0.18	20	4.81	0.25	21
200704252002	28.23	56.27	4.8	3.94	0.19	21	4.12	0.27	21
200704260403	28.23	56.24	4.6	3.61	0.13	6	3.67	0.14	8
200704260459	28.18	56.31	4.6	3.65	0.37	7	3.73	0.33	6
200704261411	28.084	56.389	4.1	3.36	0.19	4	3.65	0.16	7

200704282122	28.23	56.26	4.5	3.56	0.13	5			
200704290633	25.316	62.154	5	4.23	0.29	23	4.22	0.23	17
200705012338	28.078	56.388	3.8[I]	3.03	0.39	2	3.15	0.33	3
200705052111	38.788	42.274	4.4	4.01	0.04	2	3.88	0.01	2
200705060353	25.033	62.987	4.6	3.8	0.33	12	3.83	0.24	12
200705061057	24.955	62.941	4.8	4.17	0.2	25	4.18	0.26	20
200705080328	31.8	56.2	4.2	3.38	0.18	5	3.65	0.23	10
200705110550	34.38	54.04	4.1	2.96	0.24	6	3.26	0.28	4
200705112042	40.72	52.051	4.4	3.06	0.39	4			
200705160019	27.9	56.02	4.4	3.46	0.12	5	3.68	0.2	6
200705182303	27.734	53.161	4.7	3.93	0.22	11	3.94	0.17	10
200705262254	40.601	52.086	4.5	3.63	0.32	14	3.37	0.21	14
200705281412	30.232	51.749	4.5	3.39	0.13	9	3.59	0.25	14
200705311028	29.107	51.321	4.1	3.28	0.26	11	3.64	0.3	10
200706181429	34.414	50.852	5.1	5.09	0.21	33	5.21	0.27	30
200707040610	32.071	55.908	4.7	4.43	0.24	31	4.56	0.26	28
200707040951	31.877	56.06	4.2	3.91	0.15	21	3.92	0.21	21
200707081344	36.421	44.86	4.4	3.61	0.19	14	3.88	0.19	15
200707110651	38.751	48.598	4.9	4.24	0.29	26	4.26	0.2	23
200707231754	27.55	55.79	4.7	3.69	0.31	14	3.69	0.22	16
200707241341	42.01	48.882	4.7	3.4	0.12	8	3.22	0.16	8
200708052220	37.945	69.596	4.4	3.77	0.33	5	3.74	0.18	6
200708080328	28.139	65.857	4.5	3.51	0.21	5	3.76	0.29	11
200708191345	38.588	55.469	4.8	3.86	0.13	10	4.11	0.26	13
200708230152	40.636	48.518	4.6	3.77	0.24	18	3.73	0.19	18
200708252205	39.382	41.124	5.1	4.78	0.19	23	4.91	0.3	24
200708280930	28.17	56.74	4.9	3.89	0.18	18	4.13	0.24	23
200709051227	28.399	56.684	4.8	3.64	0.17	6	3.76	0.29	9
200709090200	30.6	69.809	5.2	5.06	0.23	33	5.2	0.27	31
200709182053	35.544	44.665	4.5	3.61	0.16	7	3.63	0.26	6
200709211021	37.343	44.272	4.5	3.72	0.21	13	3.77	0.19	18
200710190719	28.598	66.177	5.1	5.1	0.26	29	5.23	0.29	26
200710290923	37.033	29.233	4.9	4.82	0.21	27	4.83	0.25	26
200711080940	33.67	48.94	4.7	3.57	0.27	6	3.62	0.25	8
200712200948	39.417	33.212	5.2	5.35	0.19	6	5.57	0.2	17
200801050037	26.9	54.9	4.6	3.58	0.2	4	3.57	0.39	5
200801050807	31.47	49.37	4.5				3.7	0.01	2
200801061422	37.396	54.516	4	3.5	0.23	7	3.25	0.33	6
200801192141	33.319	57.307	4.4	3.75	0.18	15	3.79	0.2	20
200801280120	28.89	51.81	4.2	3.61	0.16	6	3.74	0.16	8
200802020533	26.41	52.976	4.9	3.77	0.29	8	3.76	0.33	8

200802072015	27.84	53.74	4.5	3.72	0.24	11	3.69	0.15	12
200802112347	33.26	35.416	4.3	3.7	0.84	3	3.87	0.47	5
200802151036	33.327	35.305	5	4.45	0.14	21	4.63	0.17	20
200802291957	38.498	57.258	4.7	3.71	0.19	14	4	0.24	17
200803011638	26.9	56.2	4.6				3.43	0.28	7
200803090351	33.21	59.11	4.9	4.53	0.27	18	4.73	0.3	18
200803180356	37.03	55.22	4.3	3.41	0.29	14	3.42	0.28	12
200803221551	33.41	47.71	4.4	2.97	0.59	4	3.15	0.12	5
200804161039	40.894	52.076	4.7	3.59	0.22	7	3.42	0.21	3
200804250448	37.819	29.256	4.5	4.09	0.14	17	4.07	0.23	20
200804300240	38.696	70.58	4.1	3.24	0.3	12	3.24	0.35	10
200805010015	33.86	48.59	4.5	3.7	0.18	16	3.93	0.17	19
200805052157	25.9	56.1	5.3	4.61	0.24	31	4.58	0.22	29
200805102225	39.677	52.152	4.5	3.9	0.2	9	3.6	0.22	7
200805310124	27.1	54.57	4.8 [B]	3.63	0.17	16	3.71	0.24	19
200806291537	38.992	41.225	4	3.62	0.41	7	3.54	0.28	8
200807032310	35.58	58.527	5 [N]	4.48	0.31	20	4.54	0.28	22
200808272152	32.439	47.408	5.2 [C]	5.45	0.26	28	5.65	0.29	26
200809022000	38.874	45.777	5	4.44	0.2	28	4.53	0.22	27
200809032243	32.44	47.28	5.3	4.36	0.18	18	4.5	0.38	21
200809101100	24.3	58.9	6.1	5.93	0.26	29	6.04	0.31	31
200809171208	40.01	39.979	4.8	4.04	0.25	22	4.26	0.31	20
200809171743	26.758	56.233	5.3	4.7	0.34	24	4.91	0.26	23
200810052256	33.886	69.47	6	6.09	0.23	15	6.26	0.27	15
200810252017	26.533	54.985	5.2	5	0.31	17	5.06	0.28	18
200811121403	38.841	35.524	4.8	4.62	0.27	27	4.67	0.32	28
200812081441	26.904	55.736	5.5	4.58	0.35	14	4.66	0.32	19
200812091509	26.833	55.978	5.2	4.7	0.46	20	4.69	0.46	24
200902020836	27.18	66.307	5	4.7	0.34	31	4.89	0.31	30
200902170528	39.107	29.039	4.8	4.64	0.27	21	4.66	0.32	20
200904251718	45.728	26.446	5.3	4.26	0.23	14	3.93	0.23	9
200904301004	27.753	61.431	5.2	4.42	0.43	20	4.21	0.32	14
200905101734	38.233	67.63	5.3	4.61	0.35	29	4.44	0.34	28
200906021439	40.294	52.994	4.9	4.29	0.3	21	4.29	0.31	17
200906170922	38.213	69.744	4.4	3.83	0.22	13	4	0.22	12

Table 2. Results for earthquakes in the Koran Peninsula.

Event YYYYMMDDHHMM	Latitude, ºN	Longitude, ºE	*Mw*	*Ms R*	σ_R	#R	*Ms L*	σ_L	#L
19961213041016	37.19	128.75	4.67	3.94	0.23	4	4.47	0.14	4
19970625185021	35.82	129.19	4.34	3.85	0.02	3	3.97	0.20	3
19990407144318	37.2	128.832	3.7	2.28	0.00	1	3.09	0.00	1
20001209095059	36.476	130.024	4.06	3.24	0.23	10	3.06	0.25	10
20011121014912	36.715	128.282	3.42	2.29	0.16	10	2.24	0.29	8
20011124071031	36.742	129.867	3.81	2.77	0.14	8	3.23	0.12	8
20020317002638	37.989	124.533	3.74	2.76	0.05	9	2.76	0.22	9
20020708014912	35.85	129.76	3.75	2.53	0.07	4	2.89	0.36	6
20020723124804	35.5701	122.1801	4.86	4.26	0.15	18	4.43	0.24	17
20021209224250	38.8	127.2	3.65	2.4	0.13	7	2.77	0.27	9
20030109083318	37.46	124.33	3.86	2.38	0.16	5	3.21	0.15	9
20030322203839	35	124.6	4.83	4.06	0.13	11	4.48	0.26	11
20030330111056	37.57	123.82	4.6	3.93	0.05	12	4.21	0.28	12
20030415175525	36.4	126.3	3.24	2.11	0.13	15	1.93	0.17	11
20030609011404	35.921	123.524	3.89	2.9	0.08	6	3.01	0.37	6
20031013091205	36.95	126.51	3.79	2.53	0.11	6	2.92	0.37	8
20040105164941	38.7	125.1	3.33	1.98	0.11	2	2.28	0.07	4
20040426042925	35.841	128.219	3.62	2.47	0.17	9	2.58	0.21	9
20040529101424	36.8	130.2	5.08	4.85	0.13	17	4.61	0.34	17
20040601112218	37.2	130	3.59	2.47	0.20	12	2.74	0.21	12
20040805203254	35.9	127.4	3.21	1.79	0.04	5	2.3	0.26	13
20041216185914	41.79	127.94	3.94	2.93	0.15	9	3.12	0.27	11
20050614220702	33.15	126.14	3.78	2.43	0.12	7	2.99	0.27	9
20050629141805	34.5	129.05	4.13	3.38	0.10	12	3.33	0.20	13
20051009235106	37.93	124.9	3.58	2.58	0.13	6	2.7	0.24	6
20060119033534	37.21	128.8	3.53	2.24	0.20	7	2.51	0.25	8
20060429020112	37.09	129.92	3.63	2.51	0.16	10	2.83	0.23	11
20070120115654	37.691	128.595	4.55	3.65	0.16	35	4.28	0.26	44
20080531125930	33.5	125.69	3.93	2.63	0.17	8	3.28	0.23	10
20081029002614	36.35	127.25	3.44	3.95	0.01	2	3.79	0.16	2
20090302052028	37.11	124.6	3.49	2.19	0.15	7	2.64	0.08	4

Table 3. Results for earthquakes in Italy.

Event YYYYMMDDHHMM	Latitude, ºN	Longitude, ºE	*Mw*	*Ms R*	σ_R	#R	*Ms L*	σ_L	#L
20090423151408	42.247	13.492	3.84	3.06	0.12	14	3.11	0.19	10
20090418090556	42.441	13.361	3.71	2.88	0.19	29	3.01	0.2	21
20090409224006	42.481	13.298	3.71	2.93	0.25	20	2.78	0.13	12
20090409131933	42.338	13.259	3.79	2.95	0.13	18	3.21	0.24	20
20090405204854	42.332	13.372	3.92	3.11	0.17	19	3.43	0.23	16
20090410032222	42.47	13.417	3.74	2.71	0.18	8	2.9	0.18	13
20081225030829	44.556	10.309	3.88	3.23	0.08	5	3.32	0.07	2
20090406215653	42.396	13.323	3.79	3.17	0.19	4	3.05	0.36	5
20090408042741	42.305	13.467	3.92	3.11	0.23	13	3.25	0.23	13
20090408225650	42.507	13.364	3.86	2.98	0.11	14	3.22	0.18	12
20090406022746	42.374	13.342	4.1	3.41	0.22	4	3.4	0.31	5
20090423214900	42.233	13.479	4.06	3.25	0.12	14	3.43	0.22	13
20090409043244	42.445	13.42	4.11	3.39	0.11	22	3.63	0.23	15
20090330133838	42.326	13.362	4.08	3.38	0.17	20	3.63	0.28	18
20090406163809	42.362	13.333	4.3	3.72	0.13	11	3.76	0.27	10
20090406071710	42.355	13.367	4.03	3.26	0.22	13	3.49	0.19	13
20090409031452	42.338	13.437	4.2	3.53	0.23	26	3.64	0.17	24
20090406035645	42.336	13.387	4.26	3.52	0.16	32	3.74	0.2	23
20090407213429	42.38	13.376	4.22	3.71	0.29	5	3.78	0.2	6
20090406023704	42.366	13.34	4.81	4.45	0.17	12	4.54	0.22	13
20090413211424	42.504	13.363	4.85	4.62	0.24	14	4.65	0.19	13
20090406231537	42.451	13.364	4.9	4.46	0.13	38	4.75	0.16	34
20090407092628	42.342	13.388	4.75	4.38	0.16	21	4.57	0.21	23
20090409193816	42.501	13.356	4.98	4.6	0.13	25	4.84	0.19	25
20090409005259	42.484	13.343	5.22	4.93	0.18	22	5.14	0.21	21
20081223152421	44.544	10.345	5.12	5.33	0.08	4	5.22	0.31	5
20081223215826	44.527	10.355	4.61	4.37	0.16	6	4.45	0.06	5
20090407174737	42.275	13.464	5.42	5.45	0.12	23	5.39	0.17	21
20090406013239	42.334	13.334	6.13	6.27	0.23	13	6.61	0.1	13
20090406084013	42.364	13.366	3.37	2.37	0.18	14	2.48	0.25	11
20090410191839	42.344	13.358	3.1	2.01	0.11	9	2.19	0.24	4
20090412180516	42.395	13.394	3.21	2.53	0.34	4	2.3	0.18	3
20090414205309	42.549	13.302	3.28	2.01	0.11	5	2.34	0.18	6
20090406094702	42.264	13.393	3.19	2.1	0.16	6	2.11	0.15	4
20090406141438	42.365	13.338	3.52	2.47	0.15	5	3.01	0	1
20090406200334	42.213	13.479	3.3	2.3	0.21	6	2.4	0.21	5
20090409023726	42.498	13.335	3.19	2.07	0.2	10	2.17	0.19	5
20090411195353	42.347	13.525	3.04	2.19	0.27	6	2.15	0.13	4

20090425020823	42.294	13.454	3.22	2.2	0.14	7	2.14	0.12	5
20090330134326	42.303	13.364	3.53	2.64	0.24	5	2.8	0	1
20090330215717	42.316	13.375	3.46	2.66	0.21	5	2.43	0	1
20090405223941	42.341	13.38	3.47	2.54	0.14	13	2.8	0.2	13
20090406062105	42.317	13.416	3.54	2.6	0.16	7	2.56	0	1
20090406064815	42.303	13.383	3.25	2.25	0.12	8	2.49	0.19	10
20090406073941	42.324	13.371	3.47	2.26	0.11	14	2.49	0.22	14
20090406125516	42.372	13.353	3.4	2.36	0.11	5	2.47	0.28	5
20090406165726	42.346	13.307	3.3	2.28	0.18	10	2.46	0.18	6
20090407122928	42.437	13.403	3.58	2.47	0.15	15	2.58	0.24	9
20090408175835	42.364	13.396	3.32	2.76	0.28	5	2.58	0.22	5
20090410043304	42.458	13.35	3.34	2.47	0.14	5	2.28	0.13	5
20090411070414	42.391	13.406	3.31	2.23	0.15	19	2.45	0.14	12
20090430130101	42.361	13.364	3.52	2.52	0.2	13	2.65	0.35	10
20090406103618	42.343	13.402	3.31	2.37	0.13	7	2.61	0.25	5
20090408113557	42.355	13.328	3.35	2.27	0.14	13	2.7	0.15	5
20090408231806	42.391	13.325	3.5	2.35	0.23	7	2.71	0.23	9
20090411053900	42.386	13.402	3.44	2.28	0.1	15	2.53	0.18	8
20090411065702	42.387	13.406	3.26	2.1	0.12	11	2.28	0.15	5
20090413191757	42.36	13.354	3.55	2.52	0.24	11	2.71	0.28	10
20090416054454	42.289	13.404	3.39	2.32	0.16	14	2.65	0.23	13
20090421154436	42.33	13.366	3.53	2.54	0.11	13	2.78	0.21	8
20090406044753	42.352	13.347	3.82	3.01	0.06	2	2.97	0	1
20090408030034	42.299	13.459	3.76	2.89	0.18	14	2.91	0.21	14
20090409044309	42.506	13.366	3.69	2.85	0.18	10	3.04	0.12	8
20090409151814	42.308	13.495	3.36	2.41	0.18	5	2.42	0.3	5
20090413133604	42.444	13.44	3.65	2.69	0.13	11	2.83	0.21	8
20090413190949	42.36	13.348	3.73	2.91	0.21	14	2.96	0.25	9
20090414172730	42.527	13.295	3.75	2.84	0.18	10	2.91	0.18	11
20090414201727	42.53	13.288	3.79	2.88	0.2	13	3.14	0.21	9
20090416174930	42.54	13.289	3.76	3.09	0.18	9	3.02	0.23	9
20090501051251	42.28	13.47	3.69	2.74	0.18	13	2.71	0.15	15
20090329084307	41.989	14.009	3.76	2.93	0.09	5	2.89	0.16	3
20090414135621	42.543	13.312	3.84	2.81	0.12	16	3.05	0.28	18
20090406093012	42.373	13.341	3.27	2.17	0.14	10	2.45	0.17	5
20090330190528	42.316	13.373	3.29	2.28	0.24	2	2.62	0.13	2
20090403044442	42.327	13.358	3.15	2.12	0	1	2.53	0.44	2
20090406072845	42.347	13.39	3.37	2.23	0.26	4	2.48	0.32	3
20090406095929	42.322	13.381	3.32	2.19	0.18	12	2.53	0.25	5
20090406174004	42.376	13.334	3.37	2.23	0.22	7	2.42	0.23	5
20090406234934	42.349	13.378	3.2	2.09	0.35	4	2.31	0.12	3

20090407015203	42.432	13.393	3.3	2.15	0.2	10	2.45	0.22	5
20090407213906	42.361	13.363	3.61	2.83	0.13	5	2.91	0	1
20090407222950	42.284	13.489	3.29	2.24	0.15	5	2.37	0.06	6
20090407224342	42.328	13.486	2.99	2.48	0.31	5	2.22	0.22	4
20090408103409	42.352	13.381	3.47	2.05	0.16	5	2.46	0.39	2
20090408211104	42.297	13.57	3.02	2.23	0.11	4	2.19	0.24	5
20090409034155	42.51	13.332	3.2	1.99	0.16	10	2.17	0.15	6
20090409042945	42.504	13.345	3.11	1.96	0.22	5	2.21	0.18	5
20090409061029	42.491	13.397	3.04	1.79	0	1	2.13	0.12	2
20090409093106	42.361	13.39	3.22	1.89	0.07	7	2.27	0.14	6
20090409130029	42.299	13.467	3.23	2.04	0.16	10	2.48	0.19	9
20090409204701	42.493	13.305	3.12	2.03	0.14	9	2.09	0.15	5
20090409210949	42.51	13.335	3.08	1.94	0.14	5	2.14	0.21	5
20090410064131	42.52	13.339	3.07	1.92	0.28	4	2.02	0.14	3
20090410115309	42.243	13.484	3.32	2.26	0.12	13	2.46	0.13	6
20090410190721	42.375	13.393	3.14	2.27	0.25	8	2.24	0.14	5
20090411061326	42.469	13.417	3.19	2.17	0.41	4	2.1	0.23	5
20090411154229	42.523	13.316	3.21	2.07	0.18	8	2.2	0.26	4
20090412032935	42.536	13.316	3.16	1.9	0.08	6	2.17	0.06	5
20090413070830	42.268	13.484	3.23	2.2	0.27	4	2.31	0.25	3
20090413084108	42.271	13.505	3.17	2.05	0.04	6	2.24	0.09	5
20090413200824	42.365	13.371	3.01	2	0.17	3	2.04	0.24	2
20090414192802	42.536	13.307	3.35	2.33	0.15	5	2.52	0.28	5
20090415114440	42.287	13.474	3.3	2.45	0.18	5	2.27	0.33	3
20090415193644	42.522	13.286	3.41	2.49	0.11	8	2.52	0.13	5
20090415195557	42.466	13.365	3.04	2.04	0.13	5	2.11	0.21	5
20090415225307	42.505	13.312	3.86	2.93	0.22	11	3.19	0.17	9
20090418110721	42.265	13.494	3.53	2.51	0.22	8	2.8	0.16	13
20090418130308	42.332	13.5	2.81	1.25	0	1	1.54	0	1
20090419123950	44.727	7.845	3.69	2.39	0.2	5	2.78	0.09	5
20090420071314	42.407	13.349	3.05	1.86	0.16	5	1.98	0.06	2
20090420114306	42.278	13.503	3.03	1.87	0.07	5	2.01	0.07	2
20090421162056	42.516	13.313	2.98	1.73	0.11	4	1.78	0	1
20090422123225	42.578	12.827	3.31	2.48	0.22	7	2.44	0.18	10
20090424043617	42.263	13.466	3.26	2.14	0.19	6	2.24	0	1
20090424133853	42.519	13.348	3.23	2.02	0.14	8	2.53	0.13	2
20090424142407	42.386	13.394	3.04	2.19	0.28	5	2.21	0.17	4
20090424155345	42.309	13.465	3.19	2.09	0.09	7	2.06	0.29	5
20090424225129	42.267	13.508	3.14	1.98	0.06	3	2.29	0.21	4
20090425111304	42.416	13.334	3.07	1.75	0.09	6	2.29	0.02	2
20090425131731	42.264	13.495	3.13	2.02	0.13	6	2.06	0	1

20090426175606	42.456	13.378	2.93	1.77	0.11	5	1.75	0.12	2
20090503051443	42.365	13.39	3.27	2.01	0.32	4	2.42	0.32	4
20090505104403	42.282	13.498	3.1	2.16	0.26	4	2.16	0.32	3
20090505180341	42.27	13.509	3.28	2.17	0.23	6	2.26	0.14	5
20090508010247	42.268	13.583	3.18	2.47	0.1	6	2.58	0.16	4

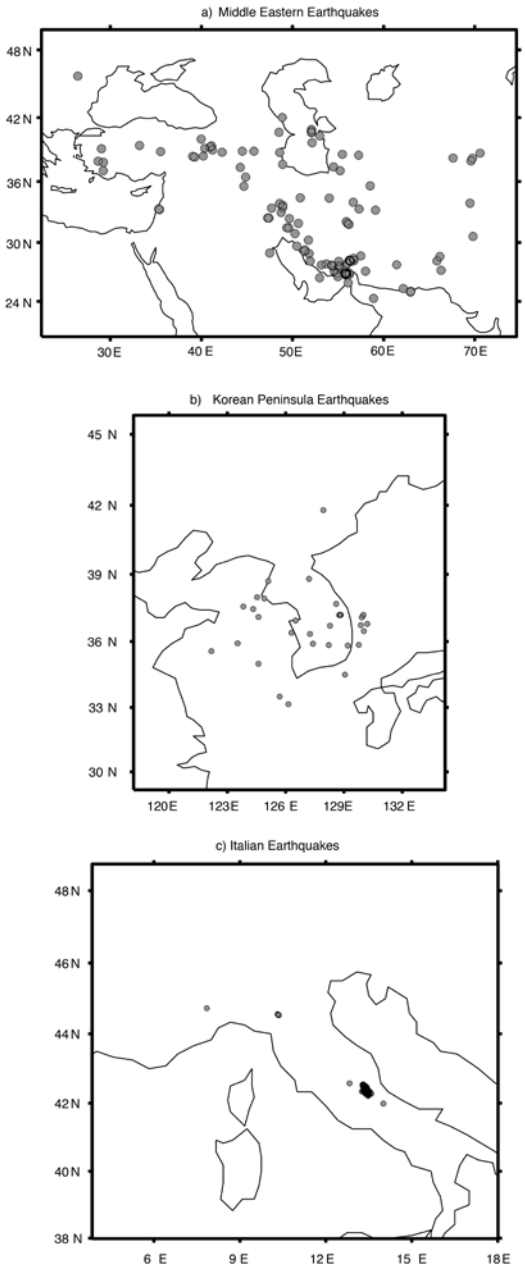

Figure 2. Map of the seismic events for which $M_s(VMAX)$-Love and Rayleigh were estimated in the a) Middle East, b) Korean Peninsula region, and in c) central Italy.

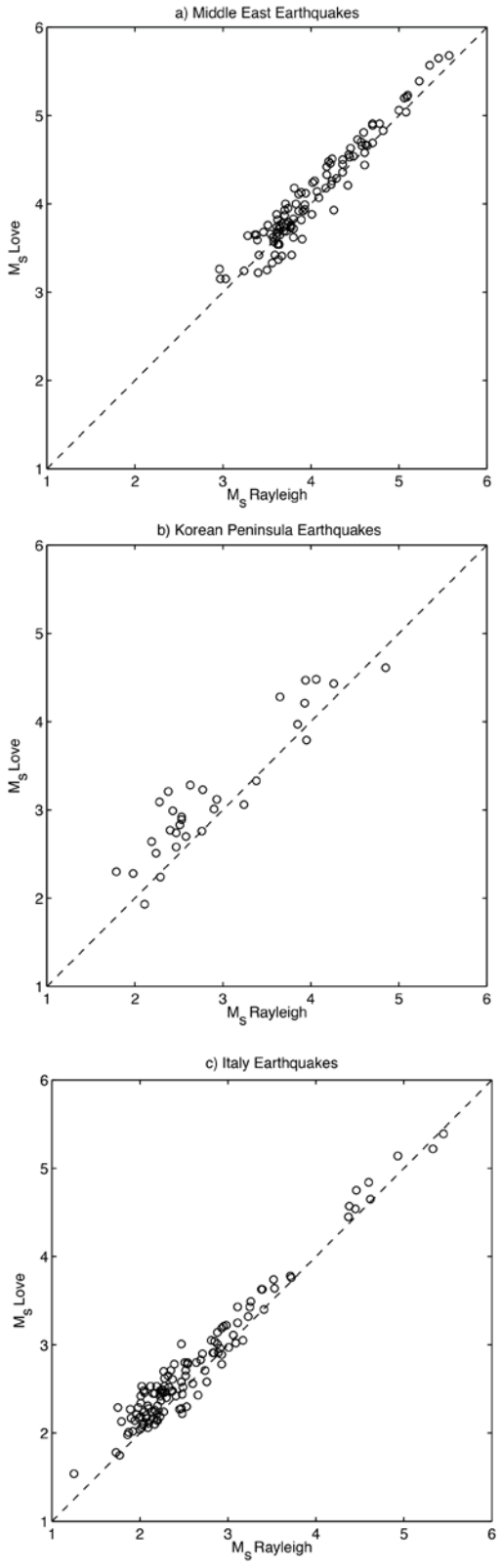

Figure 3. M_s(VMAX)-Love versus M_s*(VMAX)*-Rayleigh for earthquakes in the a) Middle East, b) Korean Peninsula region, and in c) central Italy.

We include these data in our study because the dominant focal mechanism suggests NW/SE trending normal faults (www.eas.slu.edu/eqc/eqc_mt/MECH.IT/laquila.png, last accessed July 2011; Herrmann et al., 2011a). Figure 3c shows that for the majority of these events (100 or 80%) $M_s(VMAX)$-Love was on average 0.2 m.u. larger than the $M_s(VMAX)$-Rayleigh, which is unexpected for the dip-slip focal mechanisms. The dominant period of the measurements was 8 s for Rayleigh waves and between 8 and 12 s for the Love waves. The interstation standard deviation for the Rayleigh waves averaged 0.17 m.u., which was slightly lower than for the Love waves (0.20 m.u.).

The percentage of the events with higher $M_s(VMAX)$-Love is slightly lower for the Middle East dataset than for Korea and Italy (74% vs. 80%). Possible explanations include deeper events as well as more variety in the focal mechanisms for the Middle Eastern dataset. The interstation standard deviation is slightly higher for the Middle East data, which most likely results from more laterally heterogeneous structure. Another peculiarity of the Middle East dataset is the longer dominant periods at which $M_s(VMAX)$ is calculated for both Rayleigh and Love waves. Figure 4 shows the histograms of the dominant periods for the Middle East, Korea, and Italy. Excitation due to depth alone cannot explain this period increase, because a similar feature is observed for a nuclear explosion detonated in this study region (EVID 19980528101600). The large number of Love and Rayleigh-wave observations at 25 s represents an edge effect associated with the long period limit in the current processing. Increasing this limit to 40 s will be discussed later in the report.

Explosions

We have also estimated the $M_s(VMAX)$ for Rayleigh and Love waves from 82 nuclear explosions (Table 4) at many different test sites (Figure 5). Our working hypothesis was that the Love wave magnitudes should be smaller than the Rayleigh wave estimates for explosions. This was certainly the case for all analyzed events at the Nevada Test Site, where $M_s(VMAX)$-Rayleigh averaged 0.4 m.u. larger than $M_s(VMAX)$-Love. There were some events with large Love wave magnitudes from the Shagan Test Site; however, the Rayleigh wave magnitudes were on average 0.21 m.u. larger than the Love wave estimates. For 7 Lop Nor explosions the $M_s(VMAX)$-Rayleigh are slightly larger than $M_s(VMAX)$-Love, except for one anomalous event (EVID 19920521045947 in Table 3) which had a Love wave magnitude 0.27 m.u. larger than the Rayleigh magnitude. Our dataset also included the 1998 Pakistan nuclear test, which had a Love wave magnitude slightly larger than the Rayleigh magnitude, and the 2008 Indian nuclear explosion, which had a larger Rayleigh magnitude (by ~0.2 m.u.).

We were unable to measure Love waves using openly available data for the 2006 North Korean nuclear explosion ($M_s(VMAX)$-Rayleigh=2.9). Based on background noise levels, we conclude the $M_s(VMAX)$-Love must have been less than 2.5 (similar conclusion reached by Kohl et al., 2011). For the 2009 event, the Rayleigh $M_s(VMAX)$=3.7 exceeded the Love $M_s(VMAX)$ by 0.5 m.u. As mentioned previously, the Korean events had large Rayleigh M_s estimates compared to m_b, however, the Love waves magnitudes are much smaller and provide added discrimination information.

Table 4. Results for worldwide nuclear explosions.

Event YYYYMMDDHHMM	Latitude, ºN	Longitude, ºE	*mb* (*)	*Ms R*	σ_R	#R	*Ms L*	σ_L	#L	Test Site
19790623025630	49.915	78.846	6.30	4.06	0.19	12	3.92	0.15	8	STS-B
19790707034649	50.033	78.989	5.80	4.31	0.46	9	4.22	0.41	7	STS-B
19790803150730	37.084	-116.070	4.78	3.13	0.07	3	3.01	0.07	3	NTS
19790804035656	49.903	78.888	6.10	4.16	0.18	9	3.91	0.23	7	STS-B
19790808150000	37.015	-116.008	4.85	3.38	0.04	3	3.17	0.05	3	NTS
19790818025143	49.948	78.919	6.10	3.90	0.21	9	3.73	0.21	8	STS-B
19790829150800	37.121	-116.067	4.93	3.41	0.14	4	2.83	0.09	4	NTS
19790906150000	37.088	-116.053	5.83	4.67	0.02	4	4.16	0.14	4	NTS
19790926150000	37.229	-116.364	5.73	4.60	0.05	4	3.99	0.13	4	NTS
19791028031556	49.997	78.995	6.00	4.02	0.20	10	3.87	0.14	9	STS-B
19800403140000	37.150	-116.082	4.90	3.28	0.17	4	2.84	0.01	2	NTS
19800416200000	37.100	-116.031	5.45	4.28	0.20	4	3.60	0.23	4	NTS
19800426170000	37.248	-116.422	5.66	4.60	0.05	4	4.15	0.18	4	NTS
19800612171500	37.282	-116.454	5.61	4.67	0.04	3	4.24	0.01	3	NTS
19800725190500	37.256	-116.477	5.80	4.70	0.05	4	4.12	0.07	4	NTS
19800914024215	49.937	78.797	6.20	4.08	0.19	10	4.03	0.28	9	STS-B
19801024191500	37.074	-115.999	4.43	3.00	0.12	4	2.71	0.12	3	NTS
19801031180000	37.238	-116.205	4.65	3.37	0.12	4	2.89	0.03	4	NTS
19801114165000	37.111	-116.019	4.39	3.01	0.07	4	2.82	0.07	3	NTS
19801217151000	37.325	-116.315	5.26	4.05	0.06	4	3.72	0.18	3	NTS
19810115202500	37.087	-116.045	5.56	4.41	0.02	4	3.84	0.25	4	NTS
19810606180000	37.303	-116.326	5.62	4.42	0.09	4	3.91	0.17	4	NTS
19811001190000	37.082	-116.009	5.12	3.80	0.01	3	3.32	0.08	3	NTS
19811111200000	37.076	-116.069	4.90	3.41	0.12	4	3.17	0.13	3	NTS
19811112150000	37.108	-116.049	5.38	4.17	0.05	4	3.62	0.24	4	NTS
19811216210500	37.114	-116.123	4.53	2.80	0.10	2	2.68	0.01	2	NTS
19820128160000	37.091	-116.051	5.76	4.65	0.04	4	4.26	0.30	4	NTS
19820212145500	37.224	-116.463	5.48	4.42	0.15	4	4.05	0.13	4	NTS
19820212152500	37.348	-116.316	5.76	4.45	0.06	4	4.00	0.20	4	NTS
19820417180000	37.017	-116.010	4.49	2.95	0.09	4	2.65	0.00	1	NTS
19820425180500	37.256	-116.422	5.47	4.42	0.04	4	3.91	0.06	4	NTS
19820507181700	37.069	-116.045	5.66	4.28	0.05	4	3.78	0.25	4	NTS
19820624141500	37.236	-116.370	5.73	4.57	0.09	4	4.03	0.22	1	NTS
19820729200500	37.102	-116.075	4.68	2.86	0.23	4	2.76	0.20	4	NTS
19820805140000	37.084	-116.007	5.82	4.73	0.07	4	4.16	0.06	3	NTS
19820923160000	37.212	-116.208	4.88	3.35	0.11	3	2.84	0.14	3	NTS
19820923170000	37.175	-116.089	4.90	3.49	0.13	3	3.21	0.07	3	NTS
19821210152000	37.080	-116.072	4.72	3.10	0.10	4	2.77	0.19	4	NTS
19830326202000	37.301	-116.460	5.36	4.12	0.04	3	3.72	0.13	3	NTS

19830414190500	37.073	-116.046	5.64	4.18	0.05	4	3.66	0.07	4	NTS
19830505152000	37.146	-116.089	4.37	2.65	0.09	3	2.34	0.28	2	NTS
19830526150000	37.103	-116.006	4.52	3.21	0.07	4	2.74	0.22	4	NTS
19830609171000	37.158	-116.089	4.73	2.80	0.02	2	2.65	0.14	2	NTS
19830803133300	37.119	-116.089	4.48	2.60	0.14	2	2.36	0.00	1	NTS
19830901140000	37.273	-116.356	5.52	4.22	0.11	3	3.78	0.00	1	NTS
19840301174500	37.066	-116.047	5.82	4.38	0.23	7	3.94	0.33	7	NTS
19840501190500	37.106	-116.023	5.47	4.36	0.16	8	3.86	0.09	8	NTS
19840802150000	37.017	-116.009	4.57	2.83	0.08	3	2.56	0.00	1	NTS
19870403011700	49.918	78.780	6.12	4.35	0.28	11	4.07	0.18	9	STS-B
19870802005800	49.881	78.875	5.83	3.92	0.22	8	3.86	0.24	9	STS-B
19871003151500	47.600	56.200	5.30	3.27	0.33	3	2.85	0.00	1	PNE
19871115033100	49.899	78.758	5.98	4.31	0.28	11	4.06	0.28	9	STS-B
19871213032100	49.963	78.793	6.06	4.31	0.23	8	4.07	0.18	8	STS-B
19880504005700	49.949	78.750	6.09	4.49	0.10	4	4.16	0.22	4	STS-B
19880906162000	61.361	48.092	4.80	3.26	0.14	2	2.70	0.00	1	PNE
19881123035709	49.767	78.029	5.40	3.72	0.00	1	3.48	0.00	1	STS-B
19881204052000	73.366	55.010	5.90	4.12	0.18	7	3.67	0.17	2	NZ
19881217041809	49.879	78.924	5.90	4.23	0.25	10	4.10	0.21	11	STS-B
19890122035709	49.934	78.815	6.10	4.18	0.20	10	3.94	0.20	10	STS-B
19890212041509	49.911	78.704	5.90	4.23	0.24	8	3.95	0.27	7	STS-B
19890622211500	37.283	-116.413	5.43	4.33	0.19	7	3.75	0.14	4	NTS
19890708034700	49.869	78.775	5.60	3.81	0.21	11	3.56	0.24	8	STS-B
19890902041659	50.019	78.998	5.10	3.57	0.19	5	3.33	0.16	2	STS-B
19891019094959	49.927	78.972	6.00	4.34	0.16	16	3.97	0.20	14	STS-B
19891208150000	37.231	-116.410	5.56	4.20	0.23	8	4.13	0.18	8	NTS
19900310160000	37.112	-116.056	5.16	3.75	0.23	8	3.13	0.18	5	NTS
19900613160000	37.262	-116.421	5.96	4.78	0.12	7	4.46	0.15	7	NTS
19901024145758	73.331	54.757	5.70	4.11	0.23	18	3.82	0.19	14	NZ
19901114191700	37.227	-116.372	5.46	4.34	0.20	5	3.94	0.23	5	NTS
19910404190000	37.296	-116.314	5.65	4.35	0.22	10	4.03	0.29	10	NTS
19910914190000	37.226	-116.429	5.69	4.43	0.25	12	4.13	0.34	12	NTS
19920521045947	41.510	88.770	6.50	4.82	0.20	16	5.09	0.25	16	Lop Nor
19920925075958	41.720	88.340	5.00	2.85	0.25	4	2.68	0.21	3	Lop Nor
19931005015956	41.670	88.700	5.90	4.13	0.21	19	4.17	0.21	19	Lop Nor
19940610062557	41.530	88.710	5.80	3.71	0.23	17	3.62	0.36	18	Lop Nor
19941007032558	41.660	88.750	6.00	4.07	0.18	17	4.07	0.22	12	Lop Nor
19950515040557	41.600	88.820	6.10	4.26	0.46	24	4.21	0.34	24	Lop Nor

19960608025558	41.660	88.690	5.90	4.11	0.21	9	4.08	0.11	9	Lop Nor
19960729014857	41.820	88.420	4.90	2.88	0.09	2	2.73	0.12	2	Lop Nor
19980511101300	27.078	71.719	5.20	3.21	0.20	9	3.24	0.32	10	India
19980528101600	28.830	64.950	4.90	3.41	0.23	10	3.24	0.19	8	Pakistan
20090525005443	41.294	129.082	4.70	3.72	0.18	35	3.18	0.17	13	NK

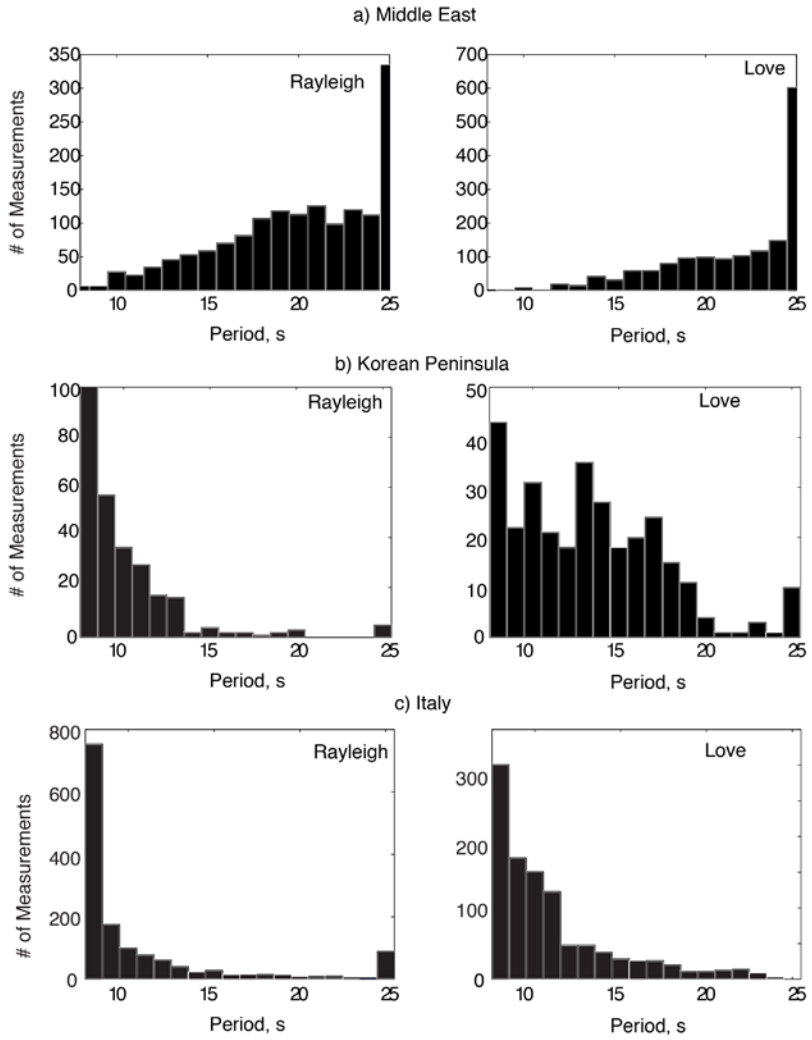

Figure 4. Histograms of the periods of maximum amplitudes for Rayleigh and Love waves in the a) Middle East, b) Korean Peninsula region, and in c) central Italy. For the Middle East dataset, varied focal mechanisms, depths, and complex regional-to-teleseismic propagation paths lead to longer period magnitude estimates. For the Korean and Italian datasets, the events are shallow and have shorter, less complex propagation paths leading to more short-period magnitude estimates.

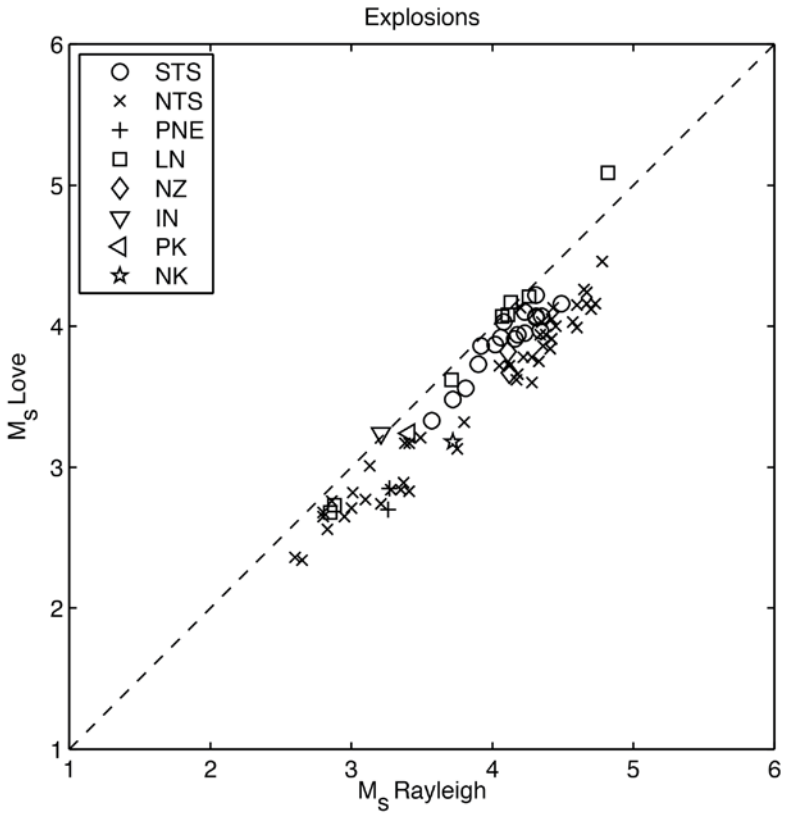

Figure 5. M_s(VMAX)-Love versus M_s(VMAX)-Rayleigh for nuclear explosions.

Event Identification with Logistic Regression

The observed differences in the Love and Rayleigh wave magnitudes for earthquakes and explosions led us to the idea that a surface wave discriminant could be developed without incorporation of an m_b. For regional events, m_b(*Pn*) is often difficult to determine, and there may be geophysical structural, data center measurement (e.g., Murphy et al., 1997), and data censoring biases that complicate the M_s:m_b interpretation. We decided to test for a possible M_s:M_s discriminant using logistic regression (Press and Wilson, 1978).

Logistic regression models the conditional probability that an event is an explosion given a regression function of event magnitudes $\underline{\boldsymbol{x}}$. The calibrated model gives the best linear combination (regression model) of magnitudes (the discriminant) that best separates the explosion and earthquake magnitude data. Using the regression model, the Bernoulli probability of an event being an explosion is expressed as

$$\pi(\underline{x}) = \frac{1}{1 + e^{\alpha + \underline{\beta}' \underline{x}}}. \tag{2}$$

For $\boldsymbol{n}$ observed events, earthquakes and explosions, the likelihood function is defined as the product of these probabilities:

$$\ell(\alpha,\underline{\beta}) = \prod_{i=1}^{n} \pi(\underline{x}_i)^{y_i} \left(1 - \pi(\underline{x}_i)\right)^{1-y_i} , \qquad (3)$$

where y_i=1 if explosion, y_i=0 if earthquake, and $\underline{x}_i$ is the vector of observed magnitudes for the event. Maximizing $\ell(\alpha,\underline{\beta})$ provides estimates (calibration values) for $\alpha,\underline{\beta}$. For a new event, $\pi(\underline{x})$ is evaluated with magnitudes $\underline{\boldsymbol{x}}$ and identification made with this value. For example, if $\pi(\underline{x})$ > 0.55 the event is identified as explosion, if $\pi(\underline{x})$ < 0.45 the event is identified as earthquake, and is indeterminate otherwise. Figure 6a gives the function $\pi(\underline{x})$,

$$\pi\left(EX \middle| M_s(Rayleigh), M_s(Love)\right) = \frac{1}{1 + e^{(4.09 + 12.14 * M_s(Love) - 12.65 * M_s(Rayleigh)}} , \qquad (4)$$

using the average jackknife parameter values (see Figures 6b,c,d), and a subset of jackknife event identifications. The indeterminate region is included on plot. We have completed a leave-one-out (jackknife) cross validation analysis (Figures 6b,c,d) on M_s*(VMAX)*-Rayleigh and Love using the decision rule above. The data included 82 explosions and 264 earthquakes. For each jackknife sample, 82+264=346 in total, calibration values for $\alpha,\underline{\beta}$ were computed using maximum likelihood estimation. These parameter values were then used to identify the hold-out event by evaluating $\pi(\underline{x})$ and applying the decision criteria above. The performance of the cross validation analysis is given in Table 5. From Figure 6e, we note that the absolute values of the slopes for earthquakes and explosions are statistically different, however the slopes may not be practically different and the logistic regression model could effectively be reduced to b_0 + b_1*(M_s(Love) - M_s(Rayleigh)).

The cross-validation analysis of the proposed M_s:M_s discriminant correctly identifies 57 of 82 explosions and 246 of 264 earthquakes. The analysis misidentifies 22 explosions as earthquakes and 11 earthquakes as explosions. These results show that there is discrimination information in an M_s(Rayleigh):M_s(Love) discriminant. Further comparative research is planned for M_s(Rayleigh):M_s(Love) versus M_s:m_b using common data. We fully expect that M_s(Rayleigh):M_s(Love) will contribute significantly to multivariate event identification. Results from this study do suggest that a M_s-Love:m_b discriminant might be more robust than M_s-Rayleigh:m_b due to the typically larger M_s-Love magnitudes for earthquakes and smaller values for explosions. However, the smaller M_s-Love estimates for explosions, while great for discrimination, are costly in terms of detection. Bonner *et al*. (2006) determined for M_s*(VMAX)*-Rayleigh to be measured at the Nevada Test Site, the m_b must be 3.6 or greater; thus the event body-wave magnitude for M_s*(VMAX)*-Love application would increase to greater than 4.0.

Table 5. Cross Validation Identification Performance with M_s Rayleigh and Love Magnitudes.

	EX	EQ	I	Total
EX	57	22	3	82
EQ	11	246	7	264

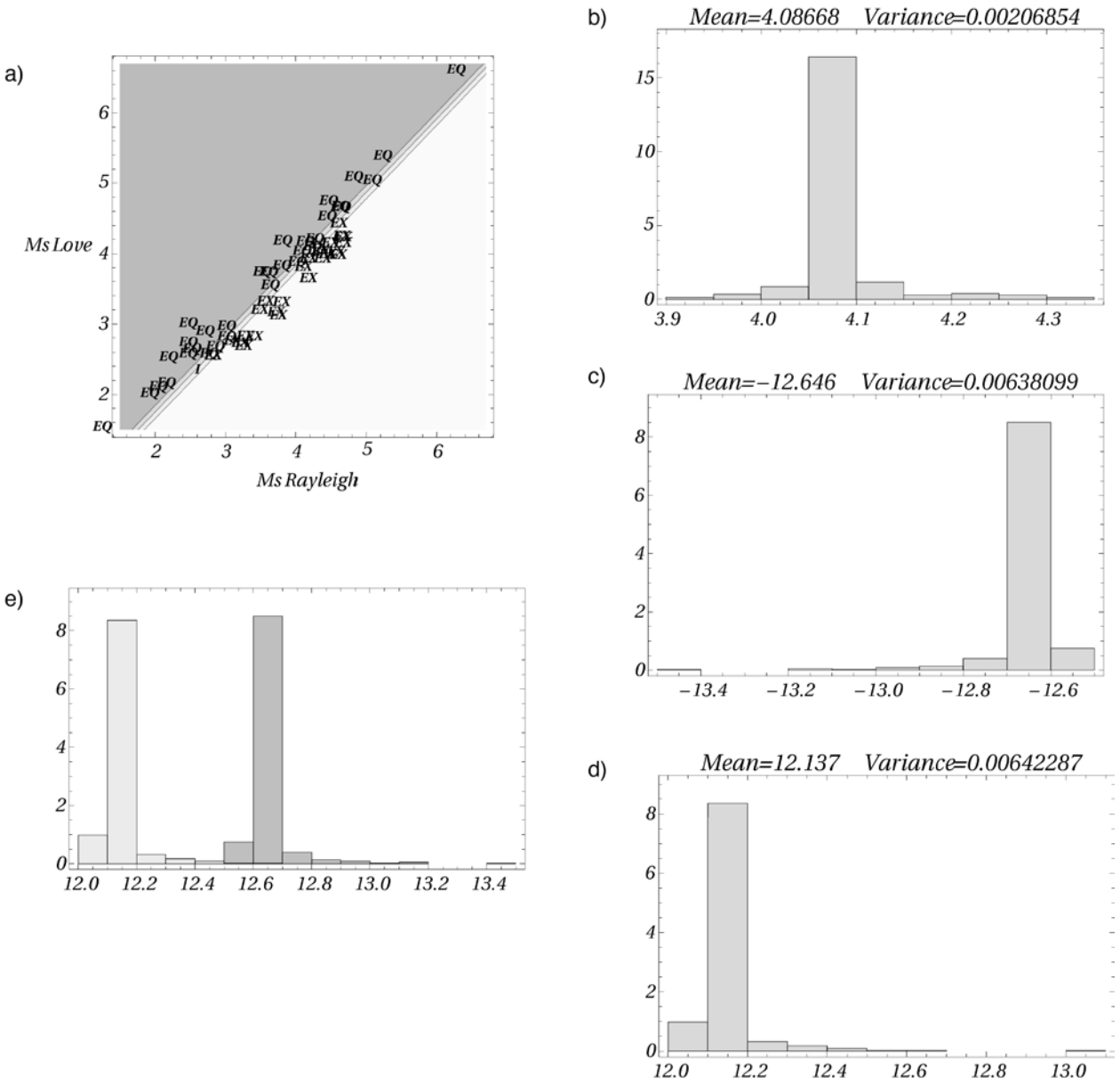

Figure 6. Logistic regression results for a possible M_s(Rayleigh):M_s(Love) discriminant. a) $\pi(\underline{x})$ using the average of jackknife parameter values. b) Jackknife α estimates. c) Jackknife estimates of Rayleigh slopes. d) Jackknife estimates of Love slopes. e) Histograms of the absolute value jackknife slopes $\underline{\beta}$. Rayleigh jackknife slopes are gray and Love jackknife slopes are light gray.

Possible Improvements to Love Wave Magnitude Estimation

The objective of this study was to evaluate Equation 1 *as is* for Love waves from both earthquakes and explosions; however, we do note that some terms in Equation 1 could change for Love waves. In the next few paragraphs, we discuss possible changes for future application of this technique, including the source excitation and attenuation corrections and the need to incorporate additional periods into the analysis.

Excitation Correction. The "source excitation" correction $-0.66 \log\left(\frac{T_0}{T}\right)$ in Equation 1 is slightly misleading, because the correction is actually for the effects of the source depth and structure at the source rather than for the actual source spectra. A shallow explosion will generate large amplitude, short-period (< 20 s) surface waves (and magnitudes) relative to T_o=20 s, where most historical measurements have been made, and thus must be reduced in order to improve explosion and earthquake discrimination and provide better agreements with historical magnitude scales. This correction accomplishes this need and is determined empirically by modeling Rayleigh waves generated by 1 km deep explosions in a variety of different velocity structures (Bonner *et al*., 2006).

Since Love waves are not generated by isotropic explosions, we determined a corresponding correction for the Love waves using a 1 km deep double-couple earthquake for different velocity structures. A similar expression for the Love wave source excitation is $-0.45 \log\left(\frac{T_0}{T}\right)$ which is similar to the one incorporated into the Russell (2006) equation. For future examination, a more rigorous and model-dependent approach to this correction, such as discussed in Stevens and McLaughlin (2001) and Stevens *et al*. (2007), could lead to improved results.

Attenuation Correction. To investigate the applicability of the attenuation correction in Equation 1 to Love waves, we first subtracted the correction $0.0031\left(\frac{T_0}{T}\right)^{1.8}\Delta$, from our estimated $M_s(VMAX)$ then computed new corrections in the form $\alpha\Delta$ for both Rayleigh and Love waves. The attenuation coefficients calculated as a result are α = 0.0037 for the Rayleigh and α = 0.0042 for the Love waves (see Chapter 5 for this study) , compared to 0.0031 in the original formula. Application of the new attenuation corrections improves the residuals for the events used in the inversion; however it did not improve the RMS residuals for the entire Middle Eastern data set. Future application of this technique could possibly incorporate 2D or 3D attenuation models for Love and Rayleigh waves (Levshin et al., 2006; Stevens et al., 2006, 2007).

Period Limitations. $M_s(VMAX)$ was originally designed for Rayleigh waves in the period range between 8 and 25 s. However for some focal mechanisms, deep events, and along complex paths, the maximum of the surface wave amplitudes may be achieved at longer periods. Limiting the period range to 25 s for the Middle East data (Figure 4) results in numerous measurements that are "pegged" at the upper limit of 25 s. Increasing the upper limit from 25 s to 40 s results in higher magnitude measurements (Figure 7; compare to Figure 4a), which

provides a more reliable estimate of source size and slightly lower standard error for both Rayleigh (e.g., 0.22 m.u. to 0.21 m.u.) and Love waves (0.22 m.u. to 0.20 m.u).

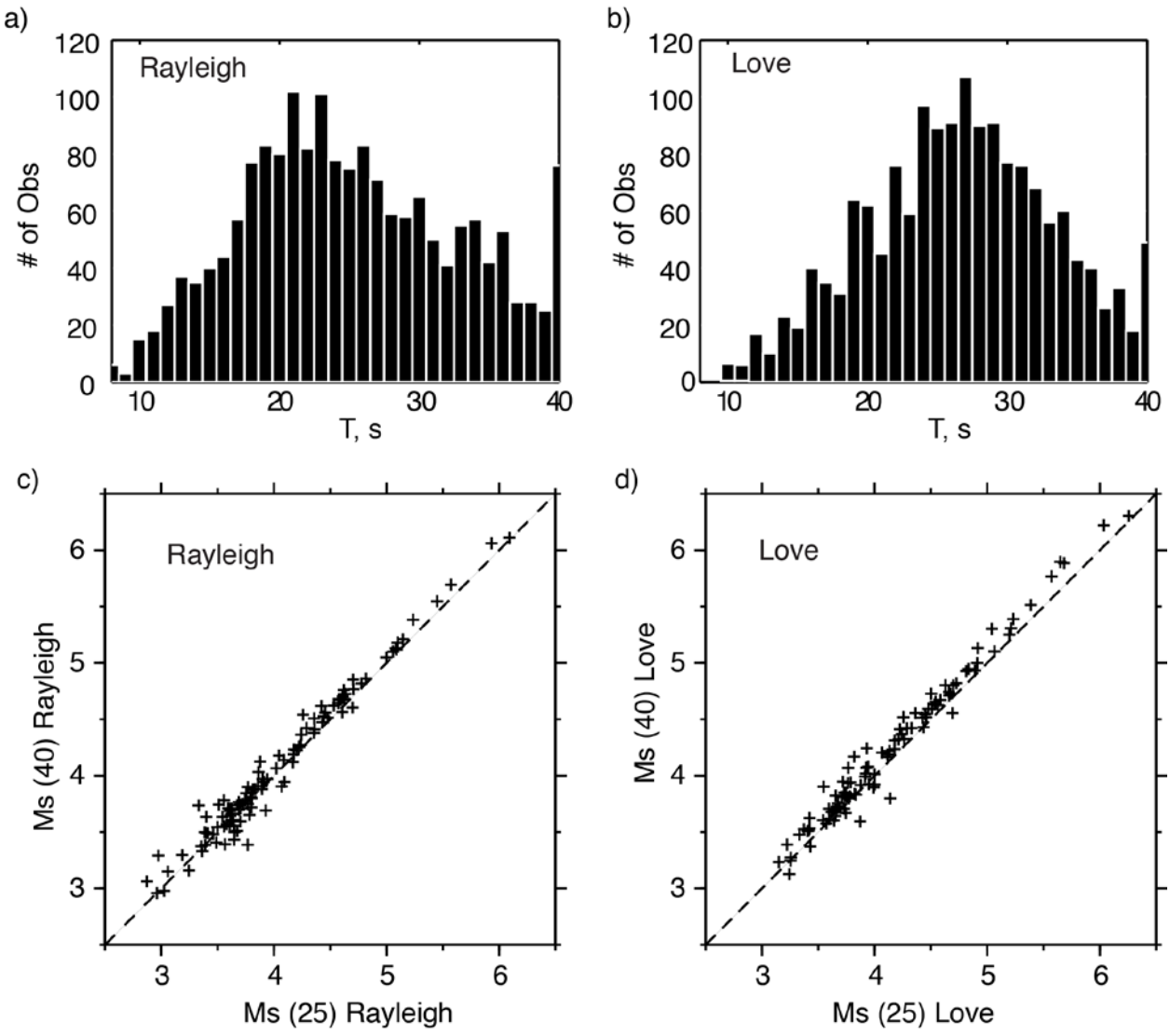

Figure 7. Results of extending to analysis periods for M_s(VMAX) to 40 s for a) Rayleigh and b) Love waves in the Middle East. The estimated c) Rayleigh and d) Love wave magnitudes are often increased by extending the analysis period to 40 s.

CONCLUSIONS

We conclude that estimating a Love wave magnitude, using the same formula and methods employed for Rayleigh waves, can lead to improved earthquake and explosion discrimination due to the fact that the earthquakes typically have a larger M_s-Love, while explosions normally exhibit a smaller M_s-Love when compared to the M_s-Rayleigh. We conclude that an M_s:M_s discriminant is possible; however does not have the same population separation that has been

historically observed for the M_s:m_b discriminant. Results also suggest that incorporation of Love waves into the analysis requires a re-examination of the period limits currently used for the M_s*(VMAX)* technique. While the M_s*(VMAX)*-Rayleigh method is currently operational at different data centers using periods between 8 and 25 s, we do believe that future processing should be extended to 40 s, especially in regions with deep earthquakes and complex paths.

DATA AND RESOURCES

We thank the United States Geological Survey, IRIS, Science Applications International Corporation, and Los Alamos/Lawrence Livermore National Laboratory and Lamont Doherty Earth Observatory for access to their invaluable data archives. Thanks also to the many seismic network operators whose dedication make this effort possible: China Digital Seismic Network, Geoscope, IRIS/USGS/CDSN Seismic Network, Lawrence Livermore southern Nevada network, IRIS/IDA network, IRIS/USGS network, Regional Seismic Test Network, and Seismic Research Observatory network. We especially would like to thank Luca Malagnini (INGV) and the Korean Meteorological Association for access to their data.

ACKNOWLEDGEMENTS

We wish to thank Drs. David Russell, Robert Herrmann, and Harley Benz for their assistance with this collaboration and research. We thank Drs. Jack Murphy, Eli Baker, Paul Richards, and Jeff Stevens for suggestions regarding datasets and future directions. We than Dr. Anton Dainty for his dedicated service to the Bulletin of the Seismological Society as an Associate Editor for nuclear explosion monitoring papers. We thank Mr. Jim Lewkowicz for his continued support and thoughtfulness. This research was funded by the Air Force Research Laboratory under Contract No. FA8718-09-C-0012.

APPENDIX 1A: SURFACE WAVE EXCITATION FROM A SHALLOW SOURCE

If the source is shallow compared to the wavelength, the surface wave excitation functions are given by (e.g. Aki and Richards, 2002; p. 328):

$$u^{LOVE}(x,\omega) = G^{L}[U_2 \sin 2\phi - U_3 \cos 2\phi] \tag{1A1}$$

$$u^{RAYLEIGH}(x,\omega) = G^{R}[U_1 + U_2 \cos 2\phi + U_3 \sin 2\phi]\,, \tag{1A2}$$

where

$$G^{L} = \sum_n \frac{ik_n l_1(h) l_1(z)}{8cUI_1} \sqrt{\frac{2}{\pi k_n r}} \exp\left[i\left(k_n r - \frac{\pi}{4} \right) \right] \times \hat{\phi} \tag{1A3}$$

$$G^{R} = \sum_n \frac{ik_n r_1(h)[r_1(z)\hat{r} + ir_2(z)\hat{z}]}{8cUI_1} \sqrt{\frac{2}{\pi k_n r}} \exp\left[i\left(k_n r - \frac{\pi}{4} \right) \right] \times \hat{\phi} \tag{1A4}$$

The radiation pattern coefficients are given by:

$$U_1 = \tfrac{1}{2}(M_{xx} + M_{yy}) - (1 - 2\beta^2/\alpha^2)M_{zz}\,,$$

$$U_2 = \tfrac{1}{2}(M_{xx} - M_{yy})\,, \text{ and } U_3 = M_{xy}$$

Here are some examples of the radiation pattern for shallow events with different focal mechanism assuming that $\alpha/\beta \approx \sqrt{3}$.

1) Dip-slip focal mechanism (M_{xx}= *1*, M_{yy}=*0*, M_{zz}= *−1*):

$$U_1 = 1\tfrac{1}{2} - 2\beta^2/\alpha^2\,,\ U_2 = \tfrac{1}{2}\,,\ U_3 = 0\,.$$

$$u^{LOVE}(x,\omega) = G^{L} \times [\tfrac{1}{2}\sin 2\phi] \tag{1A5}$$

$$u^{RAYLEIGH}(x,\omega) = G^{R} \times [1\tfrac{1}{2} - 2\beta^2/\alpha^2 + \tfrac{1}{2}\cos 2\phi] \approx G^{R} \times [\tfrac{5}{6} + \tfrac{1}{2}\cos 2\phi] \tag{1A6}$$

We expect Rayleigh wave amplitude to be larger than Love wave amplitudes.

2) Strike-slip focal mechanism (M_{xx}= *1*, M_{yy}= *−1* M_{zz}= *0*):

$$U_1 = 0\,,\; U_2 = 1\,,\; U_3 = 0\,.$$

$$u^{LOVE}(x,\omega) = G^L \times [\sin 2\phi] \tag{1A7}$$

$$u^{RAYLEIGH}(x,\omega) = G^R \times [\cos 2\phi] \tag{1A8}$$

The relationship between Rayleigh and Love wave amplitudes depend on the size of the eigenfunctions. Love wave amplitude is twice as large as the one from the dip-slip for a given moment.

3) Explosion (M_{xx}= *1*, M_{yy}= *1* M_{zz}= *1*):

$$U_1 = 2\beta^2/\alpha^2\,,\; U_2 = 0\,,\; U_3 = 0\,.$$

$$u^{LOVE}(x,\omega) = 0 \tag{1A9}$$

$$u^{RAYLEIGH}(x,\omega) = G^R \times [2\beta^2/\alpha^2] \approx G^R \times \tfrac{2}{3} \tag{1A10}$$

The Love wave is absent in this case as expected.

CHAPTER 2: DEVELOPMENT OF A COMBINED RAYLEIGH- + LOVE-WAVE MAGNITUDE DISCRIMINANT

Jonathan K. MacCarthy and Dale N. Anderson

Los Alamos National Laboratory

INTRODUCTION

We develop a calibrated mathematical formulation for an explosion discriminant that combines Rayleigh- and Love-wave magnitude values, and employs an error model that correctly accounts for estimated variances among events and among stations separately. The test statistic is applied to the announced April 2009 DPRK nuclear test, resulting in a p-value of 0.026 and decision of "reject the null hypothesis: explosion characteristics" at 95% confidence. Results are compared to an analogous treatment using Rayleigh-only data and calibrations, demonstrating comparable to improved discrimination performance in the combined Rayleigh + Love case.

It was observed by Bonner *et al.* (2011) that, for a given m_b, earthquake populations typically have larger M_s-Love magnitudes than M_s-Rayleigh magnitudes compared to nuclear explosion populations, and the converse is also typically true for explosion populations. Here, we formally test the discrimination potential of combined Rayleigh- and Love-wave magnitudes. We develop a mathematical formulation for an explosion discriminant that combines M_s(VMAX)-Rayleigh and M_s(VMAX)-Love values. Following Anderson *et al.* (in review), the formulation also accounts for estimated variances among events and among stations separately. In the following section, we describe the mathematical development of the error model and discriminant, the calibration of the statistical parameters of the error model, and the application of the discriminant via cross-validation analysis.

STATISTICAL DEVELOPMENT

Error Model for a Single Wave-Type

The single-station M_s (Rayleigh or Love) discriminant for a given body-wave magnitude ($M_s|mb$) is defined as the random variable, Y:

$$Y = M_s - \beta \times mb = \mu + Model\ Error + Station\ Noise\ , \tag{5}$$

where β is a scalar constant and *mb* is assumed fixed with no error. The right side of Equation 5 is a components-of-variance model, where μ is the population mean. *Model Error* is event-specific and arises from random source and propagation model inadequacy and is normally distributed with zero mean and variance τ^2. *Station Noise* is also normally distributed with zero mean and variance σ^2, and arises from random measurement noise and near-station effects (Anderson *et al.,* in review). The corresponding linear model representation of Equation 5 is:

$$Y_{ijk} = M_{sijk} - \beta \times mb_j = \mu_i + E_j + \varepsilon_{ijk} \qquad (6)$$
$$i = 0, A \quad j = 1,2,\ldots,m_i \quad k = 1,2,\ldots,n_{ij}$$

where Y_{ijk} is the M_s magnitude residual (Rayleigh or Love) for the explosion population (i = 0) or earthquake population (i = A) for event j at station k.

Standard Error for Two Wave-Types

We extend the above single-magnitude conceptual error model to include both Y_{ijk}-Rayleigh and Y_{ijk}-Love. In the following development, parameters in Equation 6 that are distinct for each magnitude type are subscripted "R" or "L" for Rayleigh or Love. Additionally, we assume a common population index (e.g. i = 0) and drop it for the remainder of the formulation. For a single event j = 1, $k = n_R$ stations producing Rayleigh magnitudes, and $k = n_L$ stations producing Love magnitudes, Equation 2-2 can be written in matrix form:

$$\boldsymbol{Y_{1\bullet}} = \boldsymbol{\mu} + \boldsymbol{W_{1\bullet}}\boldsymbol{V_{1\bullet}} \ , \qquad (7)$$

where $\boldsymbol{Y_{1\bullet}}$ is a vector of $n_R + n_L$ station Rayleigh and Love magnitude residuals, $\boldsymbol{\mu}$ is a vector of corresponding μ_R and μ_L means, and $\mathbf{W_{1\bullet}}$ is a linear design matrix that maps the individual Rayleigh and Love event errors (E_{1R}, E_{1L}) and station errors ($\varepsilon_{1\bullet R}$, $\varepsilon_{1\bullet L}$) in error component vector $\mathbf{V_{1\bullet}}$ into $(n_R + n_L) \times 1$ data vector, $\boldsymbol{Y_{1\bullet}}$:

$$\boldsymbol{V_{1\bullet}} = \begin{pmatrix} E_{1R} \\ \varepsilon_{11R} \\ \vdots \\ \varepsilon_{1n_RR} \\ E_{1L} \\ \varepsilon_{11L} \\ \vdots \\ \varepsilon_{1n_LL} \end{pmatrix} \qquad (8)$$

The error component vector $\mathbf{V_{1\bullet}}$ is normal with zero mean vector $\mathbf{0}$ and covariance matrix $\mathbf{\Sigma_{1\bullet}}$:

$$\mathbf{\Sigma_{1\bullet}} = \begin{pmatrix} \tau_R^2 & 0 & \cdots & 0 & \rho\tau_R\tau_L & 0 & \cdots & 0 \\ 0 & \sigma_R^2 & \ddots & \vdots & 0 & 0 & \ddots & \vdots \\ \vdots & \ddots & \ddots & 0 & \vdots & \ddots & \ddots & 0 \\ 0 & \cdots & 0 & \sigma_R^2 & 0 & \cdots & 0 & 0 \\ \rho\tau_R\tau_L & 0 & \cdots & 0 & \tau_L^2 & 0 & \cdots & 0 \\ 0 & 0 & \ddots & \vdots & 0 & \sigma_L^2 & \ddots & \vdots \\ \vdots & \ddots & \ddots & 0 & \vdots & \ddots & \ddots & 0 \\ 0 & \cdots & 0 & 0 & 0 & \cdots & 0 & \sigma_L^2 \end{pmatrix}, \qquad (9)$$

where ρ represents a correlation between Rayleigh and Love event errors. $\mathbf{Y_{1\bullet}}$ is a linear combination of elements of $\mathbf{V_{1\bullet}}$ via $\mathbf{W_{1\bullet}}$, and is thus also normal with mean $\boldsymbol{\mu}$ with $(n_R + n_L) \times (n_R + n_L)$ covariance matrix, $\boldsymbol{\Omega_{1\bullet}}$:

$$\boldsymbol{\Omega}_{\mathbf{1}\bullet} = \mathbf{W}_{\mathbf{1}\bullet}\boldsymbol{\Sigma}_{\mathbf{1}\bullet}\mathbf{W}_{\mathbf{1}\bullet}^{\top} = \begin{pmatrix} \tau_R^2+\sigma_R^2 & \tau_R^2 & \cdots & \tau_R^2 & 2\rho\tau_R\tau_L & \cdots & \cdots & 2\rho\tau_R\tau_L \\ \tau_R^2 & \ddots & \ddots & \vdots & \vdots & \ddots & \ddots & \vdots \\ \vdots & \ddots & \ddots & \tau_R^2 & \vdots & \ddots & \ddots & \vdots \\ \tau_R^2 & \cdots & \tau_R^2 & \tau_R^2+\sigma_R^2 & 2\rho\tau_R\tau_L & \cdots & \cdots & 2\rho\tau_R\tau_L \\ 2\rho\tau_R\tau_L & \cdots & \cdots & 2\rho\tau_R\tau_L & \tau_L^2+\sigma_L^2 & \tau_L^2 & \cdots & \tau_L^2 \\ \vdots & \ddots & \ddots & \vdots & \tau_L^2 & \ddots & \ddots & \vdots \\ \vdots & \ddots & \ddots & \vdots & \vdots & \ddots & \ddots & \tau_L^2 \\ 2\rho\tau_R\tau_L & \cdots & \cdots & 2\rho\tau_R\tau_L & \tau_L^2 & \cdots & \tau_L^2 & \tau_L^2+\sigma_L^2 \end{pmatrix}. \quad (10)$$

Network-Averaged Rayleigh and Love Magnitudes

The above framework for individual station Rayleigh and Love magnitudes is easily extended to network-averaged event magnitudes, $\overline{\mathrm{M}}_{sR}$ and $\overline{\mathrm{M}}_{sL}$, for n_E events. We define a new magnitude residual vector, $\overline{\boldsymbol{Y}}_{\bullet\bullet}$:

$$\overline{\mathbf{Y}}_{\bullet\bullet} = \begin{pmatrix} \overline{M}_{s_R 1} + \overline{M}_{s_L 1} \\ \vdots \\ \overline{M}_{s_L n_E} + \overline{M}_{s_L n_E} \end{pmatrix} - \mathbf{2}\beta \begin{pmatrix} mb_1 \\ \vdots \\ mb_{n_E} \end{pmatrix} = (\mu_{\mathbf{R}} + \mu_{\mathbf{L}}) + \overline{\mathbf{W}}_{\bullet\bullet}\mathbf{Y}_{\bullet\bullet}, \quad (11)$$

where $\boldsymbol{Y}_{\bullet\bullet}$ is a vector comprised of all $\mathbf{Y_{j\bullet}}$, and $\overline{\mathbf{W}}_{\bullet\bullet}$ is a $n_E \times n_E$ $(n_R + n_L)$ averaging operator that maps elements of $\mathbf{Y}_{\bullet\bullet}$ onto $\overline{\boldsymbol{Y}}_{\bullet\bullet}$. Again, $\overline{\boldsymbol{Y}}_{\bullet\bullet}$ is a linear combination of elements of $\mathbf{Y}_{\bullet\bullet}$ and is thus also normal, with mean $\boldsymbol{\mu_R} + \boldsymbol{\mu_L}$ and covariance matrix $\overline{\boldsymbol{\Omega}}_{\bullet\bullet}$:

$$\begin{aligned} \overline{\boldsymbol{\Omega}}_{\bullet\bullet} &= \overline{\mathbf{W}}_{\bullet\bullet}\boldsymbol{\Omega}_{\bullet\bullet}\overline{\mathbf{W}}_{\bullet\bullet}^{\top} \\ &= \begin{pmatrix} \tau_R^2 + \sigma_R^2/n_R + \tau_L^2 + \sigma_L^2/n_R + 2\rho\tau_R\tau_S & 0 & \cdots & 0 \\ 0 & \ddots & \ddots & \vdots \\ \vdots & \ddots & \ddots & 0 \\ 0 & \cdots & 0 & \tau_R^2 + \sigma_R^2/n_R + \tau_L^2 + \sigma_L^2/n_R + 2\rho\tau_R\tau_S \end{pmatrix}, \end{aligned} \quad (12)$$

where $\boldsymbol{\Omega}_{\bullet\bullet}$ is a block-diagonal matrix comprised of all $\boldsymbol{\Omega_{j\bullet}}$. The variance of an individual network-averaged combined $\mathrm{M_s}$, $\overline{\boldsymbol{Y}}_{j\bullet}$, is therefore $\tau^2_{\mathrm{R}} + \sigma^2_{\mathrm{R}}/n_{\mathrm{R}} + \tau^2_{\mathrm{L}} + \sigma^2_{\mathrm{L}}/n_{\mathrm{L}} + 2\rho\tau_{\mathrm{R}}\tau_{\mathrm{L}}$.

Using the formulation for variance in Equation 12, we can propose the following test statistic for a network-averaged event $\overline{\mathrm{M}}_{sR} + \overline{\mathrm{M}}_{sL}$, under the null hypothesis $\mathrm{H_0}$: explosion characteristics,

$$Z_0 = \frac{(\bar{M}^*_{sR} + \bar{M}^*_{sL}) - 2\beta \times mb^* - (\mu_R + \mu_L)}{\sqrt{\tau_R^2 + \frac{\sigma_R^2}{n_R^*} + \tau_L^2 + \frac{\sigma_L^2}{n_L^*} + 2\rho\tau_R\tau_L}} \quad , \tag{13}$$

where the asterisk (*) denotes values for the test event. The values for τ_R, σ_R, τ_L, σ_L, μ_R, and μ_L are estimated through calibration from an explosion population, described in the following section.

STATISTICAL CALIBRATION AND APPLICATION OF TEST STATISTIC

Calibration

In order to apply the test statistic in Equation 13, we assume that the statistical parameters τ_R, σ_R, τ_L, σ_L, μ_R, and μ_L are globally consistent and known for the target population. We estimate these parameters for the null hypothesis population (i = 0) through bootstrap analysis of an explosion dataset consisting of individual station M_s(VMAX)-Rayleigh, M_s(VMAX)-Love, and event *mb* values from 26 nuclear explosions from Kazakhstan, India, Pakistan, Lop Nor, and Nevada Test Site (Figure 8). A total of 235 Rayleigh + Love explosion event/station records were used in the calibration. The alternate hypothesis population (earthquakes, i = A) is represented by 124 events from the Middle East and the Korean peninsula, with a total of 1457 event/station records. M_s(VMAX) values are measured at a maximum period of 20 seconds, and *mb* values are from the International Seismological Centre (ISC) and United States Geological Survey (USGS) bulletins. All events have *mb* between 3.6 and 6.1, and occurred between 1996 and 2009.

Under the null hypothesis, we estimate the event error terms, τ, station error terms, σ, and population means, μ, for each corrected magnitude type through bootstrap analysis. In the analysis, we use β = 1 (Selby *et. al.*, 2012), and event error correlation between $E_{j\bullet R}$ and $E_{j\bullet L}$ terms is assumed to be zero (Equation 13), as its form is not readily available. We take 5000 random bootstrap populations, with replacement, from the 1692 available records, each 1692 records in size. From each bootstrap population, we estimate and record τ_R, σ_R, τ_L, σ_L, μ_R, and μ_L. The final calibrated values used to construct the test statistic in Equation (13) come from these ensemble data. Error parameters τ_R, σ_R, τ_L, and σ_L in Equation (13) are the 95th quantile values, and μ_R, and μ_L are the grand mean values. We summarize the final values in Table 6 below.

Table 6. Bootstrapped statistical parameters for null hypothesis, explosion calibration data.

Parameter	Value
τ_R	0.13
τ_L	0.16
σ_R	0.06
σ_L	0.07
μ_R	-1.74
μ_L	-1.86

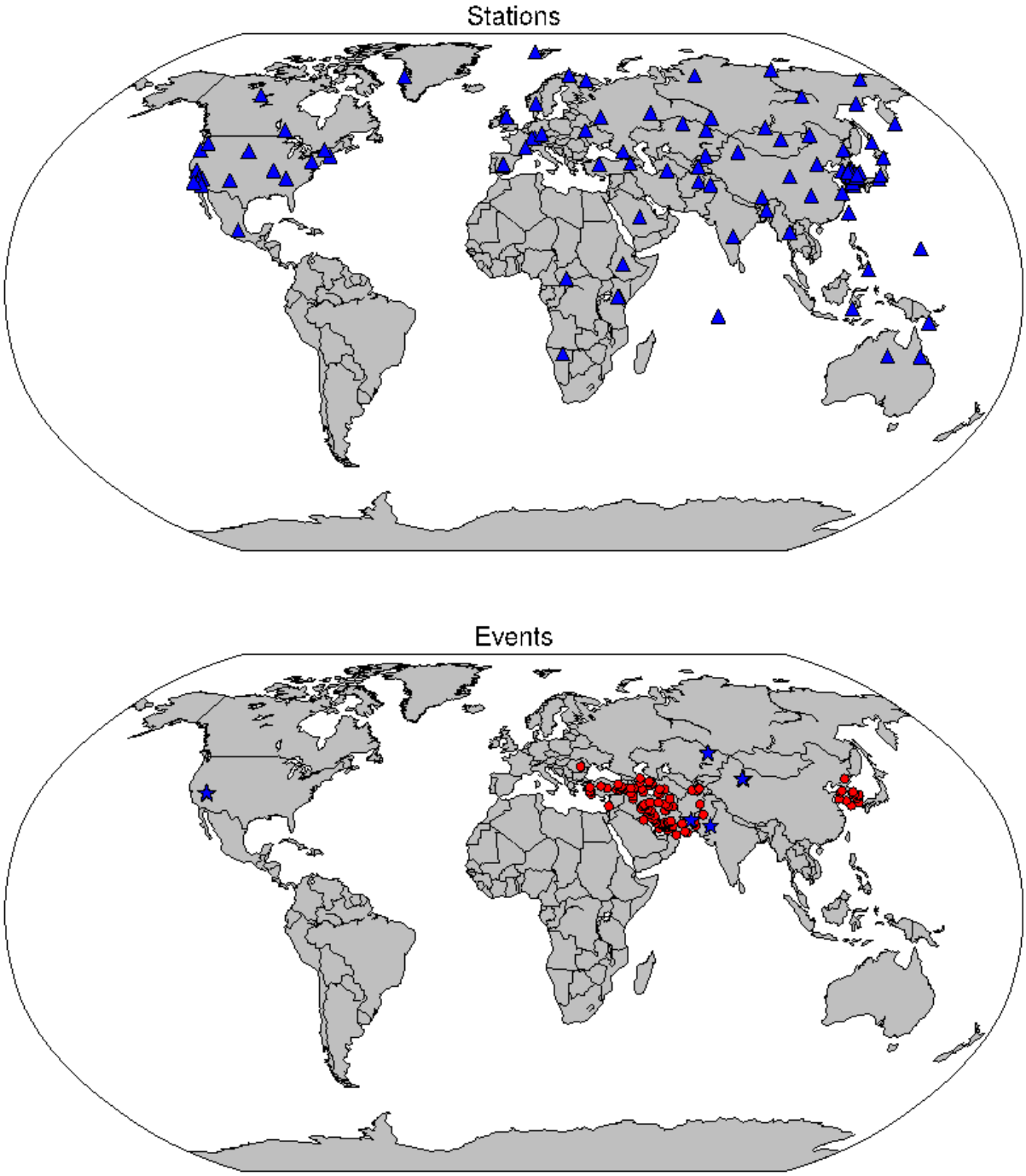

Figure 8. Stations (upper) and events (lower) used in the calibration dataset. Stars are explosion events, and red circles are earthquakes.

Application to the 2009 DPRK Announced Nuclear Test

Using the calibrated bootstrapped values from Table 6, we perform a leave-one-out analysis with Rayleigh- and Love-wave magnitudes from the announced April 2009 Democratic People's Republic of Korea (DPRK) nuclear test: $mb = 4.69$, $\overline{M}_{sR} = 3.70$, $\overline{M}_{sL} = 3.17$, with $n = 10$ stations. We calculate z-scores (Equation 13) and p-values for the excluded DPRK09 event, as well as apparent z-scores and p-values for all network-averaged calibration data (Figure 9).

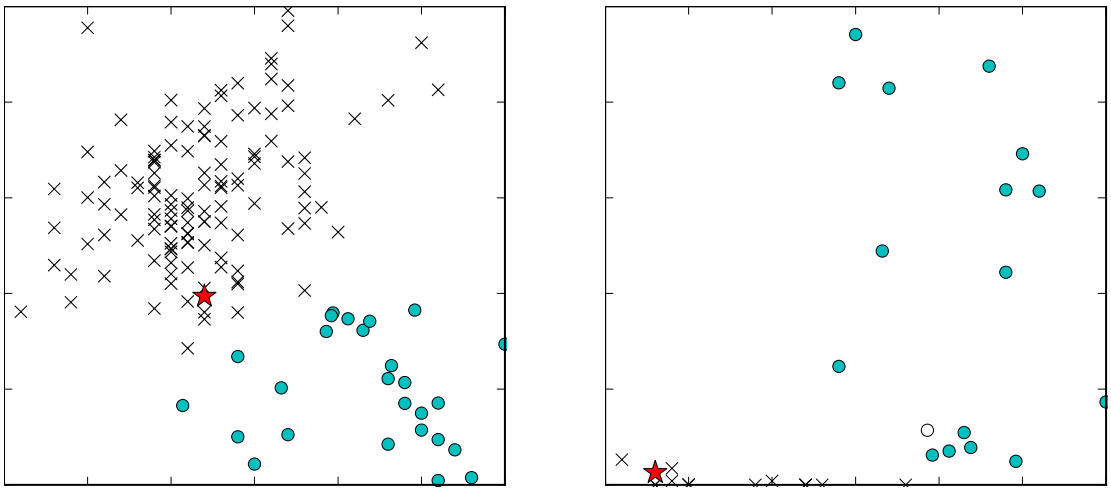

Figure 9. Apparent discriminant performance for earthquake (crosses) and explosion (circles) populations. The star represents the excluded 2009 DPRK announced nuclear event. Left: Apparent Z-score under H_0. Right: Corresponding apparent p-value. 95% confidence level is noted with a red line.

For the combined Rayleigh + Love discriminant, we find that H_0: explosion characteristics is rejected for the DPRK09 event at a confidence level of 95%. The p-value for the excluded event is 0.026. Also at 95% confidence, apparent performance demonstrates that 120 of 124 earthquakes correctly rejected H_0, and 25 of 26 explosions correctly failed to reject H_0.

While the 2009 DPRK incorrectly rejects H_0 in the above analysis, we note that *it is a nominal improvement* over the corresponding p-value using only Rayleigh calibration data. We perform similar performance analysis using only a single (Rayleigh) wave type, and recalibrated bootstrapped event and station error parameters. The corresponding p-value for the excluded DPRK09 event is 0.023, compared to 0.026 for the combined discriminant. The null hypothesis is incorrectly rejected in both analyses, but the combined discriminant does not degrade performance, and in fact nominally improves discrimination.

CONCLUSIONS AND RECOMMENDATIONS

We develop a mathematical formulation for an explosion discriminant that combines Rayleigh- and Love-wave magnitudes values, which employs an error model that correctly accounts for estimated variances among events and among stations separately. We apply the test statistic for the announced April 2009 DPRK nuclear test, resulting in a decision of "reject H_0: explosion characteristics" at 95% confidence, with a p-value of 0.026. We note, however, a nominal improvement over the Rayleigh-only case, with a p-value of 0.023, demonstrating comparable to improved discrimination performance.

The low p-value in both cases demonstrates the importance of the calibration data used to estimate the parameters of test statistic. Similar analysis using only Rayleigh-wave magnitudes from the International Seismological Center and AWE Blacknest Seismological Center yield a p-value of 0.15 (Anderson *et al.* in review), and a decision of "fail to reject H_0," which comes largely from differences in the values of calibrated statistical parameters in the test statistic. We feel that the combined Rayleigh + Love discriminant shows strong promise, and also highlights the need for a high-quality and consistent calibration data set.

CHAPTER 3: A SYNTHETIC STUDY OF SURFACE WAVE MAGNITUDES

Jessie Bonner[1], Robert Herrmann[2], and David Russell[1]

Weston Geophysical Corporation[1] and St. Louis University[2]

INTRODUCTION

We have investigated the $M_s(VMAX)$ surface wave estimation procedure (Russell, 2006; Bonner et al., 2006) using synthetic simulations. The main objective of these simulations is to determine the possible sources of bias between $M_s(VMAX)$ and historic narrow band methods for estimating M_s at periods (T) near 20 s. The simulations also allow quantification of the effects of radiation pattern and focal mechanisms, explosion emplacement media, and various attenuation models on the surface wave magnitudes. We have studied synthetics generated using the global AK135 model as well as regional velocity and attenuation models for the central United States (CUS), Italy, Korea, and the western United States (WUS). The synthetics were calculated at distances ranging from 500-6000 km. The attenuation correction used in $M_s(VMAX)$ is based on the low CUS attenuation and thus matches closely with the attenuation model used in the CUS model. Explosion synthetics generated using the CUS model show little, if any, variation in $M_s(VMAX)$ estimates with distance. Because the attenuation in the WUS is higher, the $M_s(VMAX)$ estimates show a distance trend, with 0.1 magnitude unit (m.u.) larger magnitudes estimated at regional distances than at teleseismic distances. $M_s(VMAX)$ shows no significant distance trends for synthetic earthquakes and explosions using the Korean model, whereas the largest distance trends in $M_s(VMAX)$ estimates are observed for the global AK135 and regional Italian models. For earthquakes, the synthetics allow us to determine the source of the scatter in the surface wave magnitude estimates. Improper attenuation models may account for as little as 0.1 m.u. scatter at 500-6000 km distances; however, radiation pattern effects can produce significantly larger variance in the estimates (e.g., > 0.2 m.u). We typically observe that $M_s(VMAX)$ is 0.1-0.2 m.u. larger than historic M_s measurement near T=20 s, which we attribute to two different effects. First, the historic M_s narrow band measurements are based on band pass filtered data that does not incorporate a filter correction for the amplitude reduction associated with the narrow-band filters. Second, surface wave amplitudes from some earthquake focal mechanisms can be significantly reduced near T=20 s, while $M_s(VMAX)$ is designed to seek larger amplitudes on either side of a spectral hole. For example, a 10 km deep strike slip has a significant spectral hole near T=16 s that reduces historic M_s measurements by 0.7 m.u. when compared to $M_s(VMAX)$.

OBJECTIVES

The objective of this research is to quantify the performance of $M_s(VMAX)$ (Russell, 2006; Bonner et al., 2006) using synthetic seismograms. Recent questions have been posed regarding a possible offset or bias between $M_s(VMAX)$ estimates, which are made between 8-25 s period (T), and historic narrow band M_s measurements, typically made near T=20 s, and whether inadequate attenuation correction could lead to significant magnitude errors. To answer these questions, we have completed a synthetic study that quantifies $M_s(VMAX)$ estimates for a

variety of different velocity and attenuation models at regional to teleseismic distances. The results are compared to the historical M_s estimates in the 17-23 s period band.

RESEARCH ACCOMPLISHED

Formulas

We provide a brief overview of the two magnitude formulas tested in this paper. First, Russell (2006) developed a magnitude formula that could effectively measure surface-wave magnitudes at local, regional and teleseismic distances, at variable periods, T, between 8 and 25 s. The magnitude equation is:

$$M_{s(b)} = \log(a_b) + \frac{1}{2}\log(\sin(\Delta)) + 0.0031\left(\frac{20}{T}\right)^{1.8}\Delta - 0.66\log\left(\frac{20}{T}\right) - \log(f_c) - C, \quad (14)$$

where a_b is the amplitude of the Butterworth-filtered surface waves (zero-to-peak in nanometers), Δ is the distance in degrees, and f_c is the filter frequency of 3rd order, zero phase Butterworth filters with corner frequencies of $1/T$-f_c, $1/T$+f_c, respectively, and C=0.43. Because the equation finds the maximum amplitude at variable periods, it is often referred to as $M_s(VMAX)$.

For $8 \leq T \leq 25$, the equation is corrected to T=20 s, accounting for frequency-dependent source effects, attenuation, and dispersion. The second term of Equation 14, 0.5 log(sin(Δ)), is a correction for the geometrical spreading; the third term, $0.0031(20/T)^{1.8}\Delta$, is a period-dependent attenuation correction; and the fourth term, 0.66log(20/T), is a period-dependent excitation correction. The constant, C, is determined to be 0.43 to scale the equation at T=20 s to von Seggern's formula (1977), which is scaled to Vaněk et al. (1962) at Δ=50 degrees.

For the "historic" magnitude formula, we used:

$$M_s = 1\log10(A/T) + \log10(\Delta) + 1.12 \quad (15)$$

where A is the peak-to-trough trace amplitude in nanometers and Δ is the epicentral distance in degrees. This equation represents the Prague formula (Vaněk et al., 1962) scaled to Δ=50 degrees (Yacoub, 1988). In order to measure the amplitudes at each period of interest and simplify time domain processing of data, we construct a 2nd-order Butterworth bandpass filter that emulates the Gaussian filters originally designed by Yacoub (1983) for pseudo-spectral magnitude estimation (Figure 10). Following Herrmann (1973), Yacoub (1983) utilized a narrow band Gaussian filter of the form

$$H = exp\left[-16\pi\left(\frac{\omega-\omega_0}{\omega_0}\right)^2\right] \quad . \quad (16)$$

A zero phase Butterworth filter can be designed with the same maximum time domain amplitude as the Gaussian, using the method outlined in Russell (2006). For the Gaussian and Butterworth filter, the maximum time domain amplitudes are respectively, $A/(2T)$, $A \cdot 2\pi b_n f_c$, where A is the frequency domain amplitude at period T, b_n is the

Butterworth gain for an n^{th} order filter (Russell, 2006), and f_c is the one-sided bandwidth of the Butterworth filter. Equating the maximum time domain amplitudes and solving for f_c gives

$$f_c = \frac{1}{4\pi b_n T}. \quad (17)$$

For a Butterworth filter of order *n*, using f_c as defined above will give an equivalent maximum time domain amplitude as the Gaussian filter defined by Yacoub (1983).

The filters are combed through the data at periods between T=17-23 s allowing 7 magnitudes to be estimated using Equation 15. The maximum magnitude is selected as the final magnitude for comparison with $M_s(VMAX)$ after we add 0.3 m.u. to the constant in Equation 15 to effectively render it a zero-to-peak measurement. We refer to this method as the historic magnitude or M_s estimate in this paper.

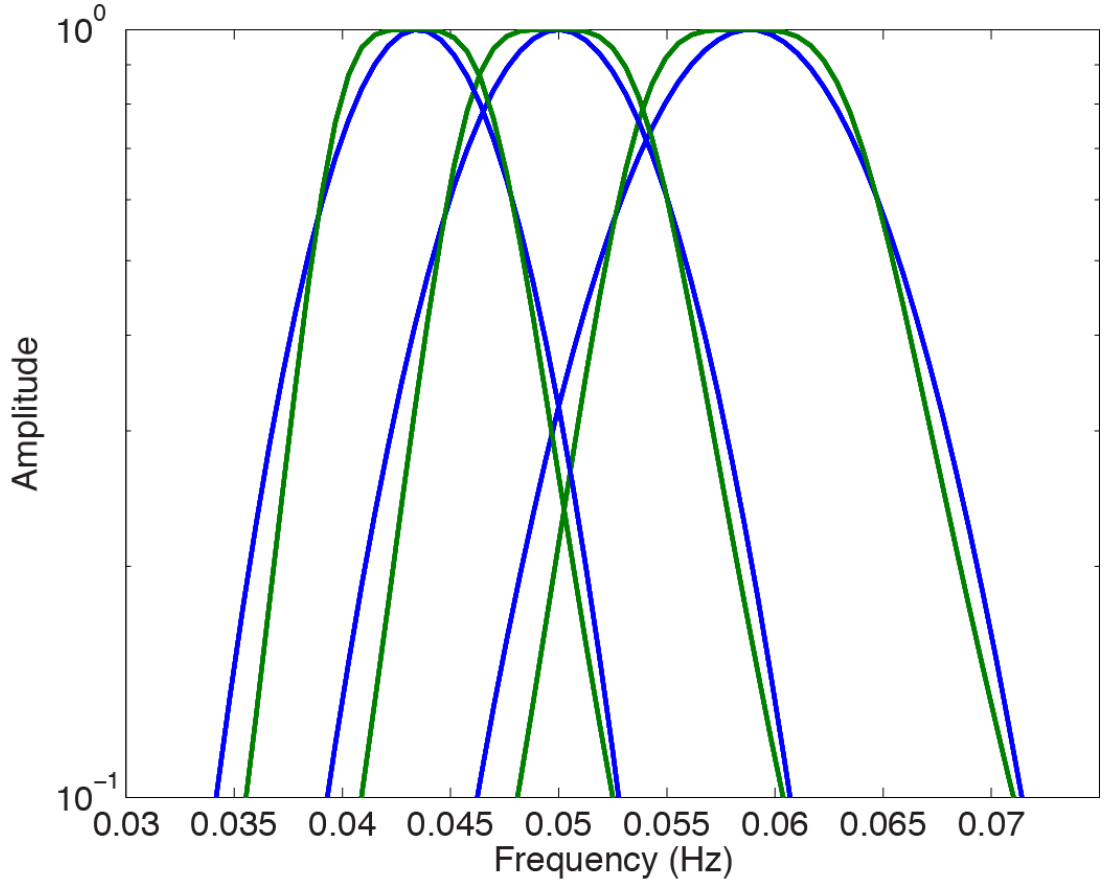

Figure 10. Comparison of the Gaussian filters (blue) suggested by Yacoub (1983) at T=17s, 20s, and 23 s used for filtering surface waves for magnitude estimation and an emulated 2nd order Butterworth version used in our study. Both the Gaussian and Butterworth filters have the same maximum time domain amplitudes.

Models

We chose five different velocity and attenuation models for the comparison of the magnitude formulae using synthetics. The models include the global average AK135 model (Kennett et al., 1995; tak135sph.mod), central and western United States crustal models (Herrmann and Mitchell, 1975; Herrmann et al., 2011b; CUS.mod, WUS.mod), a Korean Peninsula model (Cho et al., 2007; t6.invSNU.CUVEL.mod), and a model for the central Italian Apennines (Herrmann et al., 2011a; nnCIA.mod). Examples of the layered shear wave velocity are shown in Figure 11a.

The other aspect of the study is to propagate the motions from the source regions to large distances. The CUS and WUS model Q values are based on work at St. Louis University by Mitchell and Herrmann, and perform quite well in defining the fundamental surface wave propagation observed from current permanent and temporary broadband stations in North America. The AK135 model has Q_{kappa} and Q_{mu} values which were converted to Q_P and Q_s. The Q values for the Korea and Central Italy models have not been thoroughly tested because of the short distance of observations. The period-dependent attenuation coefficients for each model are shown in Figure 11b. We note that the way the scripts are set up to run these programs, any velocity and Q map could easily be tested in a similar manner.

The $M_s(VMAX)$ formula uses an attenuation correction of the form:

$$B_{att} \left(\frac{To}{T}\right)^p \Delta, \tag{18}$$

where p describes the power law decay for the attenuation coefficient with frequency, and B_{att} is a magnitude correction defined by:

$$B_{att}(T) = \log(e)\, \kappa\, \gamma_0 \tag{19}$$

where κ is a degree to km conversion (111.2 km/deg) and γ_0 represents the attenuation coefficient in km^{-1} at the reference period (T_o) = 20 s. We note that for the Russell (2006) $M_s(VMAX)$ formula, the B_{att} and p were based on central United States attenuation values (e.g., Q_{20}=800; Herrmann and Mitchell, 1975) and determined to be 0.0031 and 1.8, respectively for T=8-25 s surface waves. This results in a similarity between the Russell (2006) and CUS attenuation coefficients shown in Figure 11.

We selected these models as a representative set of crustal structures, some of which are relevant to areas of monitoring interest. The CUS model is applicable to stable cratons, the WUS model to regions with lower velocities in the upper 6 km, and the Central Apennines model for central Italy which has even lower upper crustal velocities. The Korean Peninsula model was selected due to monitoring interest, while the AK135 continental model is a standard reference model for travel times.

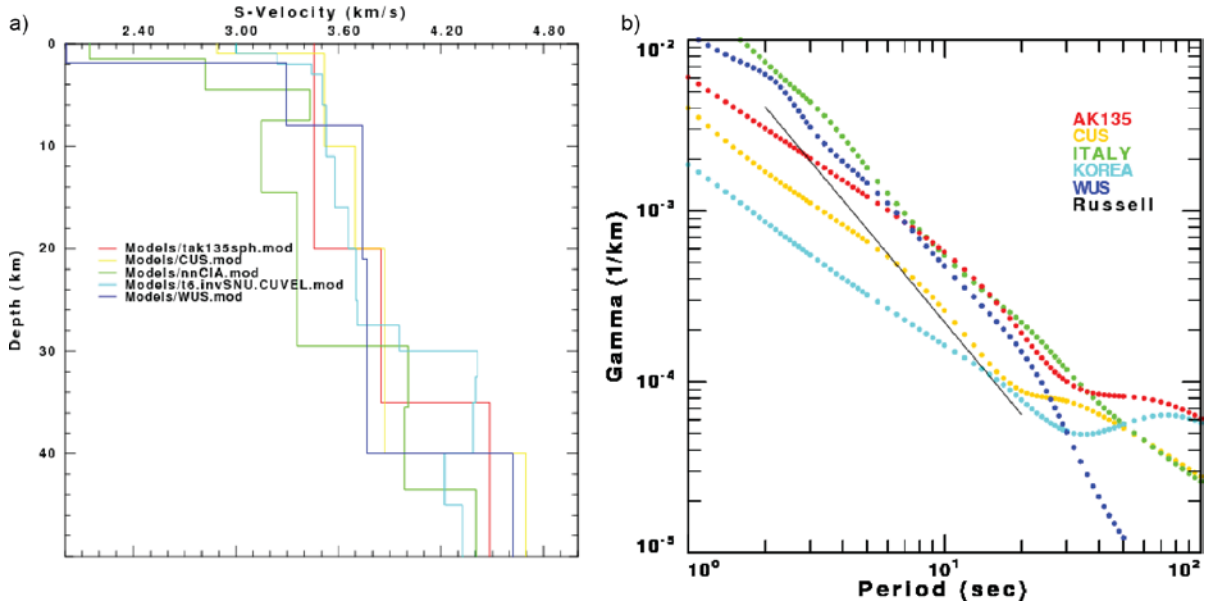

Figure 11. Velocity and attenuation models used in the synthetic study. a) Shear wave velocity profiles for five different models including AK135 (tak135sph.mod), central United States (CUS.mod), central Italian Apennines (nnCIA.mod), the Korean Peninsula (t6.invSNU.CUVEL.mod), and the western United States (WUS.mod). The period-dependent attenuation coefficients for each model as well as the period-dependent attenuation correction term for the Russell (2006) M_s(VMAX) formula are also shown.

Explosion Synthetics

For the first comparison of the two magnitude formulas, we synthesized a shallow explosion (M_w=5.0) in each velocity/attenuation model. We used modal summation (Herrmann, 2004) to generate the vertical-component synthetics at stations placed every 500 km starting at 500 km and ending at 6000 km. The synthetics at each station were then analyzed and an M_s*(VMAX)* and M_s estimated. Plots were produced for each model that have four subplots. The first panel represents the M_s*(VMAX)* selected for each distance based on the period of maximum amplitude (red dot) and the M_s*(VMAX)* computed for each period (red curves). The second panel is the M_s*(VMAX)* as a function of distance (red dots) and historic M_s vs. distance (blue dots). The third panel shows a set of plots to test the assumption that the M_s*(VMAX)* processing effectively results in pseudo-spectral amplitudes (black dots) based on time-domain measurements, and that these amplitudes are equivalent to actual spectral amplitudes (red line). The final panel shows the historic M_s period as a function of distance and will be a number between 17 and 23 s.

Figure 12 shows the magnitude results for the CUS model, which as mentioned previously, has a similar attenuation structure to what was incorporated into the Russell (2006) M_s*(VMAX)*. Figure 12a shows that the M_s*(VMAX)* spectra are essentially flat between 8-25 s and overlay each other. One of the objectives of the M_s*(VMAX)* formula development was to apply excitation corrections that attempted to flatten the spectra for an explosion. These results suggest that the excitation and attenuation corrections for M_s*(VMAX)* are well suited for earth

structures similar to the stable cratonic features of the central United States. As shown in Figure 12c, the explosion spectra at short distances have increased short period amplitudes that will bias the magnitude estimate high if not corrected for using an excitation correction, which would degrade M_s:m_b performance.

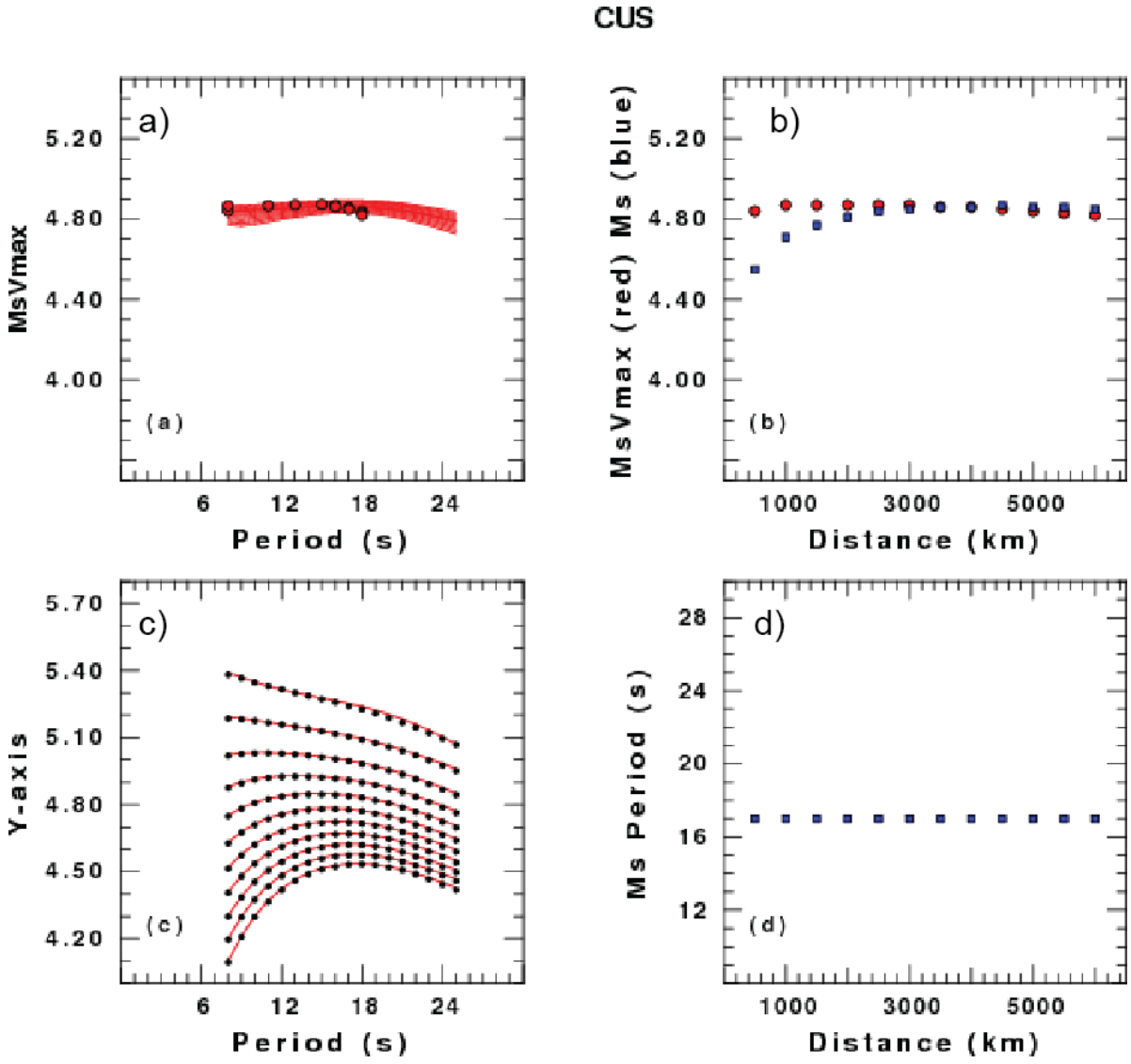

Figure 12. M_s and M_s(VMAX) processing results for the CUS model. a) M_s(VMAX) selected for each distance based on the period of maximum amplitude (black dot) and the M_s(VMAX) computed for each period (red curves). b) M_s(VMAX) as a function of distance (red dots) and historic M_s vs. distance (blue dots). c) M_s(VMAX) pseudo-spectral amplitudes (black dots) derived from the peak amplitude in the filtered time series compared to actual spectral amplitudes (red line). d) historic M_s period as a function of distance.

The $M_s(VMAX)$ is distance independent as shown in Figure 12b for the CUS model; however, we note that the M_s has smaller magnitudes than $M_s(VMAX)$ at regional distances. There are two reasons for these differences. First, the filter combs emulated from Yacoub (1983) are too narrow and introduce error into the estimation of magnitudes, whereas $M_s(VMAX)$ has a $-\log(f_c)$ correction to correct for this problem. We derived a correction to M_s (see Appendix 3A) and restricted the analysis of both magnitudes to T=20 s, and thus were able to show that this corrects for the narrow band error, resulting in very close magnitudes for both formulas. The second reason for differences in the two magnitude estimates is related to the actual Rayleigh-wave excitation spectra between T=8-25 s. At shorter distances, $M_s(VMAX)$ migrates to shorter periods for the final estimate (see Figure 12a), whereas the M_s is restricted to 17-23 s, is actually pegged at T=17 s, and would prefer to migrate to lower periods with larger amplitudes. One of the primary objectives of the $M_s(VMAX)$ development was to use these shorter periods at regional distances, which lowers the detection capabilities to smaller magnitudes (Bonner et al., 2006). At teleseismic distances, both formulas are using T~17 s amplitudes to produce the magnitude estimates thus resulting in similar results.

Results for the western United States (WUS) model are shown in Figure 13. With this analysis, we begin to see the effects of an attenuation model that differs from the Herrmann and Mitchell (1975) attenuation incorporated into $M_s(VMAX)$. Figure 12a shows that the $M_s(VMAX)$ magnitude "spectra" do not overlay each other and are not all flattened as was the case for the CUS model. The magnitude "spectra" at regional distances show a slight increase in magnitudes at the shorter periods, which has been noted on analyses of NTS explosions at WUS stations at regional distances (Figure 14). With the attenuation model differences, the $M_s(VMAX)$ period of maximum amplitude migrates from 8 s at 500 km to 24 s at 6000 km, which reduces the scatter in the final magnitude estimates to less than 0.15 magnitude unit (m.u.). The $M_s(VMAX)$ estimates are distance dependent with larger magnitudes at regional distances. Notice also how the bias between $M_s(VMAX)$ and M_s increases at regional distances, which is problematic if only regional data are used for smaller magnitude explosions. These results suggest the possible need to regionalize the $M_s(VMAX)$ formula for attenuation.

For example, based on the WUS model, a regionalized Q for the WUS would include a B_{att} and p of 0.0070 and 1.7, respectively, for T=8-25 s. Using the regionalized Q, the standard deviation in the final magnitudes would be reduced from 0.05 m.u. to 0.02 m.u.

Figure 15 shows the processing results for the final three models. The results show that both $M_s(VMAX)$ and M_s have significant distance dependencies for the AK135 and Italian models. The Q values for the latter model have not been thoroughly tested. In all three models, we see a bias between $M_s(VMAX)$ and M_s that averages ~0.1 m.u. (Figure 16) and is larger at regional distances and smaller at teleseismic distances. We note that for the Korean Peninsula model, we observe that the $M_s(VMAX)$ magnitude "spectra" overlay one another but are not flattened. This suggests that the excitation correction could be improved for this region to better flatten the spectra. However, even with this problem, the $M_s(VMAX)$ estimates are approximately distance-independent, whereas M_s has some distance dependence.

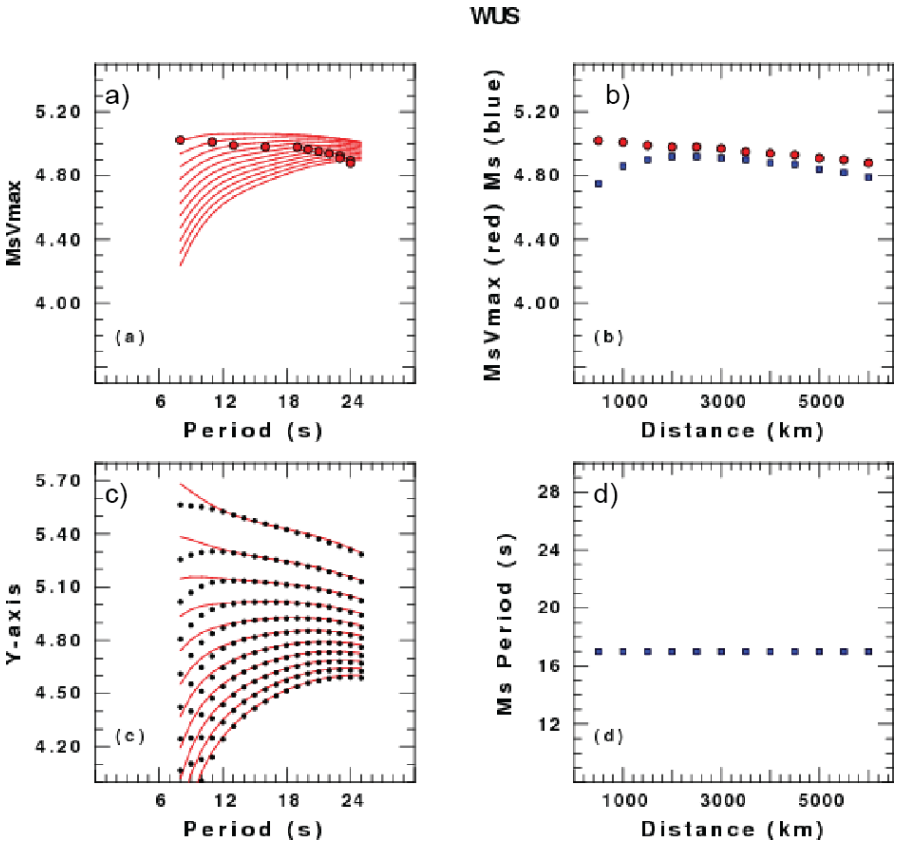

Figure 13. M_s **and** M_s**(VMAX) processing results for the WUS model.**

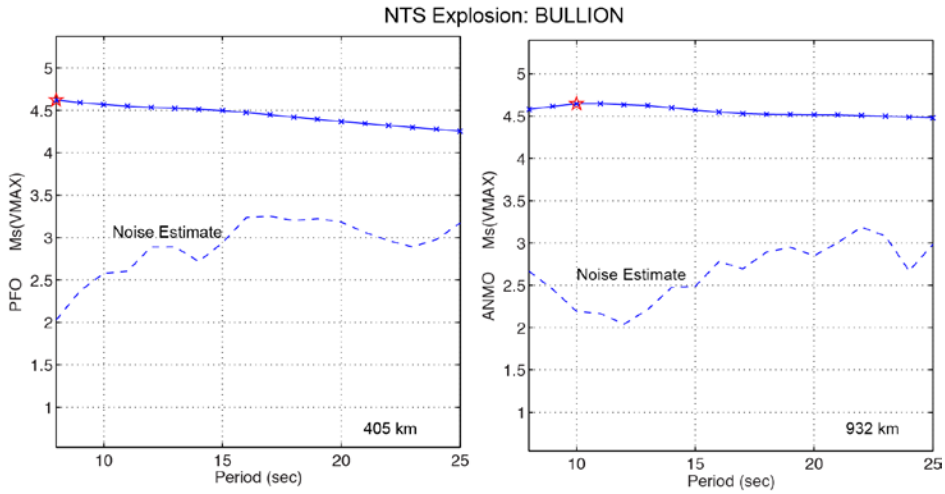

Figure 14. M_s**(VMAX) processing for two stations (Pinon Flats-left; ANMO-right) that recorded the Nevada Test Site explosion BULLION. The** M_s**(VMAX) results suggest slightly larger magnitudes at shorter periods that synthetic results (Figure 13a) suggest is a result of the differences between the real earth attenuation and the** M_s**(VMAX) attenuation correction.**

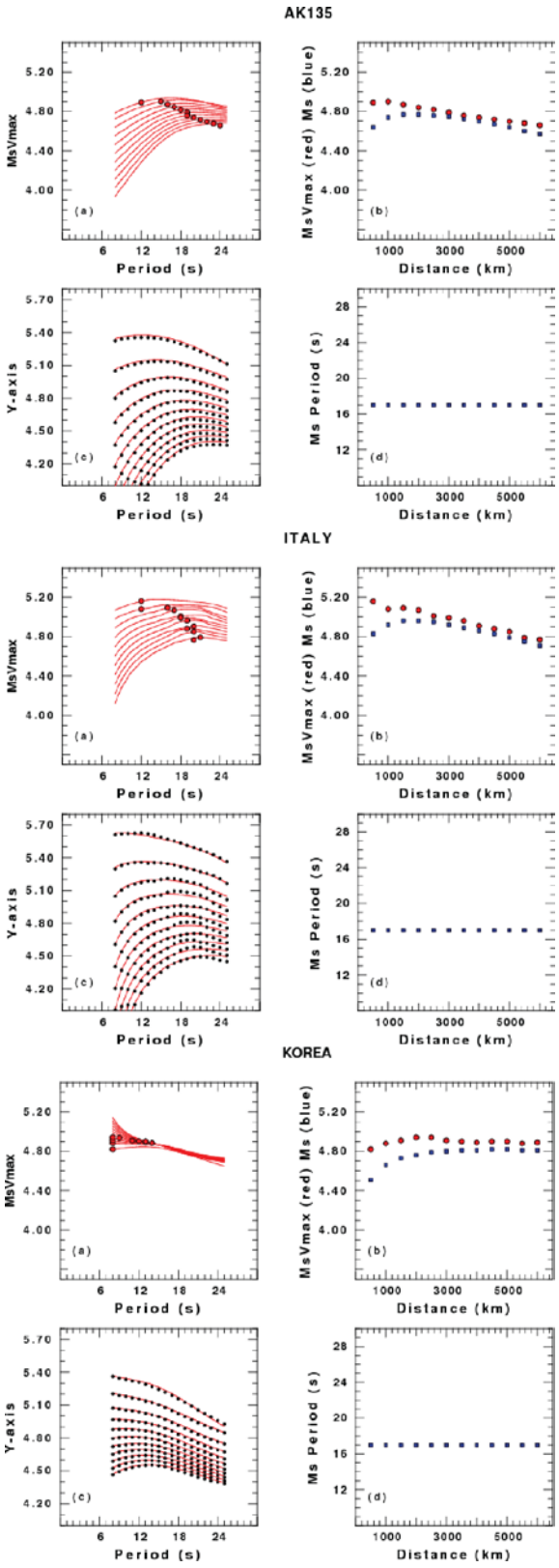

Figure 15. Processing results for the AK135, Italian, and CUS models.

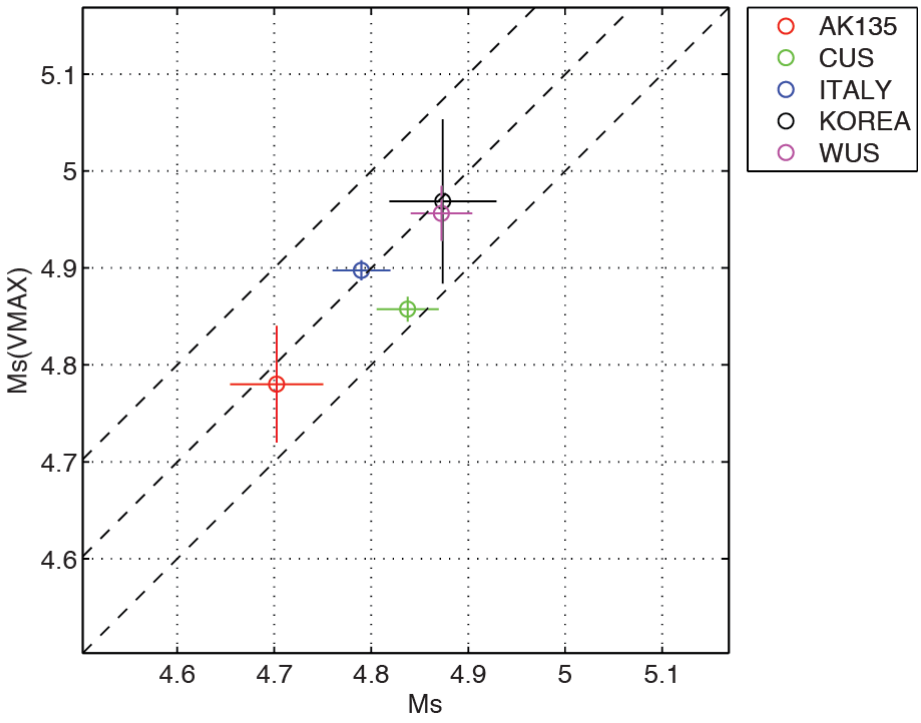

Figure 16. Bias between averaged M_s(VMAX) and M_s for explosion synthetics at distances between 500 and 6000 km for five different models. For most of the models, we observe that M_s(VMAX) is ~ 0.1 m.u. larger than the historic M_s estimates.

Earthquake Synthetics

For the second comparison of the two magnitude formulas, we synthesized earthquakes (M_w=5.0) at depths of 1, 10, 20, 30, 40, and 50 km. We considered normal (Strike 40/Dip 45/ Rake -90) and strike slip (30/90/0) fault focal mechanisms. We again used modal synthetics to synthesize fundamental-mode Rayleigh waves at distances between 500 and 6000 km; however, we varied the source-to-station azimuth from 0 to 352 as a function of distance. For example, station 1 was located at 500 km and 0 degrees azimuth, station 2 was at 1000 km at 32 degrees azimuth, station 3 was at 1500 km and 64 degrees, and this pattern continued until the final station was located at 6000 km and 352 degrees.

Figure 17 shows the results for a normal fault source generated and propagated through the CUS model at source depths ranging from 1 to 30 km. Some of the interesting features include:

- For the 1 km depth event, the scatter in the magnitudes caused by the radiation pattern is very large, with magnitudes ranging from 4.4 to 5.2. The magnitude scatter is much less for the deeper events.

- An odd effect is observed for the 10 km depth in which the $M_s(VMAX)$ and M_s are approximately mirror images of each other. This is caused by the shape of the Rayleigh wave spectra due to a spectral hole near T=20 s for some azimuths.

- When the radiation pattern effects are removed, we see a similar small distance dependent bias between $M_s(VMAX)$ and M_s that was observed for explosions, which we believe is due to filter and excitation effects for the CUS model, while for other models, the differences can also be attributed to attenuation model mismatch.

Figure 18 shows an example where the bias between $M_s(VMAX)$ and M_s can be significantly larger than 0.1 m.u. In this case, a 10 km deep strike slip event creates a very large spectral hole near T=16 s. $M_s(VMAX)$ straddles this hole and chooses peak amplitudes either at T=8-10 s or T=25 s period, while M_s tries to move as far away from the hole as possible at T=23 s period. The result is a 0.4 m.u. difference in the two magnitude estimates, with $M_s(VMAX)$ providing an estimate that is much closer to the seismic moment used to generate the synthetics.

CONCLUSIONS AND RECOMMENDATIONS

We have learned several important features about $M_s(VMAX)$ from this synthetic study. These include:

- For explosions, $M_s(VMAX)$ is biased high by ~0.1 m.u. when compared to a historic M_s for most of the models studied in this research. For earthquakes, the bias can be significantly larger depending on depth and focal mechanism. We hypothesize that in most cases, the $M_s(VMAX)$ provides an estimate that is closer to the true moment of the event.
- The $M_s(VMAX)$ measurement procedure does correctly estimate the Rayleigh-wave spectra, however, the extrapolation of that spectral amplitude back to a 1 km distance for explosions could be improved with regionalized attenuation models and excitation corrections.
- Regionalized Q models will not significantly reduce the scatter for the earthquake magnitude estimates, as most of it is due to radiation pattern effects. We are investigating other methods to reduce this scatter, which include using both the Rayleigh and Love waves in a combined magnitude.
- In most cases, we see only a small distance dependent bias between $M_s(VMAX)$ and M_s, thus, we recommend using a simple bias correction of 0.1 m.u. since we believe that we have isolated the cause in terms of Q effects, filter effects, and excitation.

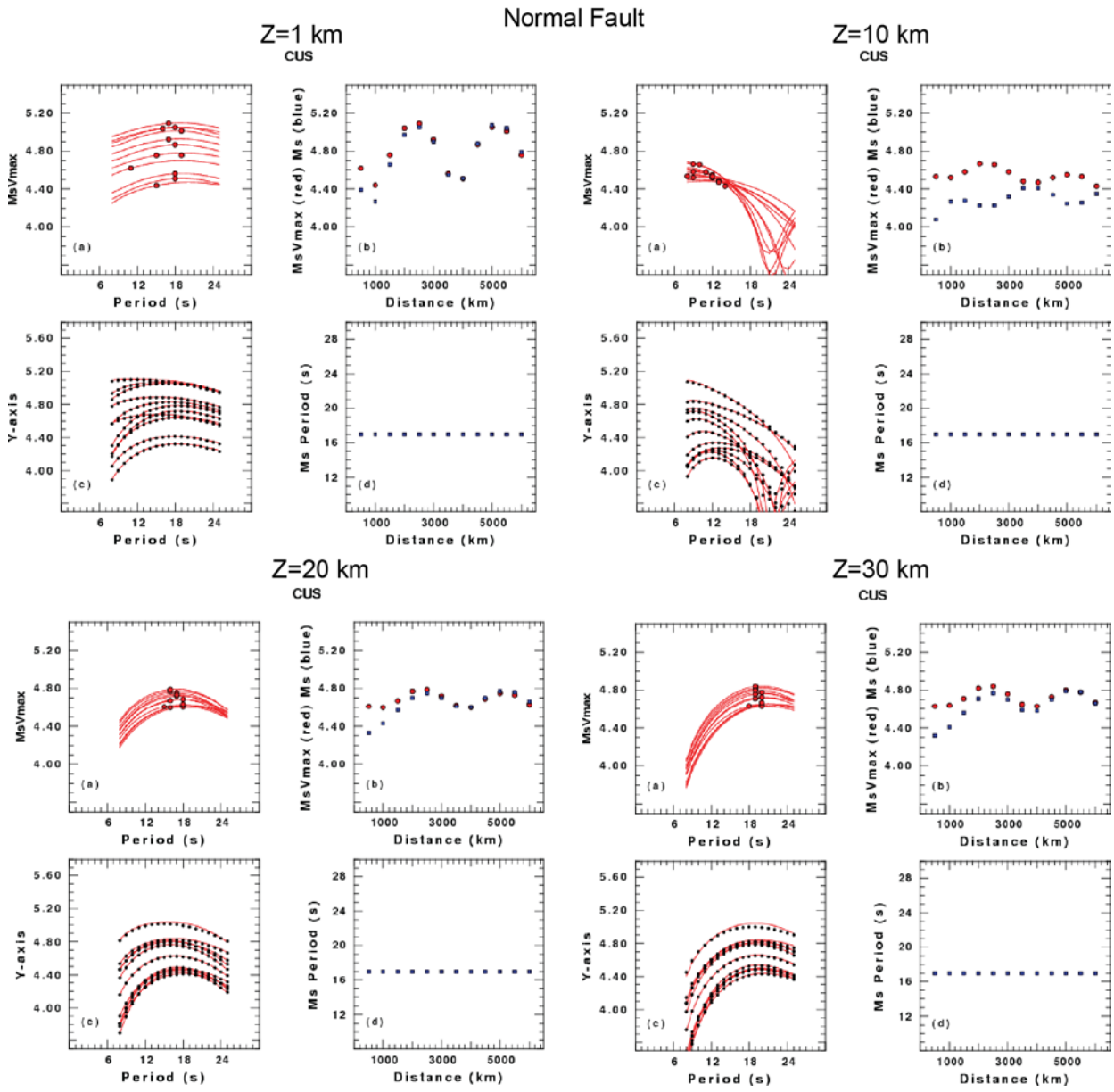

Figure 17. M_s and M_s(VMAX) processing results for a normal fault earthquake in the CUS model at depths of 1 km, 10 km, 20 km, and 30 km.

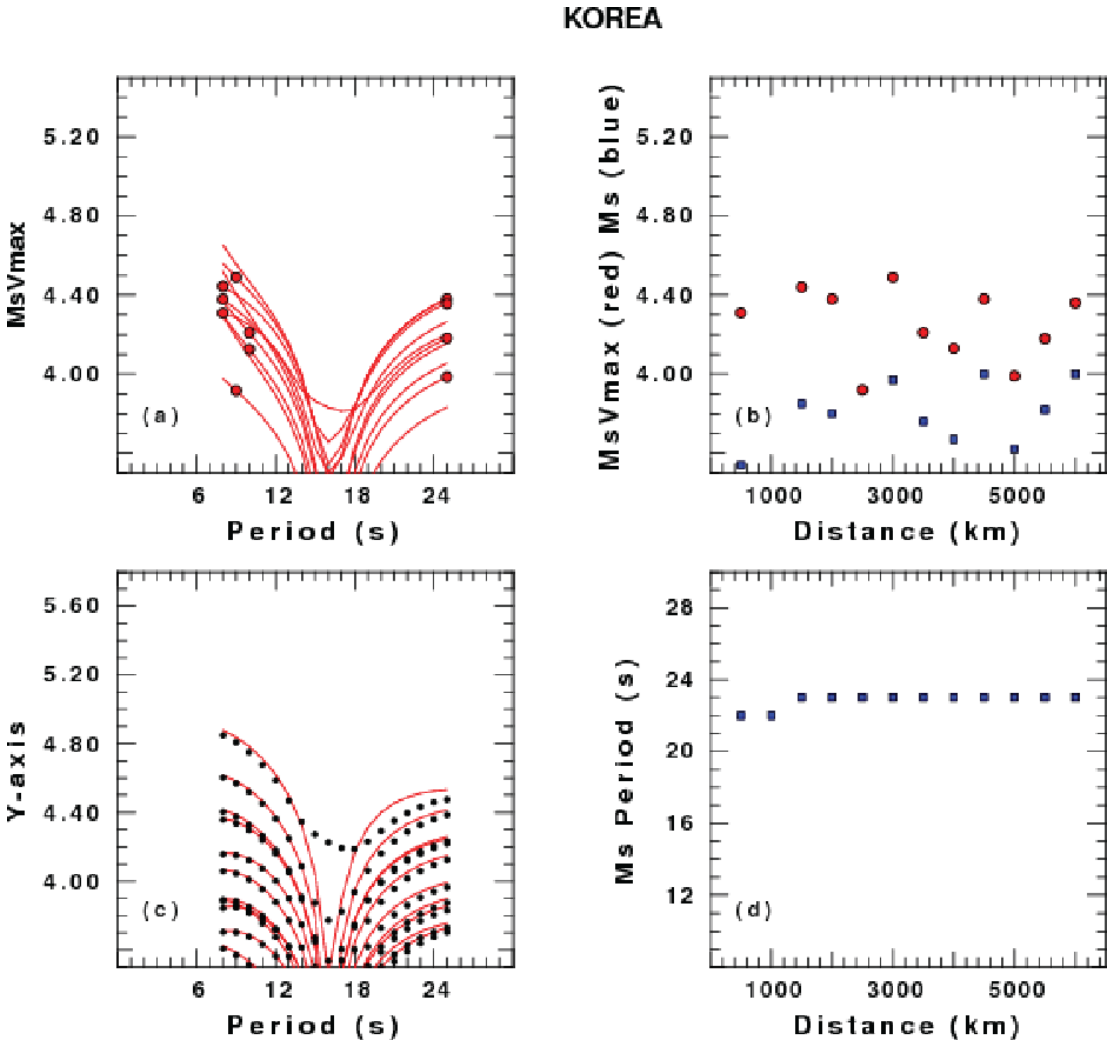

Figure 18. M_s and M_s(VMAX) processing results for a strike-slip fault earthquake in the Korean Peninsula model at depths of 10 km.

APPENDIX 3A: Correction in narrow band historic M_s formula

Yacoub's (1988) fundamental method is to calculate a spectral amplitude in the frequency domain using a Gaussian filter of the form $exp[-c(\omega - \omega_0)^2]$, FFT it back to the time domain, and insert the maximum envelope amplitude into a standard magnitude formula such as von Seggern (1977). The problem with this direct approach to utilizing the spectral magnitude is that it does not modify the standard magnitude formula to account for the Gaussian filter, in that it has no correction for the filter value "c" in the standard magnitude formula. Newer results using equivalent Butterworth filters in $M_s(VMAX)$ correct for the filter width in the final magnitude formula by the term $\log(f_c)$, where f_c the one-sided width of the Butterworth filter. That this can cause significant errors can be easily seen by putting a very large value of *"c"* in the Gaussian, which would result in a vanishing small time domain maximum. The actual error is a complicated term, but it can be analytically calculated for typical crustal structures as shown below.

Following (Russell, 2006), a dispersed surface wave can be mapped from the frequency to time domain using

$$a = A/\sqrt{\pi\alpha} \tag{3A1}$$

Where A is the frequency domain amplitude, a is the time domain amplitude and

$$\alpha = \frac{x}{4\pi}\frac{T^2}{U^2}\frac{dU}{dT} \tag{3A2}$$

x=epicentral distance (km), T=period of interest (sec), U= group velocity at period T (km/sec), and dU/dT=derivative of group velocity with respect to period, evaluated at period T (km/sec^2). If the same signal is filtered with a sufficiently narrow Gaussian bandpass filter of the form $exp[-c(\omega-\omega_0)^2]$, it can be mapped from the frequency to time domain using

$$a_f = A/\sqrt{\pi c} \tag{3A3}$$

"Sufficiently" means that $c > \alpha$, that is, the Gaussian filter is narrower than the earth's dispersion filter coefficient α in (3A2), thus (3A3) controls the process. To transform the unfiltered time domain amplitude in (3A1) to the filtered amplitude in (A3), equate frequency domain amplitudes A for

$$a_f = \sqrt{\alpha/c}\, a \tag{3A4}$$

Substituting into (3A4) the expanded value for α in (3A2) gives

$$a_f = \sqrt{\frac{x}{4\pi c}\frac{T^2}{U^2}\frac{dU}{dT}}\, a \tag{3A5}$$

In Yacoub (1988), he references his earlier paper (Yacoub, 1983) for the exact form of the exponential filter he is using, which follows Herrmann (1973):

$$H = exp\left[-c'\left(\frac{\omega-\omega_0}{\omega_0}\right)^2\right] \tag{3A6}$$

where c' is now normalized to ω_0^2, and therefore $c = c'/\omega_0^2 = c'T^2/(4\pi^2)$. Substitute into (3A5) and rearrange for

$$a_f = \sqrt{\frac{\pi}{c'U^2}\frac{dU}{dT}x}\, a \tag{3A7}$$

Herrmann (1973) recommends a value of $c' = 16\pi = 50.27$, which Yacoub (1983, 1988) uses. Notice in this case that the width of the Gaussian filter is inversely proportional to the square of the period T, but not to the distance x. In the derivation for *Ms(VMAX)* (Russell, 2006) the equivalent Butterworth filter used has a bandwidth inversely proportional to both period and

distance, i.e., $f_c \propto 1/(xT)$, where the constant of proportionality is calculated to ensure that the filter bandwidth is always less than the earth dispersion bandwidth. Substituting $c' = 16\pi$ into (3A7) gives

$$a_f = \frac{1}{4U}\sqrt{\frac{dU}{dT}\,x}\;a \tag{3A8}$$

For a typical continental crust (Russell, 2006), at T=20 sec let U=2.9 km/sec, and dU/dT= 0.02 km/sec^2 in (3A8) for

$$a_f = (0.0122\sqrt{x})\;a \tag{3A9}$$

Equation (3A9) can now be used to determine the effect of using filtered amplitudes in standard magnitude dispersion curves. Notice that in (3A9), at a distance of x=6730 km, $a_f = a$, which means that beyond this point the Gaussian filter has a filter bandwidth greater than the earth dispersion filter and no longer controls the maximum amplitude. Equation (3A9) no longer applies for distances beyond this point, for the particular crustal and period values used. However, for distances less than 6730 km, an error will be introduced into standard magnitude formulas due to not correcting for the bandwidth in the formula, as will be shown below.
Yacoub (1988) takes the filtered amplitudes and directly inserts them into a time domain magnitude formula of the form:

$$M_s = \log\left(\frac{a}{T}\right) + F(x,T) \tag{3A10}$$

The reason to use this general formula is to show that the error does not depend on the explicit form of the magnitude formula, as long as the measured amplitude enters only into the first log term. Substituting the filtered amplitude (3A9) into (3A10) gives:

$$M_s = \log\left(0.0122\sqrt{x}\frac{a}{T}\right) + F(x,T) \quad = \quad \log\left(\frac{a}{T}\right) + F(x,T) + \frac{1}{2}\log(x) - 1.914 \tag{3A11}$$

Thus, for the period and crustal parameters used, there is an error introduced of

$$Error = \frac{1}{2}\log(x) - 1.914 \tag{3A12}$$

Notice that in (3A12), closer epicentral distances mean larger errors. Notice also that the error is independent of the particular event magnitude. Figure 3A1 shows the error as a function of distance, for Gaussian filters, 20 sec periods, and a typical continental crust. Yacoub (1988) noted that he found an average decrease in his spectral amplitudes of 0.17 magnitude units for all station distances used in his NTS teleseismic study, which is consistent with these results. Subtracting Equation (3A12) from the historical magnitude formula will correct it for the width of the Gaussian filter.

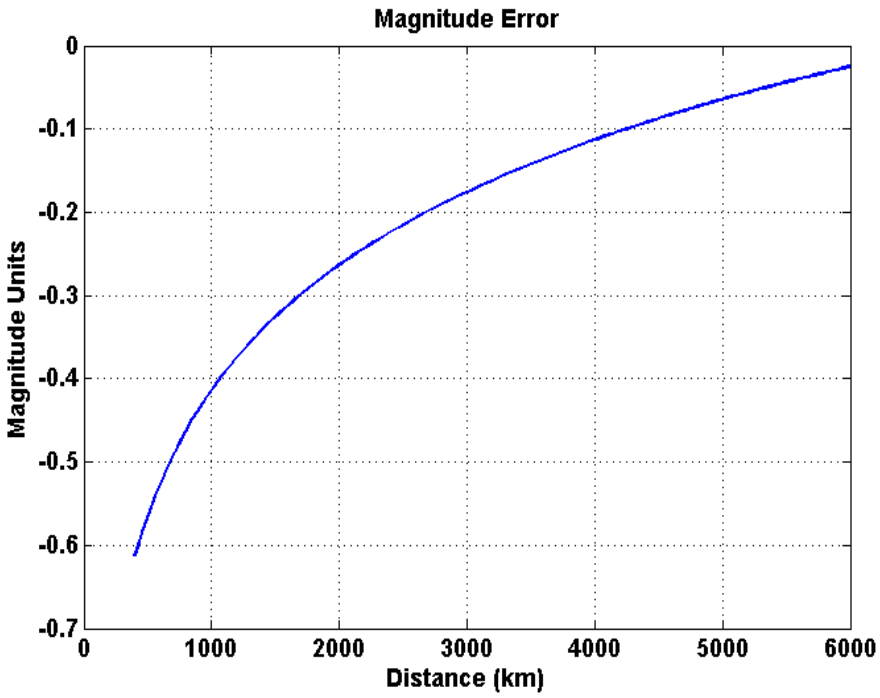

Figure 3A-1. Magnitude errors as a function of distance due to Gaussian filter methods.

CHAPTER 4: IMPROVING M_s:m_b DISCRIMINATION USING MAXIMUM LIKELIHOOD ESTIMATION: APPLICATION TO MIDDLE EAST EARTHQUAKE DATA

Anastasia Stroujkova and Jessie Bonner

Weston Geophysical Corporation

INTRODUCTION

We evaluated the detection thresholds for both Rayleigh and Love waves for a series of stations used for surface wave magnitude estimation in the Middle East. We estimated the $M_s(VMAX)$ magnitudes using the Maximum Likelihood Estimation (MLE) approach and compared it with conventional averaged estimates for the dataset consisting of approximately 120 events located in the Middle East. The major differences between the two estimates are observed for the magnitudes smaller than 4 m.u.. The MLE estimates with $M_s(VMAX) > 4$ m.u. are identical to the results of the averaging. MLE does not improve the standard error of the estimated values, it simply reduces the bias of the mean.

During the application of the $M_s(VMAX)$ methods (Russell, 2006) to small-to-intermediate sized events (e.g., $m_b < 4.5$), we began to note possible magnitude biases that could have been associated with data censoring produced by variable signal-to-noise conditions in the recording networks. If some of these smaller events were being lost in the noise at various stations, the averaged magnitude based only on a few observed data points could be biased toward the higher values. To quantify and reduce this bias we have estimated the M_s detection thresholds for European and Asian Global Seismographic Network (GSN) stations and applied a Maximum Likelihood Estimator of variable-period surface-wave magnitudes. The Maximum Likelihood Estimate (MLE) was proposed by Ringdal (1976) for the seismic event magnitude (m_b) estimation in order to reduce the network bias due to non-detection. It was applied to spectral-based surface wave magnitudes by Stevens and McLaughlin (2001). We studied different detection thresholds for the stations recording the event (direct and indirect estimation methods). In this chapter, we extended the MLE estimate to both Rayleigh and Love waves for a dataset consisting of approximately 100 earthquakes and two nuclear explosions located in the Middle East (Figure 19).

RESEARCH ACCOMPLISHED

Maximum Likelihood Magnitude Estimate

Using the Maximum Likelihood Estimate (MLE) to reduce the network bias due to non-detection was proposed by Ringdal (1976). Generalization of this procedure to include data clipping was proposed by von Seggern and Rivers (1978). The network magnitude bias is caused by the loss of information from non-reporting stations. For small and intermediate size events, this means that the stations with the magnitude measurements below a certain threshold

may not report the signal and therefore get ignored. This effect is called "censoring." A number of studies have shown that the magnitude bias could be significant, particularly for the events close to the detection threshold (Ringdal, 1976; Evernden and Kohler, 1976).

The MLE method is based on the assumption that for a given event the magnitude estimates follow a Gaussian distribution with unknown mean and variance $M_s \sim N(\mu, \sigma)$. We assume that an event is detected by a station if the station magnitude exceeds a certain threshold magnitude a_i ($i = 1,\ldots, n$), where n is a number of the stations in the network. Ringdal (1976) provided an expression for the maximum likelihood estimate of an event magnitude with a true magnitude μ:

$$L(m_1 \ldots m_n / \mu, \sigma) = \prod_{i, m_i > a_i} \frac{1}{\sigma} \phi\left(\frac{m_i - \mu}{\sigma}\right) \prod_{j, m_j < a_j} \Phi\left(\frac{a_j - \mu}{\sigma}\right), \tag{20}$$

where ϕ and Φ are the Gaussian PDF and CDF respectively. This expression is maximized numerically in order to obtain a maximum likelihood estimate of the magnitude μ.

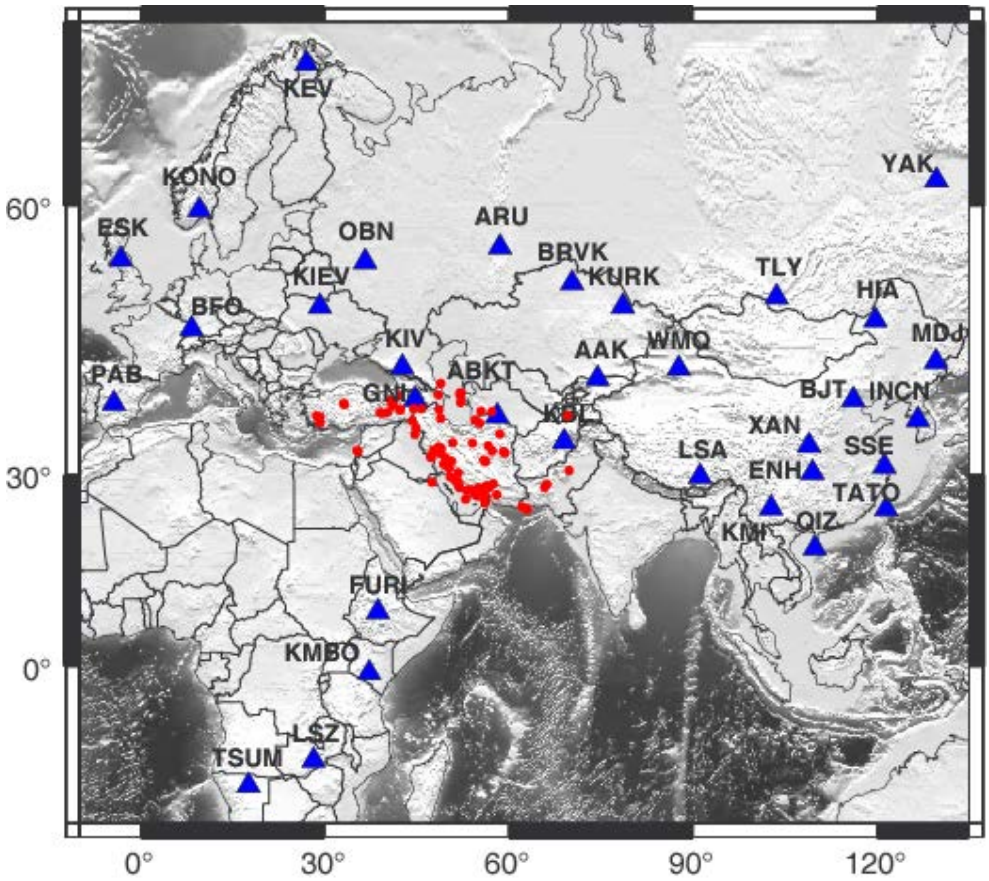

Figure 19. Map of the seismic events (red circles) and stations (blue triangles) used for M_s(VMAX) study.

The threshold values for each station a_i could be estimated using a "noise magnitude" for each event-station pair. We converted the broadband ambient noise estimates for the Global Seismographic Network (GSN, e.g., Berger et al., 2004) from decibels to nanometers (nm) and input them into the $M_s(VMAX)$ formula (1) for variable-period surface waves. We propagated these noise estimates at periods (T) between 8 and 40 s to distances (Δ) corresponding to each earthquake-station pair. Table 7 (columns 4-5) shows the estimates of the magnitude threshold for a representative event in the region (2006.06.03).

An important part of the MLE application is evaluation of the detection thresholds for the stations recording the event. Ringdal (1976) discussed three basic ways of estimating the station detection threshold: a) *the indirect estimation method* based on seismic noise studies; b) *the recurrence curve estimation method* based on magnitude-frequency distribution of the seismicity; and c) *the direct estimation method* based on the percentage of events of each magnitude actually detected by the station. The *indirect* method can be applied by estimating a "noise magnitude" for each event-station pair using the broadband ambient noise estimates for the GSN (e.g., Berger et al., 2004). The computation of the percentages of the detected events required for the *direct* method can be complicated since some of the stations may be off-line at different periods of time. Ringdal (1976) applied the *direct* estimation method by averaging the three smallest magnitudes recorded by each station. The second and third columns in Table 7 show the values estimated using this approach. Figure 20 shows the correspondence between the estimates made with different methods for different periods for the stations with both estimates available. The magnitude thresholds show the best agreement for the period T=20 sec for both Rayleigh and Love magnitudes. Notice that a different set of stations was used for the thresholding application. The threshold values using the minimum $M_s(VMAX)$ approach are missing for the stations with not enough $M_s(VMAX)$ measurements to obtain a reliable threshold. Some of the noise floors were not reported, which resulted in missing values in columns 4-5 of Table 7.

An important issue to consider is which stations should be added to MLE estimate as censored values. Ringdal (1986) divided all stations into: a) detecting stations, b) non-detecting stations due to noise; and c) non-detecting stations due to maintenance issues. For the third group of stations, Ringdal suggests computing the probabilities of each station of being off-line and adding them randomly. We, however, only used the reporting stations to use as either measured or a censored (threshold) value.

Another issue, mentioned in Ringdal (1986) is the increase of noise due to special circumstances, such as time intervals coinciding with large events and their aftershocks overlapping with the event in question. In this case we did not estimate the magnitudes even though they were significantly above the detection threshold. These events require special attention, for instance using the information about the noise amplitude just before the event to establish the detection threshold.

It was noted by Ringdal (1976) that the estimate of the true magnitude μ depends on the inter-station magnitude variance σ. Figure 21 shows the histograms of $M_s(VMAX)$ RMS residuals for the Middle East dataset for both Rayleigh and Love waves. In both cases the mean values of the RMS are approximately 0.2.

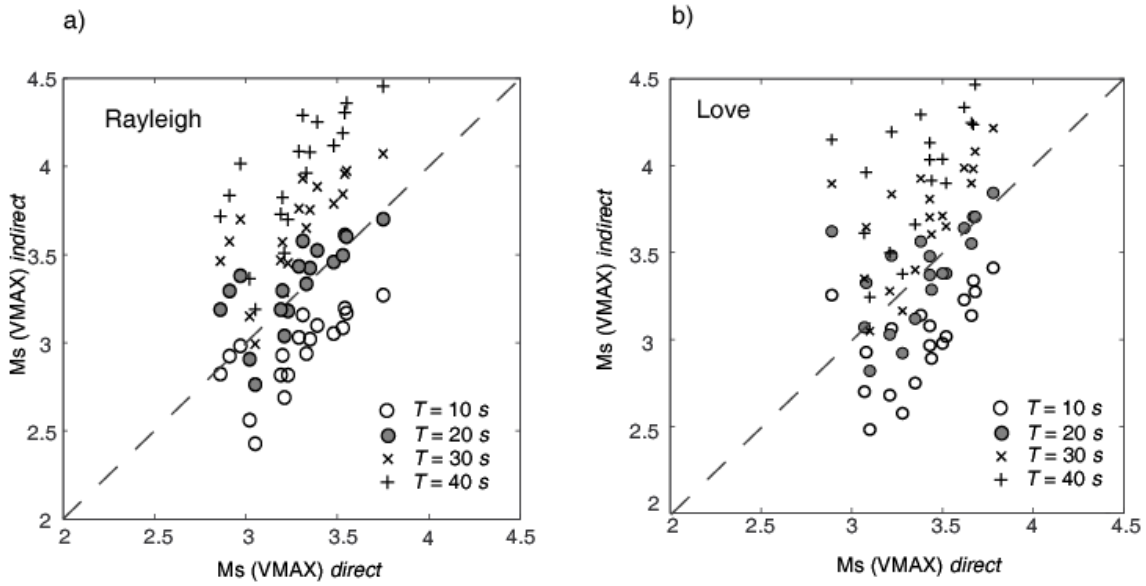

Figure 20. Comparison of the magnitude thresholds computed with different methods with each circle corresponding to one station having both threshold values defined in Table 7 using: a) Rayleigh $M_s(VMAX)$, and b) Love $M_s(VMAX)$. Horizontal axis: detection threshold computed by averaging 3 lowest magnitudes actually detected by the station (Ringdal, 1976); vertical axis: detection threshold computed using the noise floors for different periods for a representative event (2006.06.03). The best agreement (dashed line) is for T=20 sec.

Application of MLE Technique to the Middle East Dataset

We estimated $M_s(VMAX)$ using the standard approach (station average) and an MLE approach for the Middle East dataset discussed earlier. We applied the method to both Rayleigh and Love $M_s(VMAX)$ measurements using the threshold values listed in Table 7. For the events with the magnitudes significantly larger than the threshold magnitude with missing stations due to unusually high noise, we did not use the threshold values if the average magnitude exceeded the threshold value by more than 0.6 m.u., which corresponds to a standard error multiplied by 3. For the events with measured values below the threshold, we used the measured values.

Figure 22 show comparison between the traditional (mean) and the MLE estimates of the $M_s(VMAX)$ using both types of thresholds described earlier for Rayleigh and Love waves. Figure 22a shows the cross-plot between the mean and the MLE estimate of $M_s(VMAX)$ using *min* magnitude thresholds (*direct* method). The results for both types of measurements show similar trends. Above the magnitude of approximately 4.1 both MLE and conventional estimates are essentially equal. Below this point there is a significant positive bias for the conventional network average estimate. Figure 22b shows comparison between the Rayleigh and Love wave measurements for mean and MLE. Again, the character of the distribution is very similar. Similar computations obtained using noise floor thresholds (*indirect* method) produce similar results (Figure 22 c-d).

Table 7. Comparison of the magnitude threshold values for one event computed using the two approaches described in the article. The omitted threshold values in columns 2 and 3 mean that there were not enough $M_s(VMAX)$ measurements to obtain a reliable threshold. The values in the columns 4-5 were skipped for the stations for which the noise floors were not reported.

Station	Minimum $M_s(VMAX)$ Rayleigh	Minimum $M_s(VMAX)$ Love	Magnitude thresholds computed for the event 2006.06.03 (T=20 s)	
			Rayleigh	Love
AAK	3.21	3.21	3.04	3.03
ABKT	-	-	2.73	2.71
ANTO	2.94	3.22	-	-
ARU	3.20	3.67	3.30	3.71
BFO	3.33	3.44	3.33	3.29
BJT	3.54	3.66	3.61	3.55
BRVK	3.23	3.52	3.18	3.38
ENH	3.48	3.43	3.46	3.37
ERM	-	-	3.70	3.82
ESK	3.53	3.62	3.50	3.64
FURI	-	-	3.14	3.23
GNI	3.05	3.10	2.76	2.82
GRFO	3.19	3.26	-	-
GUMO	-	-	3.55	3.75
HIA	3.31	3.22	3.58	3.48
INCN	3.55	3.68	3.60	3.71
KBL	2.78	3.10		
KBS	3.39	3.38	3.52	3.56
KEV	3.35	3.50	3.42	3.38
KIEV	3.19	3.35	3.19	3.12
KIV	3.02	3.28	2.91	2.92
KMBO	3.51	3.69	-	-
KMI	-	-	3.42	3.44
KONO	3.29	3.43	3.43	3.48
KURK	2.86	2.89	3.19	3.62
LSA	2.91	3.07	3.29	3.07
LSZ	-	-	3.67	3.64
MDJ	-	-	3.57	3.50
OBN	-	-	3.21	3.27
PAB	-	-	3.48	3.37
PMG	-	-	3.99	4.11
QIZ	-	-	3.56	3.48
SSE	-	-	3.51	3.47
SUR	-	-	3.78	3.73
TATO	-	-	3.63	-
TLY	2.97	3.08	3.38	3.32
TSUM	3.75	3.78	3.70	3.84
WMQ	-	-	3.22	3.28
XAN	-	-	3.48	3.45

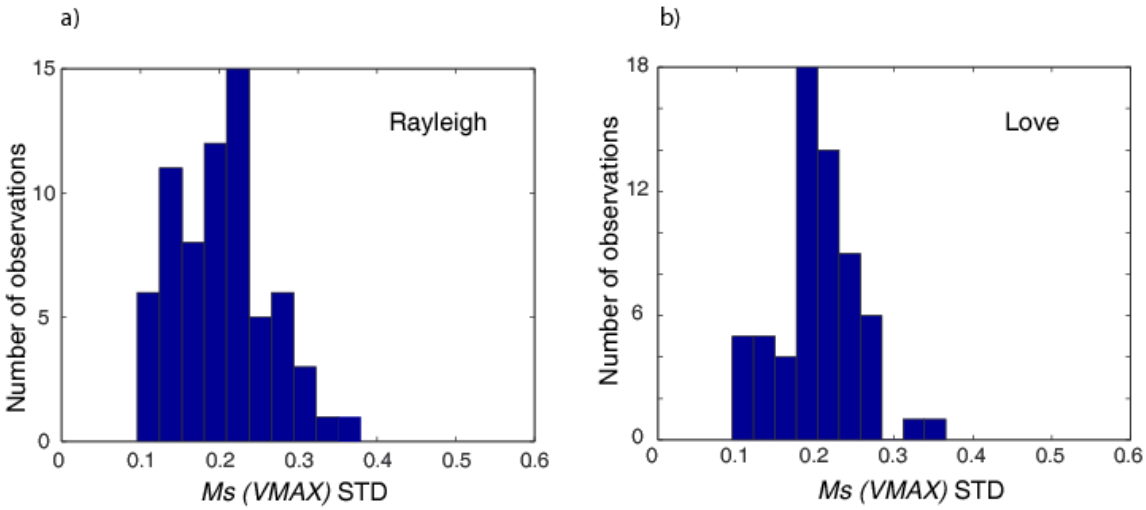

Figure 21. Histogram of M_s(VMAX) RMS residuals for the Middle East dataset: a) using Rayleigh waves; b) using Love waves.

The standard errors of $M_s(VMAX)$ estimation using both traditional and MLE techniques are shown in Figure 23. Notice that the MLE confidence intervals almost always exceed the standard deviation. It was noted earlier (*e.g.* McLaughlin, 1988) that MLE method does not reduce the confidence intervals compared to the traditional (averaging) approach; it merely improves the bias in the expected value.

CONCLUSIONS

We evaluated the detection thresholds for both Rayleigh and Love waves for the series of stations used for the magnitude estimation in the Middle East. We estimated the $M_s(VMAX)$ magnitudes using MLE approach and compared it with conventional averaged estimates for the dataset consisting of approximately 120 events located in the Middle East. The major differences between the two estimates are observed for the magnitudes smaller than 4 m.u.. The MLE estimates above $M_s(VMAX) > 4$ m.u. are identical to the results of the averaging. MLE does not improve the standard error of the estimated values, it simply reduces the bias of the mean.

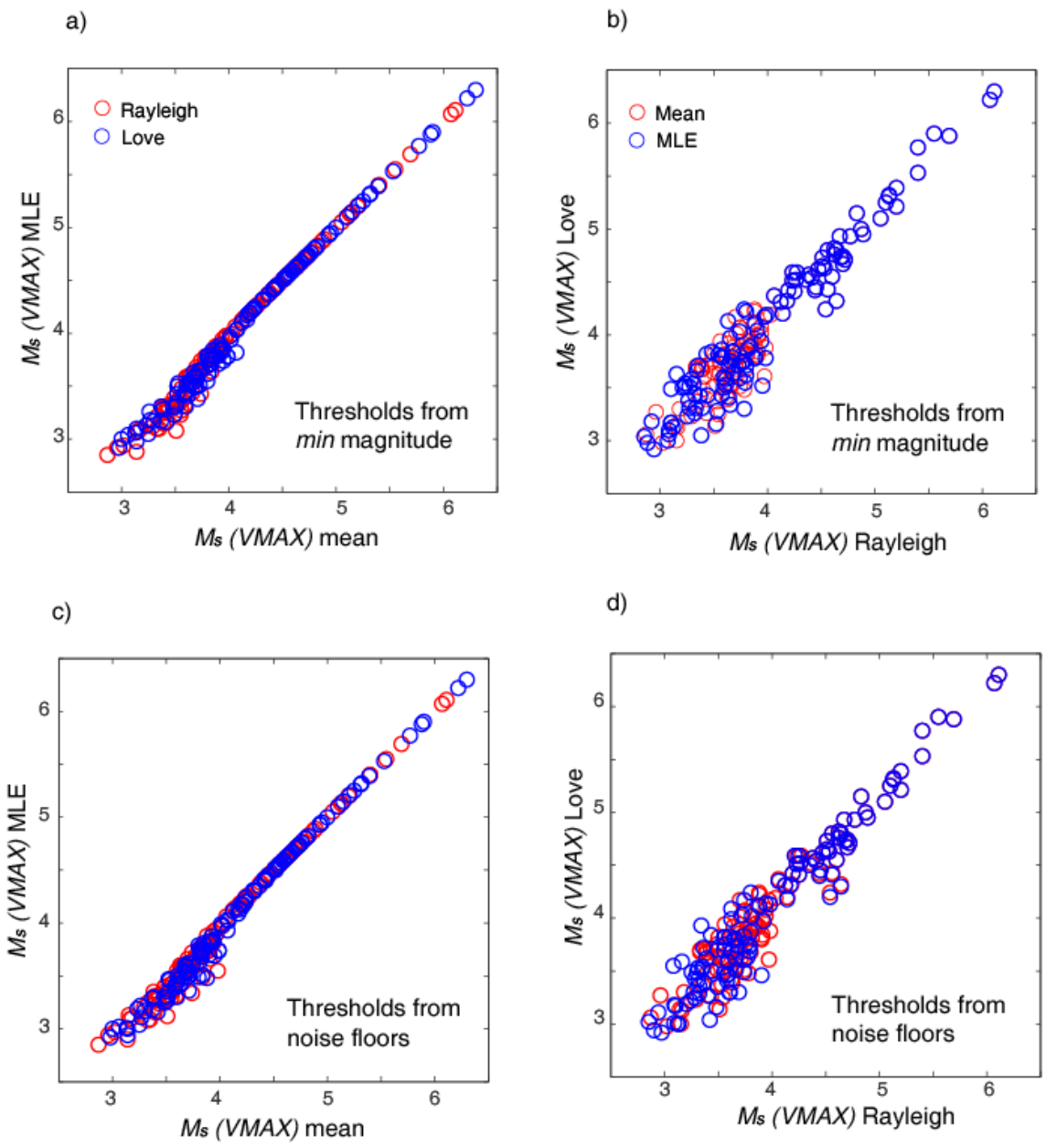

Figure 22. a) Comparison between the traditional (mean) and the MLE estimates of the $M_s(VMAX)$ using *direct* method to estimate thresholds applied to the Middle East event dataset using Rayleigh (red) and Love (blue) waves; b) Comparison between Rayleigh and Love the $M_s(VMAX)$ for mean (red) and MLE (blue) estimates using *indirect* method to estimate thresholds; c) Comparison between the mean and the MLE estimates of the $M_s(VMAX)$ using *direct* method applied to the Middle East event dataset using Rayleigh (red) and Love (blue) waves; d) Comparison between Rayleigh and Love the $M_s(VMAX)$ for mean (red) and MLE (blue) estimates using *indirect* method.

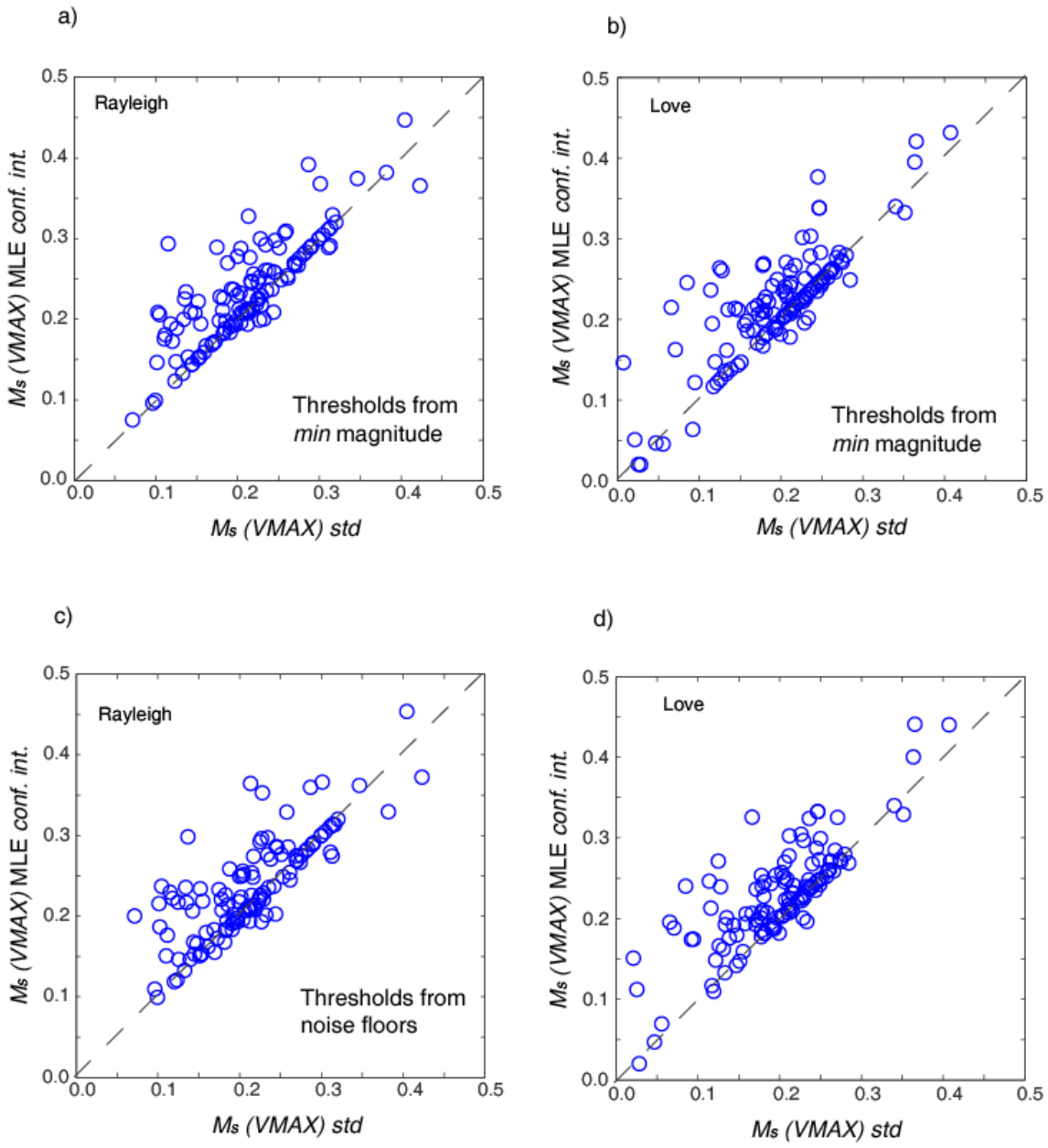

Figure 23. a) Comparison between the inter-station standard deviation for the traditional and the confidence intervals MLE estimates of the $M_s(VMAX)$ using *direct* method thresholds applied to the Middle East event dataset (Rayleigh waves); b) Comparison between the inter-station standard deviation for the traditional and the MLE estimates of the $M_s(VMAX)$ using *direct* method thresholds applied to the Middle East event dataset (Love waves); c) Comparison between the inter-station standard deviation for the traditional and the MLE estimates of the $M_s(VMAX)$ using *indirect* method thresholds applied to the Middle East event dataset (Rayleigh waves); d) Comparison between the inter-station standard deviation for the traditional and the MLE estimates of the $M_s(VMAX)$ using *indirect* method thresholds applied to the Middle East event dataset (Love waves).

CHAPTER 5: DEVELOPING EMPIRICAL RELATIONSHIPS FOR IMPROVED LOVE- AND RAYLEIGH-WAVE MAGNITUDES

Anastasia Stroujkova and Jessie Bonner

Weston Geophysical Corporation

INTRODUCTION

We studied the suitability of the Russell (2006) formula for Love waves. We computed the attenuation correction by fitting a linear regression to uncorrected $M_s(VMAX)$ measurements. We used two slightly different approaches to find the coefficients for the empirical Russell formula suitable for the Middle East region. We found the best fitting attenuation constants for both Rayleigh and Love waves are 0.0037 and 0.0042, respectively. The value of the attenuation term used in the Russell formula is 0.0031.

Russell (2006) developed a time-domain method and formula (Equation 1) for measuring surface waves with minimum digital processing using zero-phase Butterworth filters ($M_s(VMAX)$; Bonner et al., 2006). We extended application of the $M_s(VMAX)$ technique to Love waves in attempt to improve seismic event screening using the properties of Rayleigh and Love waves. In this chapter we develop a Love-wave magnitude formula that is complementary to the Russell (2006) formula for Rayleigh waves. To obtain the empirical formula we use two slightly different approaches to calculate the coefficients for the attenuation term. We used linear regression to find the dependency of the magnitude estimate on the event-station distance and the period at which the magnitude maximum is reached.

DEVELOPING EMPIRICAL EXPRESSIONS

In this chapter, we attempt to either show the validity of the Russell (2006) Rayleigh-wave equation for Love waves or to develop a new formula, which takes into account the excitation and attenuation of Love waves. For this task we needed in some instances to use the Russell formula without the attenuation and/or excitation corrections to evaluate the role of each one on Love wave magnitudes. Recalculating $M_s(VMAX)$ without corrections is a time-consuming process, therefore we chose to simply subtract the correction values from already computed $M_s(VMAX)$ values.

Approach 1

To study the correction performance on our Middle Eastern dataset (Figure 24) we plotted the measured station $M_s(VMAX)$ as functions of period at which $M_s(VMAX)$ was picked. In each case we found linear fits of the form:

$$\delta M_s = \left(M_s(VMAX) - \overline{M_s(VMAX)}\right) = a\Delta_j^i + b \text{ and} \quad (21)$$

$$\delta M_s^i = \left(M_s(VMAX)_j^i - \overline{M_s(VMAX)^i}\right) = cT_j^i + d\,, \quad (22)$$

where Δ_j^i is the great circle (GC) distance in degrees between event *i* and station *j*, and T_j^i is a period in sec, the bar above the magnitude value indicates the mean $M_s(VMAX)$ for each event.

Figure 24 shows the individual $M_s(VMAX)$ measurements for two representative events from our dataset. The event 2006.09.26 (Figure 24a) has limited number of stations available for $M_s(VMAX)$ estimation. The range of the periods where $M_s(VMAX)$ is determined for using Rayleigh waves is limited to the interval between 15s and 30s. If there is a systematic trend in the measurement as a function of period, computing the mean may result in a biased value. To avoid computing the biased value we used events with at least 20 measurements of $M_s(VMAX)$.

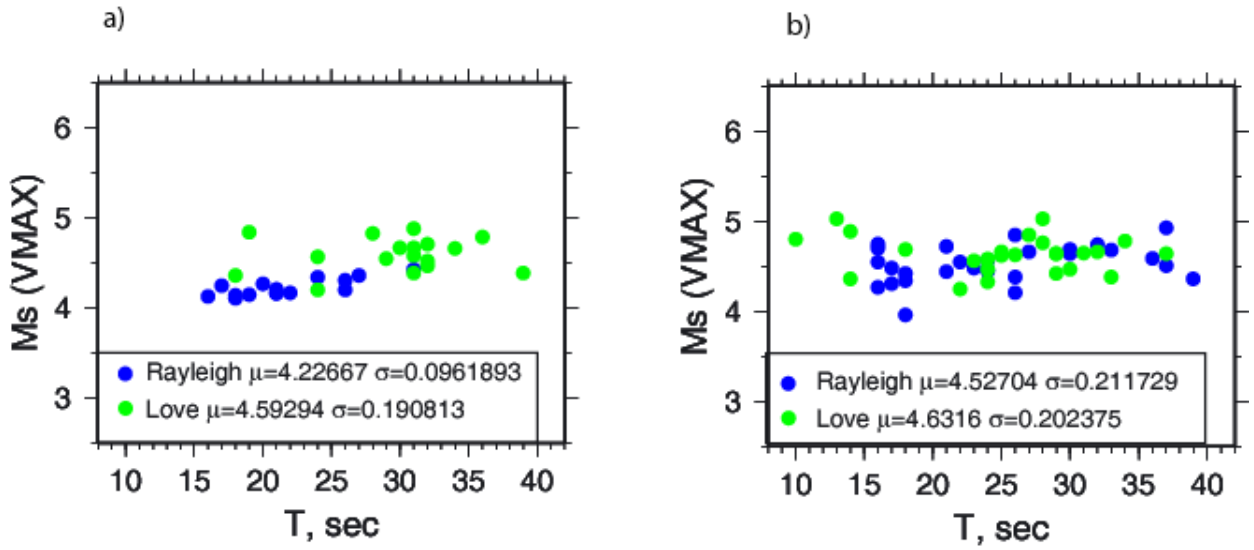

Figure 24. Individual station $M_s(VMAX)$ computed using Russell formula (Equation 1) for two events plotted against the measurement period: a) Event 2006.09.26 08:14 (31.909º N, 50.653 º E, Depth 29.9 km, M_w =4.5), and b) Event 2008.09.02 20:00 (38.874º N, 45.777 º E, Depth 25 km, M_w=5.0).

Event 2008.09.02 shown in Figure 24b has more stations where $M_s(VMAX)$ was determined; however it does not have a single linear trend. Russell (2006) deals with it by adding a period-dependent factor $(T_0/T)^{1.8}$. However, the period dependent behavior varies between events, and appears to be depth and/or focal mechanism dependent. Therefore the inversion was performed without the period-dependent factor.

We computed the regression coefficients for $M_s(VMAX)$ values estimated using Russell's formula. Then we estimated the linear fit to the $M_s(VMAX)$ with different terms removed to see how the different corrections improve the estimation. We considered four different cases: 1)

Russell formula with all corrections applied; 2) no corrections for the attenuation and the source excitation; 3) no correction for the attenuation; 4) no correction for the source excitation. The reasoning behind removing the source excitation for this experiment is that it was developed for the Rayleigh waves from shallow explosions. It is applied to the Rayleigh waves from the earthquakes to improve discrimination. However, it is not clear what the source excitation correction for the Love waves should be. We also removed the attenuation correction to study differences in Rayleigh and Love attenuation.

Table 8. The linear fit coefficients using the events with at least 20 $M_s(VMAX)$ measurements

Description	Wave type	$M_s(VMAX) = a\,\Delta + b$			$M_s(VMAX) = cT + d$		
		a	*b*	RMS	*c*	*d*	RMS
Russell formula, all corrections	R	-0.0010	0.0456	0.2329	0.0032	-0.0791	0.2355
	L	-0.0018	0.0833	0.2238	0.0027	-0.0711	0.2305
No attenuation or radiation correction	R	-0.0035	0.1608	0.2315	-0.0015	0.0367	0.2539
	L	-0.0042	0.1896	0.2228	-0.0022	0.0582	0.2496
No attenuation correction	R	-0.0030	0.1374	0.2426	0.0088	-0.2198	0.2640
	L	-0.0036	0.1614	0.2330	0.0082	-0.2144	0.2581
No source radiation correction	R	-0.0015	0.0690	0.2373	0.0071	-0.1773	0.2395
	L	-0.0025	0.1115	0.2282	-0.0077	0.2014	0.2346

The estimated linear fit was a function of either distance or period at which $M_s(VMAX)$ was computed (Figure 25). Ideally the corrections should remove the bias introduced by either the attenuation, dispersion or the source excitation. Therefore, the smallest values of the coefficients would correspond to the best estimation. Table 8 shows the regression coefficients computed using the events with at least 20 $M_s(VMAX)$ measurements, for better mean value estimate. The highlighted lines in Table 8 correspond to the case where the linear fit was applied to the magnitudes uncorrected for both the source excitation and the attenuation. The smallest RMS residuals are observed in case when the attenuation correction is applied as a function of station-event distance. Note, that the RMS residuals are computed only for those events used for the inversion.

Approach 2

As we mentioned earlier, the first approach may not give a correct answer if strong trends as a function of the distance or the period exist in the data. The second approach does not rely on the unbiased mean estimate of $M_s(VMAX)$. In order to find this correction we first need the values without the attenuation and the excitation corrections.

$$M_s^0(VMAX) = \log(a_b) + \frac{1}{2}\log\left(\sin(\Delta)\right) - \log(f_c) - 0.43 \tag{23}$$

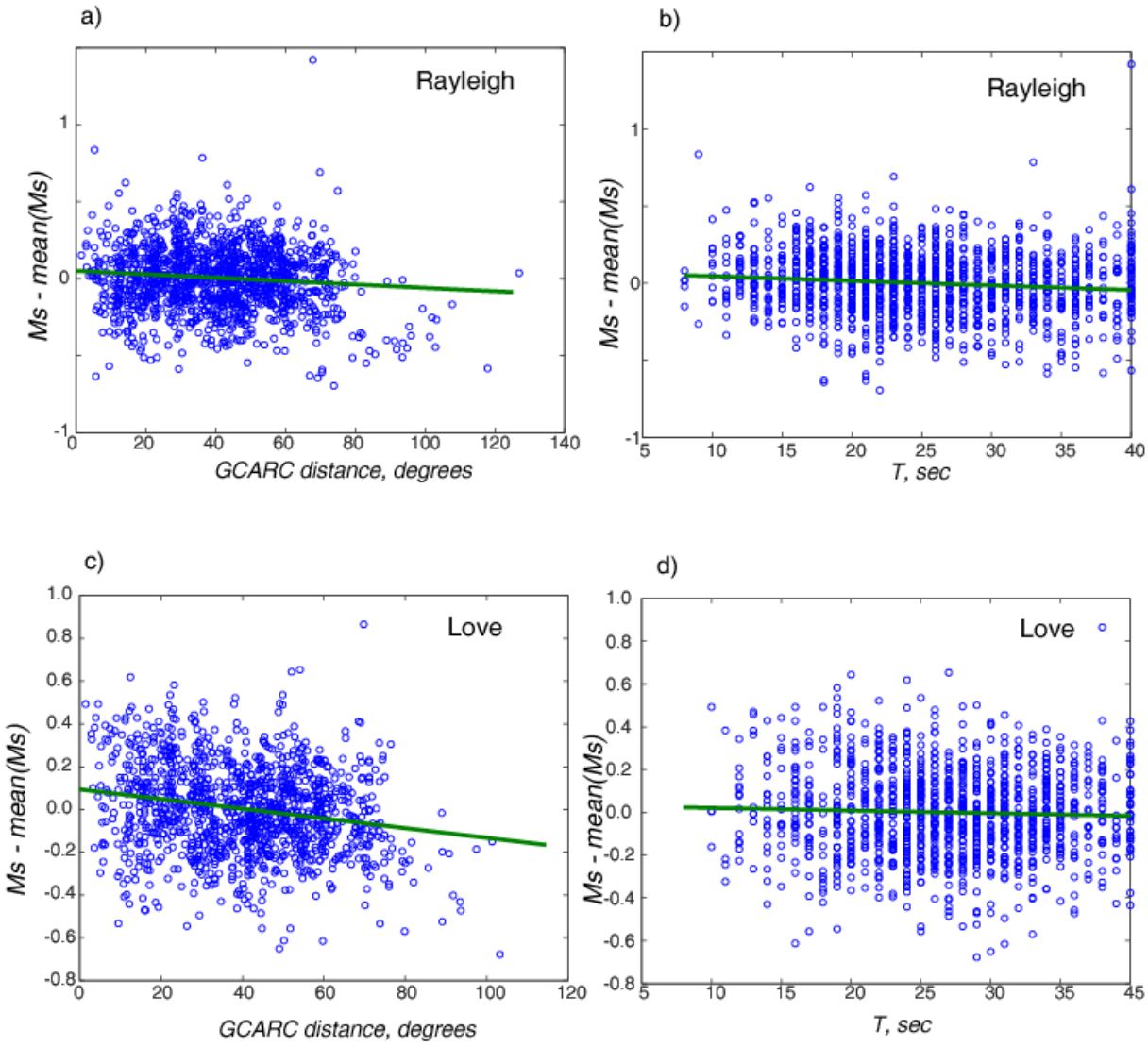

Figure 25. a) Individual station $M_s(VMAX)$ computed using Rayleigh waves with removed mean value for each event plotted against the GC distance between the event and the station; b) Individual station Rayleigh $M_s(VMAX)$ with removed mean value for each event plotted against the period (T) at which the max value was detected; c) Individual station Love $M_s(VMAX)$ computed using Rayleigh waves with removed mean value for each event plotted against the GC distance between the event and the station; d) station Love $M_s(VMAX)$ with removed mean value for each event plotted against the period T. The green lines show the linear fit with parameters provided in Table 8 rows 1 and 2 (Russell formula, all corrections applied).

We then solve a system of equations:

$$M_s^{0,i} = M_s^i - a\Delta_j^i \tag{24}$$

where Δ_j^i is the distance between the i^{th} event and the j^{th} station and $M_s^{0,i}$ is the uncorrected magnitude values obtained using (3), to obtain the corrected magnitudes M_s^i and the attenuation parameter a.

The solution of the inverse problem is shown in Table 9. We tried to incorporate the dependence on the period T into the inverse problem, but it didn't improve the RMS residuals. The final formulas with the distance correction are:

$$M_{s_s}^{R*}(VMAX) = \log(a_b) + \frac{1}{2}\log(\sin(\Delta)) + 0.0037\Delta - \log(f_c) - 0.43 \tag{25}$$

$$M_s^{L*}(VMAX) = \log(a_b) + \frac{1}{2}\log(\sin(\Delta)) + 0.0042\Delta - \log(f_c) - 0.43 \tag{26}$$

The attenuation coefficients are very close to the value obtained by Russell (0.0031 in the original formula (Equation 1) vs. 0.0037 for the Rayleigh waves (Equation 25) and 0.0042 for the Love waves (Equation 26) in our expression. Adding the period-dependent factor did not improve the solution, therefore it was omitted. The results are very similar to the corresponding results obtained with our first approach. The attenuation correction for the Rayleigh waves is 0.0035 (1st) and 0.0037 (2nd), while the Love wave attenuation factor is the same in both cases (0.0042). The standard error however is slightly lower as a result of our second approach. It shows that there is a slight bias due to a limited bandwidth of some estimates.

We compared the magnitude values $M_s(VMAX)$ estimated with Russell formula and with Equations 25 and 26 (Figure 26). The regression lines are given by the following equations:

$$M_{s_s}^{R*}(VMAX) = 1.0085 M_s^{RUS}(VMAX) - 0.0424 \tag{27}$$

$$M_s^{L*}(VMAX) = 1.0201 M_s^{RUS}(VMAX) - 0.0817 \tag{28}$$

Table 9. **The attenuation coefficients obtained by solving the system of Equations 24.**

Wave type	Attenuation coefficient *a*	RMS residuals
Rayleigh	0.0037	0.22
Love	0.0042	0.22

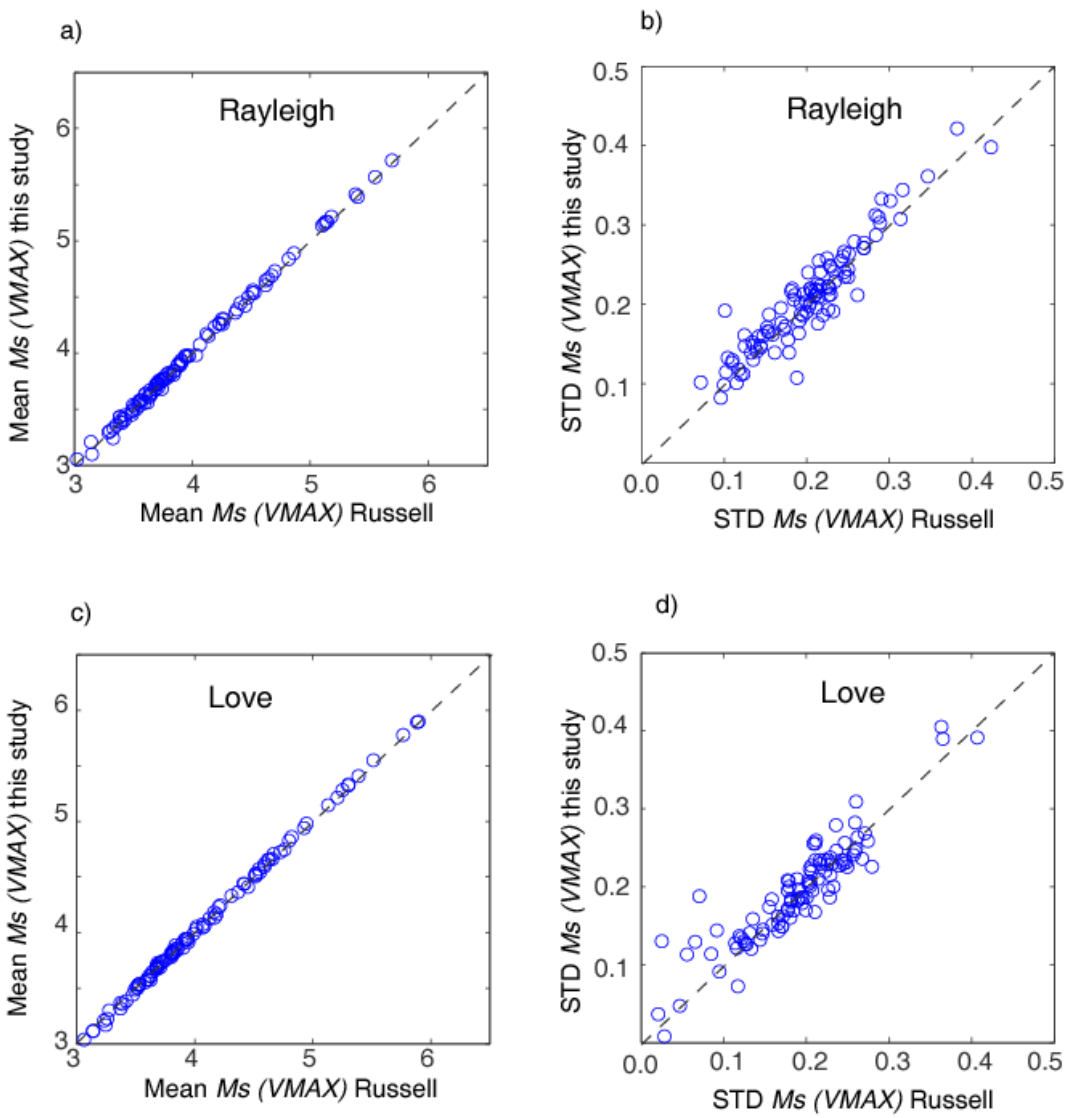

Figure 26. a) Comparison between the $M_s(VMAX)$ estimates obtained using Russell formula (horizontal axis) and Equation 27 (vertical axis) for Rayleigh waves; b) Comparison between the standard errors of $M_s(VMAX)$ estimates obtained using Russell formula (horizontal axis) and Equation 27 (vertical axis) for Rayleigh waves; c) Comparison between the $M_s(VMAX)$ estimates obtained using Russell formula (horizontal axis) and Equation 28 (vertical axis) for Love waves; d) Comparison between the standard errors of $M_s(VMAX)$ estimates obtained using Russell formula (horizontal axis) and Equation 28 (vertical axis) for Love waves.

CONCLUSIONS

We studied the suitability of the Russell (2006) formula for Love waves. We computed the attenuation correction by fitting a linear regression to uncorrected $M_s(VMAX)$ measurements. We used two slightly different approaches to find the coefficients for the empirical Russell formula suitable for the Middle East region. The main difference between the two approaches is the different ways of removing the mean value from the measurements for individual earthquakes. In the first approach we subtract the arithmetic mean and then find linear fits to the equation as a function of either distance or the period. The second approach includes the estimation of the mean as well as the linear trend as a part of the inverse problem.

In application of our first approach we found that the smallest RMS residuals correspond to the case when the attenuation correction is applied as a function of station-event distance to the $M_s(VMAX)$ with both attenuation and the source excitation correction removed. The RMS residuals are computed only for those events used for the inversion. The attenuation coefficient obtained in this case is slightly higher for Love waves (0.0042 for the Love waves *vs*. 0.0035 for the Rayleigh waves). This is expected, since shear waves typically have lower Q. The value of the attenuation used in Russell formula is 0.0031.

We found the best fitting attenuation constants for both Rayleigh and Love waves. The attenuation coefficients calculated as a result are 0.0037 for the Rayleigh and 0.0042 for the Love waves. The attenuation coefficients computed using the two approaches are similar for the Rayleigh waves (0.0035 *vs*. 0.0037) and identical for the Love wave. The standard error however is slightly lower as a result of our second approach, because in addition to fitting the slopes we also adjusted the intercepts. Application of the new corrections improves the residuals for the events used in the inversion; however it does not improve the RMS residuals for the entire data set.

CHAPTER 6: SOURCE AND PATH EFFECTS ON LOVE AND RAYLEIGH WAVE MAGNITUDES IN THE MIDDLE EAST

Anastasia Stroujkova and Jessie Bonner

Weston Geophysical Corporation

INTRODUCTION

We analyzed Rayleigh and Love waves for 120 Middle Eastern events and correlated source information with interpretation of M_s(*VMAX)* magnitude measurements. Most of the events have Love-wave M_s (M_s *L*) greater than M_s Rayleigh (M_s *R*); however for some events, the magnitudes are either equal or M_s *R* greater than M_s *L*. The majority of the events with M_s *R* greater than M_s *L* belong to either (or both) of the two categories: a) deep events (depth greater than 30 km), and b) thrust or dip-slip events. This observation is interesting because this reverse relationship between M_s *R* and M_s *L* is also true for the explosions. Smaller Love wave magnitudes also correlate with low M_s vs. m_b. Scattering of the surface waves could be a significant source of bias in magnitude estimation. Significant heterogeneities along the plate boundaries are the most likely causes of such scattering.

We have applied the M_s*(VMAX)* formula (Russell, 2006; Bonner et al., 2006) using both Love and Rayleigh waves to approximately 120 events (Table 10) located in the Middle East with reported body wave magnitudes (m_b) between 3.8 and 6. Many of these events have the focal mechanism information from the Harvard CMT catalog, while some of the events are deep (depth > 50 km). Figure 10 shows the map of the events of the updated dataset.

As mentioned in Chapter 1, we noted that for the majority of the events in our Middle Eastern earthquake dataset, the M_s*(VMAX)* computed using the Rayleigh waves (M_s *R*) are smaller than the one computed using the Love waves (M_s *L*). Out of 120 events of the dataset, 32 events have M_s *R* > M_s *L* (26%) and 4 events have M_s *R* = M_s *L* (3%) (Figure 28). These events are interesting for monitoring purposes because the Love waves from explosions, if they can be measured or exist, typically have smaller amplitudes than the Rayleigh waves. Therefore, identifying the types of earthquakes with similar features would allow differentiating them from the explosions. Our analysis of events with known focal mechanisms and well-constrained depths shows that the majority of events with higher Rayleigh wave magnitude are either deep events, or events with thrust (normal) focal mechanism, or both. In addition, some of these events also show anomalous M_s:m_b ratios (as discussed later and shown in Table 28). We later show that an additional way to separate the shallow from deep events is by identifying the surface wave higher modes.

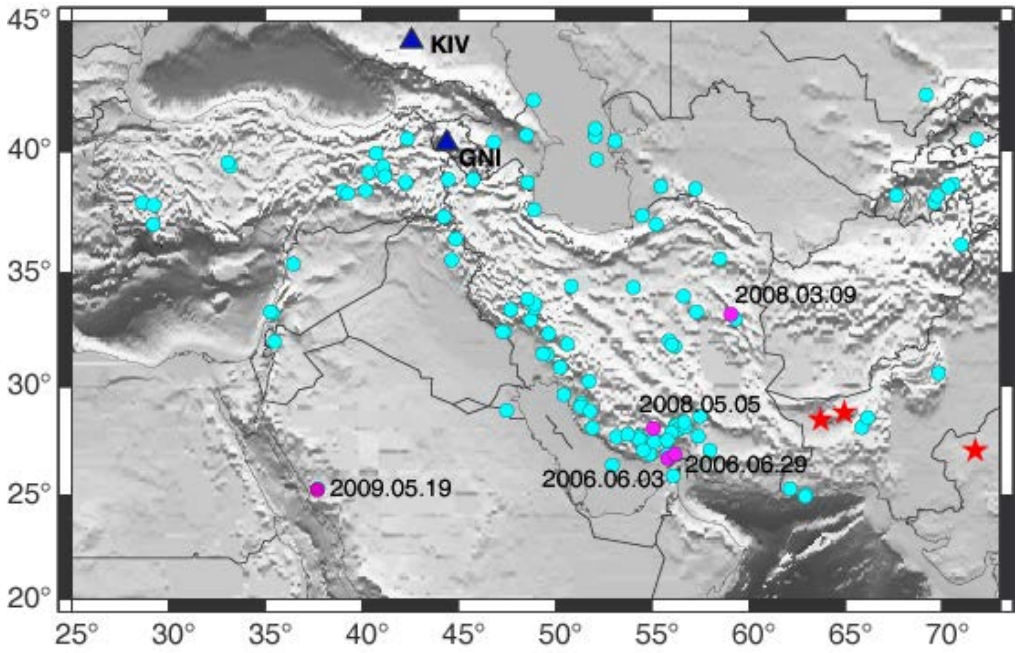

Figure 27. Map of the seismic events (blue circles) for which $M_s(VMAX)$ Love and Rayleigh was estimated. The red stars show the nuclear explosions conducted near the research area. Events highlighted in pink are discussed in this chapter.

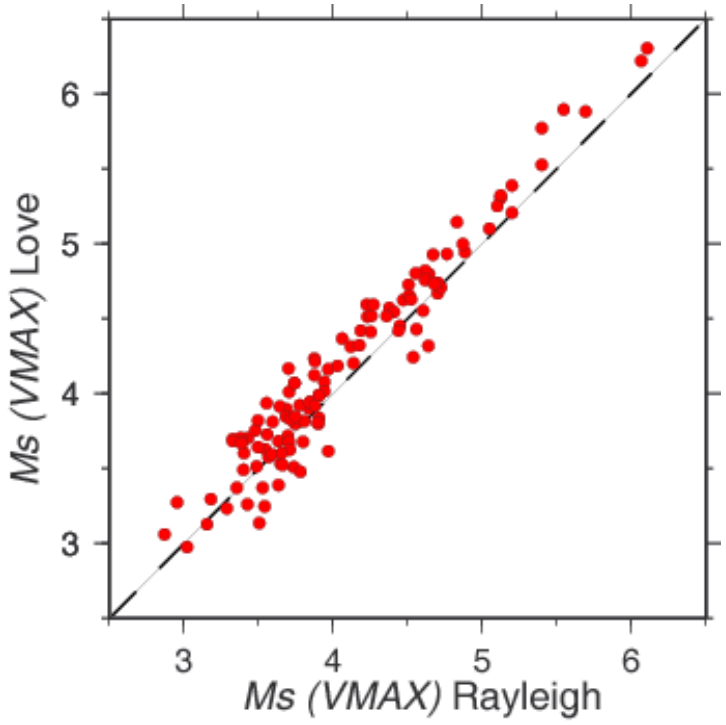

Figure 28. Comparison of M_s computed using Rayleigh and Love waves from 120 events in the Middle East.

Table 10. Updated event catalog used for M_s studies. The events with $M_s\ R > M_s\ L$ are highlighted with blue; the events with $M_s\ R = M_s\ L$ are highlighted with yellow. In the last column, T stands for thrust, SS for strike-slip, and O for oblique.

Event date and time	Latitude, °N	Longitude, °E	Depth, km	m_b (*)	$M_s\ R$	$M_s\ L$	CMT avail.
2006.06.03 07:15	26.759	55.843	12.1	5.40	4.64	4.80	+ (T)
2006.06.03 14:40	39.151	40.362	26-28	4.40	3.88	4.24	
2006.06.05 04:23	37.933	28.675	31-34	4.40	3.91	3.99	+ (T)
2006.06.28 21:02	26.925	55.866	15-16	5.80	5.68	5.88	+ (T)
2006.06.29 16:41	26.798	55.906	15-16	4.60	3.91	3.84	
2006.06.30 05:38	26.8	55.9	21-23	4.60	3.77	3.82	
2006.06.30 15:06	26.9	55.8	26-28	4.40	3.63	3.69	
2006.07.02 19:39	39.274	40.96	11	4.70	4.27	4.59	+ (O)
2006.07.17 22:01	26.72	55.82	15-16	4.40	3.84	3.90	
2006.09.09 04:58	32.02	35.49	1	4.50	4.62	4.76	
2006.09.10 08:57	27.72	54.32	25-28	4.70	4.38	4.55	+ (O)
2006.09.14 02:25	29.255	51.35	19-20	4.90	3.85	3.95	
2006.09.26 08:14	31.909	50.653	29-32	4.50	4.23	4.59	+ (SS)
2006.10.13 10:19	27.62	54.36	17-19	4.60	3.78	3.93	
2006.10.19 21:00	39.927	40.768	5	4.40	3.95	4.14	
2006.11.05 20:06	37.63	48.92	16-18	4.80	4.23	4.51	+ (O)
2006.11.11 02:19	32.37	49.67	9	4.50	3.74	3.51	
2006.11.13 10:59	27.646	55.088	10	4.50	3.65	3.53	
2006.12.29 10:22	28.937	47.496	10	4.60	3.62	3.42	
2007.01.03 14:42	38.716	42.302	4.5	4.40	3.69	3.27	
2007.01.07 15:32	33.986	56.652	37.6	4.50	3.78	3.48	
2007.01.19 05:47	32.97	48.75	26.7	4.50	3.43	3.26	
2007.01.19 10:11	31.45	49.6	15	4.90	3.61	3.53	
2007.01.26 08:20	38.418	40.216	5.5	4.60	4.26	4.52	+ (SS)
2007.02.09 02:22	38.39	39.043	2.6	5.10	5.13	5.30	+ (O)
2007.02.12 18:30	29.63	50.471	10	4.40	3.69	3.89	
2007.02.17 08:45	40.51	42.357	5	4.60	4.25	4.26	
2007.02.21 11:05	38.318	39.275	6	5.60	5.38	5.51	+ (O)
2007.02.27 22:28	28.1	55.08	28	4.50	4.19	4.42	+ (T)
2007.03.06 22:32	33.49	48.93	16	4.70	4.06	4.37	
2007.03.17 14:20	27.091	58.021	14.1	4.90	3.71	4.17	
2007.03.18 14:19	28.129	51.939	39.1	4.30	3.51	3.14	
2007.03.23 21:38	27.47	55.15	14	4.80	4.41	4.54	+ (T)
2007.03.26 11:00	28.65	57.49	5-75(?)	4.60	3.90	3.80	
2007.04.09 21:26	38.88	44.487	5	4.40	3.80	3.68	
2007.04.18 00:14	30.88	50.27	15	4.60	3.50	3.82	
2007.04.25 04:19	28.19	56.22	15.9	5.10	4.67	4.93	+ (T?)
2007.04.25 20:02	28.23	56.27	32-35	4.80	3.97	4.17	
2007.04.26 04:03	28.23	56.24	12-15	4.60	3.56	3.73	
2007.04.26 04:59	28.18	56.31	14-16	4.60	3.43	3.71	

2007.04.26 14:11	28.084	56.389	3-6	4.10	3.33	3.70	
2007.04.28 21:22	28.23	56.26	14.1	4.50	3.55	3.63	
2007.04.29 06:33	25.316	62.154	28.8	5.00	4.25	4.41	
2007.05.01 23:38	28.078	56.388	24.2	3.80[I]	3.14	3.14	
2007.05.05 21:11	38.788	42.274	26-28	4.40	3.98	3.88	
2007.05.06 03:53	25.033	62.987	27-29	4.60	3.72	3.83	
2007.05.06 10:57	24.954	62.941	27-29	4.80	4.12	4.31	
2007.05.08 03:28	31.8	56.2	24	4.20	3.50	3.64	
2007.05.11 05:50	34.38	54.04	6	4.10	2.96	3.27	
2007.05.11 20:42	40.72	52.051	37.4	4.40	3.15	3.00	
2007.05.16 00:19	27.9	56.02	7	4.40	3.48	3.75	
2007.05.18 23:03	27.734	53.161	32	4.70	3.94	4.08	
2007.05.26 22:54	40.601	52.086	37	4.50	3.66	3.52	
2007.05.28 14:12	30.232	51.749	10	4.50	3.38	3.71	
2007.05.31 10:28	29.107	51.321	5.9	4.10	3.41	3.60	
2007.06.18 14:29	34.414	50.852	17-18	5.10	5.12	5.31	+ (T)
2007.07.04 06:10	32.071	55.908	15-16	4.70	4.47	4.62	+ (OSS)
2007.07.04 09:51	31.877	56.06	0	4.20	4.02	4.02	
2007.07.08 13:44	36.421	44.86	32.8	4.40	3.64	3.92	
2007.07.11 06:51	38.751	48.598	27-29	4.90	4.36	4.52	+ (OT)
2007.07.23 17:54	27.55	55.79	16-17	4.70	3.70	3.72	
2007.07.24 13:41	42.01	48.882	66.5	4.70	3.63	3.39	
2007.08.05 22:20	37.945	69.596	41.9	4.40	3.61	3.67	
2007.08.08 03:28	28.139	65.857	24.6	4.50	3.74	4.07	
2007.08.19 13:45	38.588	55.469	30	4.80	4.03	4.19	
2007.08.23 01:52	40.636	48.518	33-35	4.60	3.75	3.85	
2007.08.25 22:05	39.382	41.124	10	5.10	4.82	5.13	+ (OSS)
2007.08.28 09:30	28.17	56.74	23-25	4.90	3.88	4.22	
2007.09.05 12:27	28.399	56.684	14	4.80	3.56	3.94	
2007.09.09 02:00	30.6	69.808	0	5.20	5.10	5.25	+ (SS)
2007.09.18 20:53	35.544	44.665	13-33(?)	4.50	3.71	3.68	
2007.09.21 10:21	37.343	44.272	14-23(?)	4.50	3.75	3.80	
2007.10.19 07:19	28.598	66.177	0	5.10	5.18	5.39	+ (SS)
2007.10.29 09:23	37.033	29.233	5	4.90	4.86	4.95	+ (T)
2007.11.08 09:40	33.67	48.94	14.1	4.70	3.39	3.68	
2007.12.20 09:48	39.417	33.212	10	5.20	5.40	5.77	+ (O)
2008.01.05 00:37	26.900	54.9	24	4.60	3.57	3.58	
2008.01.05 08:07	31.47	49.37	29.7	4.50	4.45	4.45	
2008.01.06 14:22	37.396	54.516	10	4.00	3.54	3.25	
2008.01.19 21:41	33.319	57.307	27.9	4.40	3.84	3.94	
2008.01.28 01:20	28.89	51.81	3	4.20	3.69	3.85	
2008.02.02 05:33	26.41	52.976	10	4.90	3.90	3.81	
2008.02.07 20:15	27.84	53.74	9	4.50	3.86	3.91	
2008.02.11 23:47	33.26	35.416	0	4.30	3.59	3.59	
2008.02.15 10:36	33.327	35.305	10	5.00	4.56	4.80	+ (OSS)
2008.02.27 11:10	33.00	59.34	5	3.80[I]	3.33	3.68	
2008.02.29 19:57	38.498	57.258	10	4.70	3.71	4.01	
2008.03.01 16:38	26.88	56.19	5	4.60	3.53	3.37	
2008.03.09 03:51	33.21	59.11	31	4.90	4.62	4.82	+ (OSS)
2008.03.15 10:15	39.566	33.074	10	4.40	4.22	4.43	

2008.03.18 03:56	37.03	55.22	22	4.30	3.49	3.51	
2008.03.22 15:51	33.460	47.570	6	4.40	3.29	3.23	
2008.04.16 10:39	40.894	52.076	13	4.70	3.71	3.62	
2008.04.25 04:48	37.819	29.256	5	4.50	4.14	4.20	+ (OT)
2008.04.30 02:40	38.696	70.580	55.8	4.10	3.16	3.13	
2008.05.01 00:15	33.86	48.59	16	4.50	3.74	4.07	
2008.05.05 21:57	28.429	54.082	50	5.30	4.70	4.67	+ (T)
2008.05.10 22:25	39.677	52.152	22	4.50	3.97	3.62	
2008.05.31 01:24	27.1	54.57	14	4.80[B]	3.60	3.81	
2008.06.29 15:37	38.992	41.225	3.9	4.00	3.66	3.60	
2008.07.03 23:10	35.58	58.527	25	5.00[N]	4.51	4.65	+ (T)
2008.08.27 21:52	32.439	47.408	10	5.20[C]	5.54	5.87	+ (SS)
2008.08.28 06:06	40.477	71.799	60.9	4.00	3.18	3.30	
2008.09.02 20:00	38.874	45.777	25	5.00	4.53	4.63	+(SS)
2008.09.03 22:43	32.434	47.358	30	5.30	4.51	4.73	+(T)
2008.09.10 11:00	26.743	55.828	12.0	6.10	6.07	6.22	+(T)
2008.09.17 12:08	40.010	39.979	5.4	4.80	4.18	4.32	+(SS)
2008.09.17 17:43	27.025	56.182	24.6	5.30	4.87	5.00	+(T)
2008.10.05 22:56	33.886	69.470	10	6.00	6.11	6.30	+(SS)
2008.10.25 20:17	26.533	54.985	28.8	5.20	5.05	5.10	+(OT)
2008.11.12 14:03	38.841	35.524	10	4.80	4.68	4.73	+(OSS)
2008.12.08 14:41	26.920	55.850	6.1	5.50	4.70	4.74	+(OT)
2008.12.09 15:09	26.753	55.695	26.8	5.20	4.60	4.55	+(T)
2009.02.02 08:36	27.180	66.307	10	5.00	4.77	4.93	+(SS)
2009.02.17 05:28	39.107	29.039	7	4.80	4.72	4.71	+(OT)
2009.04.25 17:18	45.676	26.527	101.0	5.30	4.54	4.24	+(T)
2009.04.30 10:04	27.753	61.431	70.0	5.20	4.64	4.32	+(O)
2009.05.10 17:34	38.233	67.630	22	5.30	4.56	4.43	+(T)
2009.05.19 16:54	25.25	37.70	10	5.10	4.53	4.51	
2009.05.19 17:35	25.292	37.744	2	5.70	5.67	5.54	+(T)
2009.06.02 14:39	40.294	52.994	51	4.90	4.44	4.42	+(OSS)
2009.06.17 09:22	38.213	69.744	19	4.40	3.88	3.92	

* Most of the event locations and m_bs were determined by the NEIC. Values for the few events for which NEIC results were not available were determined by the [I] – ISC, [B] – BJI, [C] – CSEM, or [N] – NNC.

Table 11. Analysis of the events which failed one or more discrimination criteria. Two nuclear explosions are added for comparison.

Event date and time	Latitude, ºN	Longitude, ºE	Depth, km	m_b (NEIC/ IDC)	*Ms*	M_s*(VMAX)* *R/L*	M_s *L* - M_s *R*	Murph. Discr IDC	Murph. Discr M_s*(VMAX)* NEIC	Murph. Discr M_s*(VMAX)* IDC	*pP* depth	Higher modes
Earthquakes												
2007.01.19 10:11	31.45	49.6	15	4.90/ 4.10	3.6	3.61 / 3.53	-0.08	0.55	0.08/-0.01	0.59/0.51	-	+
2007.04.26 04:59	28.18	56.31	14.1	4.60/ 4.30	3.2	3.43 / 3.71	0.28	-0.08	0.28/0.56	0.15/0.43	16	
2007.05.11 20:42	40.72	52.051	37.4	4.40/ 4.10	3.2	3.15 / 3.00	-0.15	0.17	0.25/0.1	0.12/-0.03	46	+
2007.07.24 13:41	42.01	48.882	66.5	4.70/ 4.40	3.4	3.63 / 3.39	-0.24	0	0.45/0.11	0.23/-0.01	68	+
2008.02.02 05:33	26.41	52.976	10	4.90/ 4.70	3.5	3.90 / 3.81	-0.09	-0.28	0.37/0.29	0.12/0.03	-	
2008.08.28 06:06	40.477	71.799	60.9	4.00/ 4.10	2.9	3.18 / 3.30	0.12	-0.13	0.78/0.9	0.15/0.27	-	
2009.04.25 17:18	45.676	26.527	101.0	5.30/ 5.10	4.0	4.54 / 4.24	-0.30	-0.28	0.51/0.21	0.26/-0.03	101	+
2009.04.30 10:04	27.753	61.431	70.0	5.20/ 5.00	4.1	4.64 / 4.32	-0.32	-0.05	0.74/0.42	0.49/0.17	70	+
Explosions												
1998/05/11 10:13	27.078	71.719	0.0	5.20/ 5.10	3.8	3.30/ 3.35	0.05	-0.48	-0.60/ -0.55	-0.98/-0.93	15	
1998/05/28 10:16	28.903	64.893	0.0	4.80/ 4.90	3.6	3.35/ 3.25	-0.10	-0.42	-0.05/ -0.15	-0.67/ -0.77	-	

RESEARCH ACCOMPLISHED

Velocity Model Development, Focal Mechanism and Depth Computation

The velocity structure of Iran is highly heterogeneous and is not well constrained due to poor station coverage. We obtained a regional velocity model using the surface wave amplitude inversion technique (Herrmann and Ammon, 2002). Surface wave inversion was performed using program *surf96* (Herrmann and Ammon, 2002). This code implements an iterative weighted inversion to obtain velocity structure from dispersion curves. The inversion of the surface waves is highly non-unique. The resulting velocity model was later used to invert the spectral amplitudes of Rayleigh and Love waves for event depth and focal mechanism using source inversion codes (Herrmann and Ammon, 2002) in the Computer Programs in Seismology (CPIS). We used the program *srfgrd96*, which performs a grid search over a model space of moment M_0, focal depth h, and mechanism (strike ϕ, dip δ, and rake λ) to minimize the misfit between observed and predicted surface-wave amplitude spectra. The input required for the inversion consists of the amplitudes of the fundamental Rayleigh and Love waves and a 1-D regional Earth model.

We performed the velocity inversion in two steps. A first inversion was performed by fixing layer depths and changing the velocities. For this procedure we selected a two-layer crust to match the common *iasp91* model and set the crustal depth to 35 km. A second inversion was

performed by fixing and varying the layer depths. The results with different layer thicknesses are shown in Figure 29a-b. The starting model in both cases was *iasp91*. Figure 29a shows the inversion (2-step procedure) results for a 2-layer crust and 2 layer mantle (model *iran1*). For the second inversion (model iran2) we divided the crust into 5 km layers and the mantle into 10 km layers.

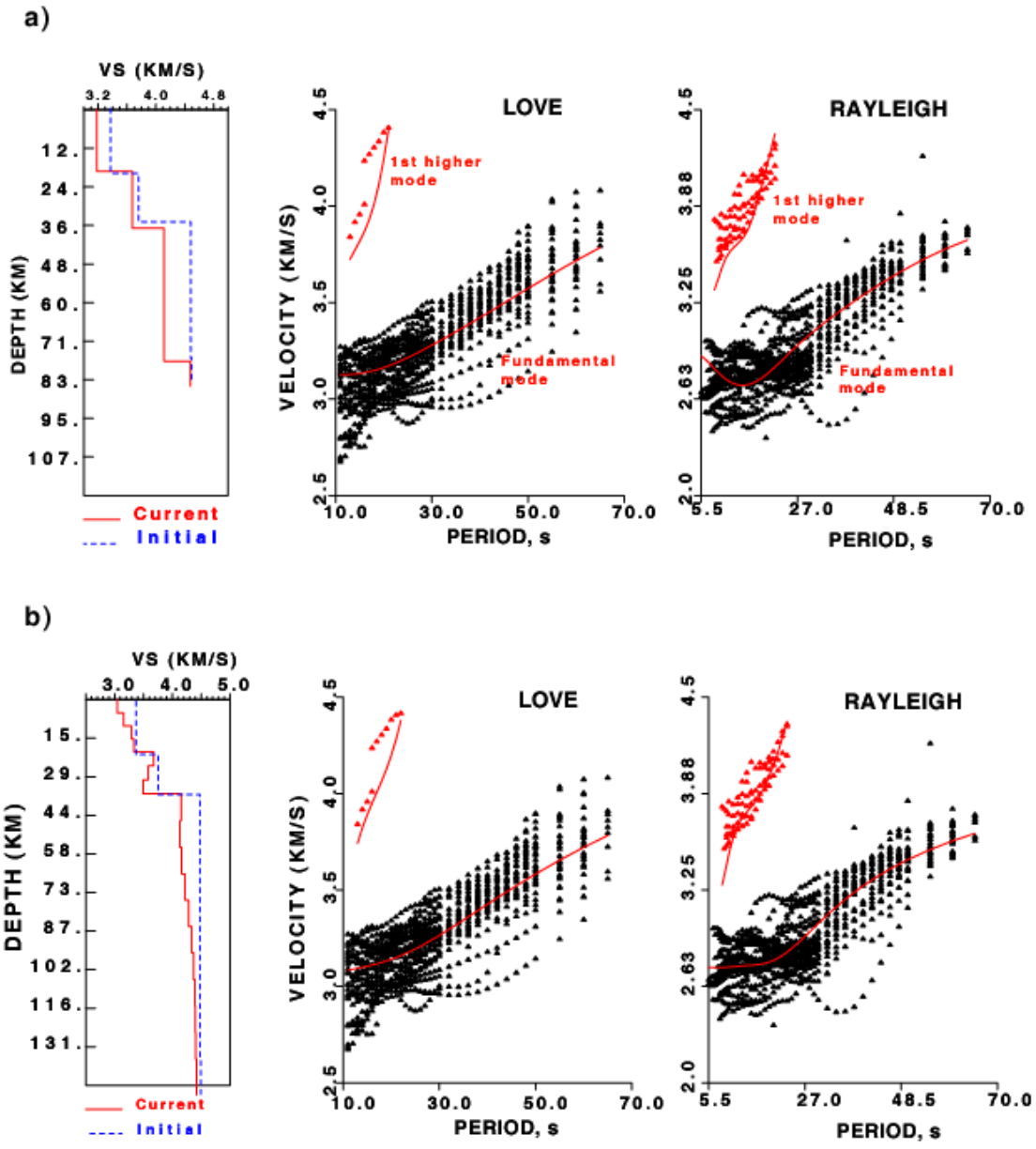

Figure 29. a) Shear velocity profile derived from inversion of surface wave dispersion curve using 2-layer crust (*iran1*); middle panel shows the dispersion curves (Love waves) picked from the data (black dots) and a theoretical curve (red line) for the best fit model; the right panel shows the dispersion curves for Rayleigh waves. Red triangles show picks for suspected 1st higher mode. b) Shear velocity profile derived from inversion of surface wave dispersion curve using 7-layer crust (*iran2*).

Both velocity models have slower velocities below the Moho than *iasp91*. These results contradict some other velocity studies in the area (e.g. Hatzfeld et al., 2003). The model iran2 has also a peculiar velocity inversion in the lower crust. The presence of a low-velocity layer below the Moho was predicted from a receiver function study by Doloei and Roberts (2003).

The surface-wave amplitude spectra needed for the inversion were obtained by applying multiple-filter analysis (Herrmann, 1973; Bhattacharya, 1983) to surface waves observed at regional distances from our study events. For this study, we applied the method to estimate the moment magnitudes (*Mw*), depths and focal mechanisms for the 40 events with known focal mechanisms (Table 10). Figure 30 shows a comparison between the moment magnitudes from CMT bulletin and the values obtained in this study.

Figure 31 shows a comparison between some of the focal mechanisms obtained using the srfgrd96 and the corresponding Harvard CMT solutions. The surface wave inversion method can produce spurious results if the incorrect velocity model is used. This can be potentially troublesome, especially in areas with strong lateral velocity variations, including active tectonic belts, continental shelves etc. Strike-slip mechanisms are usually better resolved than the dip-slip or oblique mechanisms.

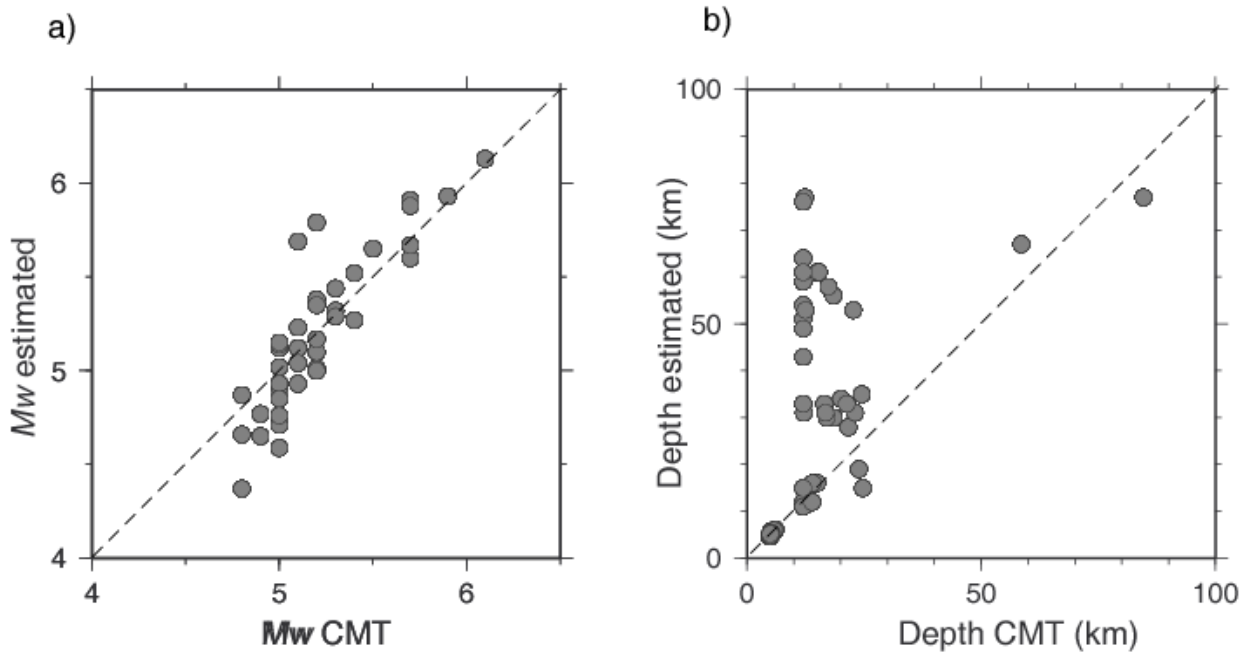

Figure 30. Comparison of M_w (a) and depth (b) computed using *srfgrd96* program (Herrmann, 2004) and the values reported in the CMT bulletin.

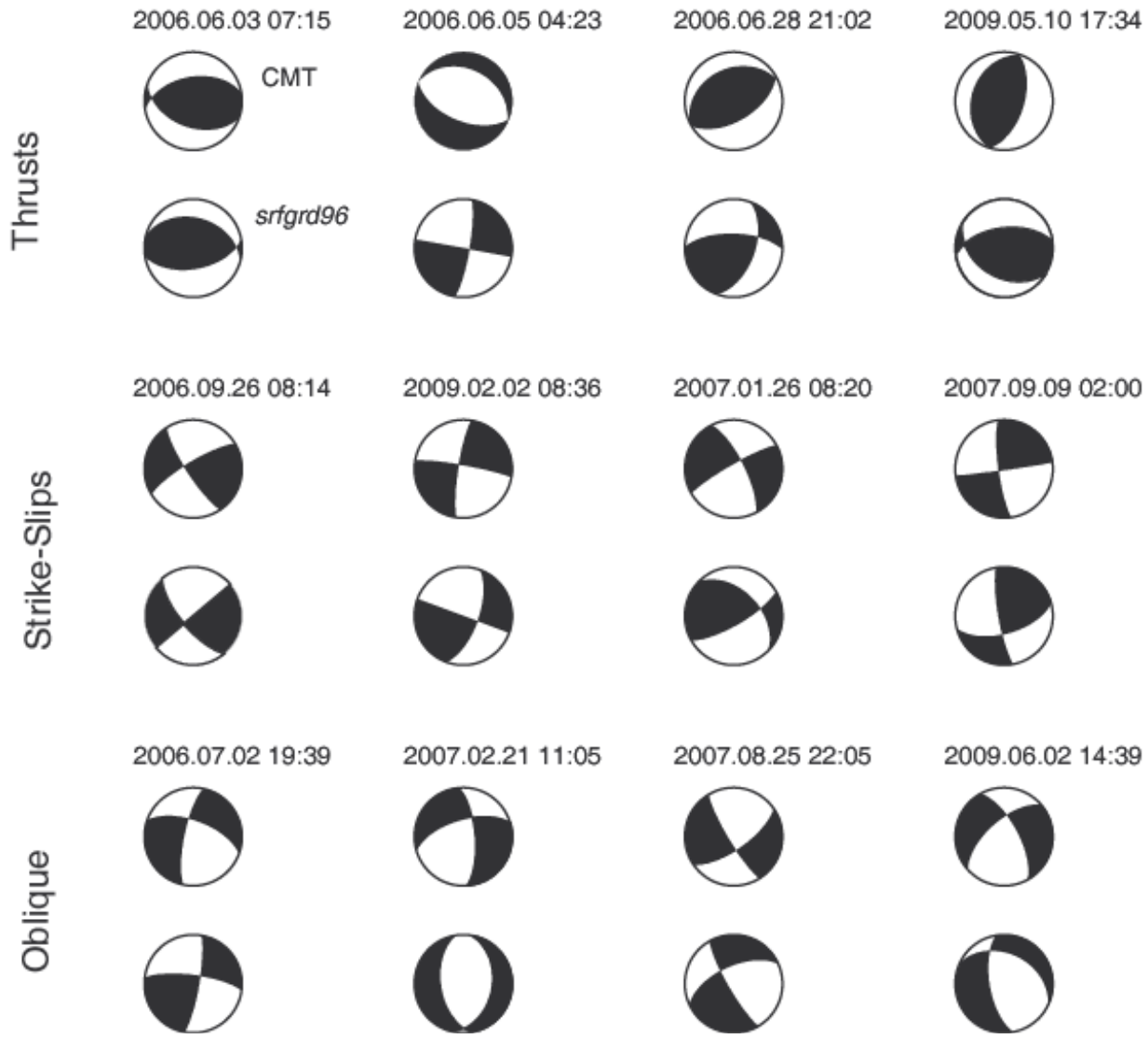

Figure 31. Comparison of the focal plane solutions from Harvard CMT bulletin and the solutions computed using srfgrd96 program (Herrmann, 2004).

Figures 32 and 33 show some examples of events with $M_s(VMAX)$ Rayleigh greater than Love. Both of the events have thrust source mechanisms, even though the event 2009.05.19 is very shallow. It appears that the deep events typically have *Ms R* > *Ms L* regardless of their focal mechanism, while shallow events with *Ms R* > *Ms L* are more likely to be normal or thrust events.

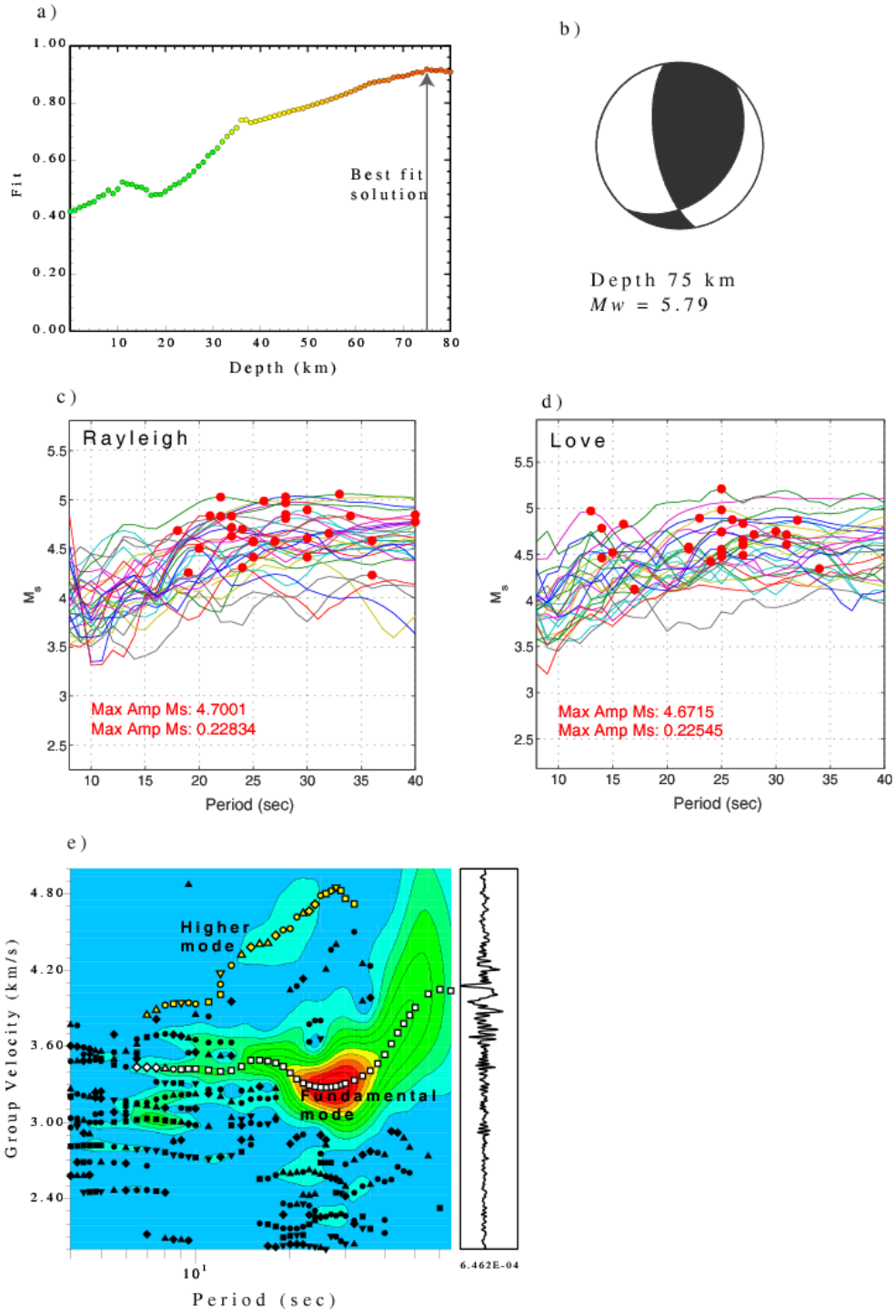

Figure 32. a) The results of the depth estimate for the event 2008.05.05 (USGS depth 50 km). The maximum of the fit function indicates the solution for depth. b) The focal plane solution. c) $M_s(VMAX)$ estimate using the Rayleigh waves. d) $M_s(VMAX)$ estimate using the Love waves. e) The multiple filter analysis for the event 2008.05.05 recorded by station GNI (Z component). In addition to a fundamental model of the Rayleigh waves the higher mode can also be observed.

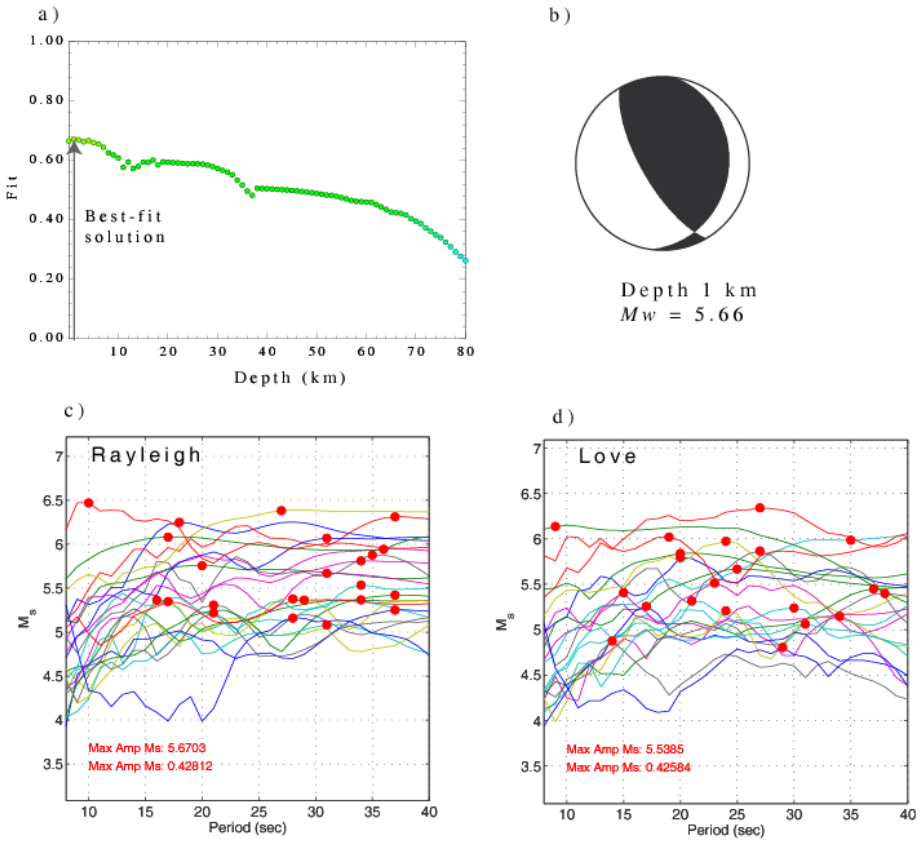

Figure 33. a) The results of the depth estimate for the event 2009.05.19 (USGS depth 2 km). The maximum of the fit function indicates the solution for depth. b) The focal plane solution. c) $M_s(VMAX)$ estimate using the Rayleigh waves. d) $M_s(VMAX)$ estimate using the Love waves.

Higher Modes

Surface wave higher modes are typically observed for deeper events and the events with a dip-slip type of the source mechanism. This happens because the excitation of the fundamental mode becomes less efficient with depth. Figures 34 and 35 show the data and synthetics for events 2006.06.29 and 2009.05.19. The synthetics were computed for different depths, including the estimated event depth. Notice increase of the relative amplitude of the higher modes with increased depth. The data from the shallow event (2009.05.19) do not show any amplitude increase associated with the higher modes, while the mid-crustal event (2006.06.29) has higher modes with appropriate amplitudes for the inferred depth.

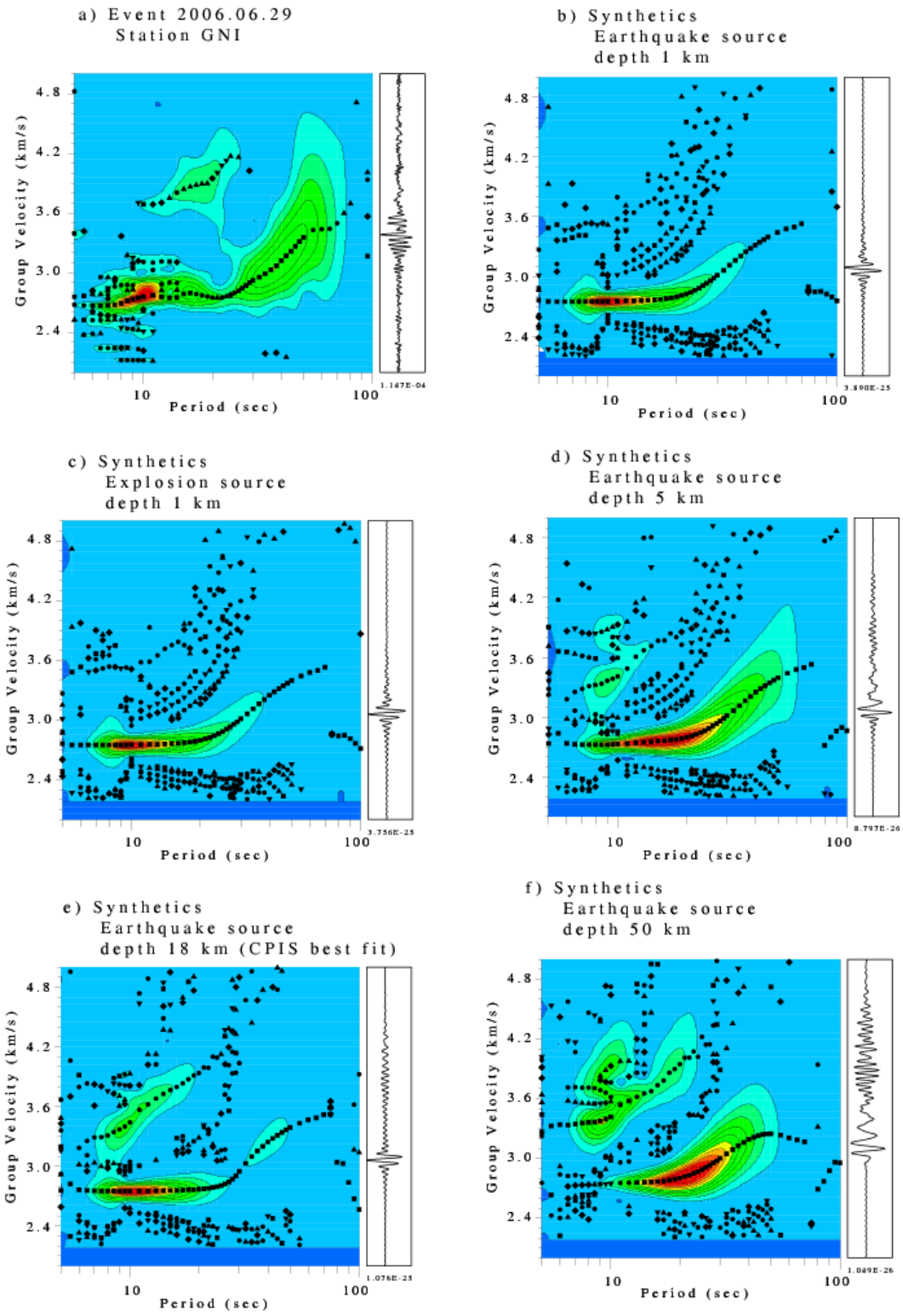

Figure 34. a) Multiple filter analysis for event 2006.06.29 recorded by station GNI; b)-f) synthetics for the same event-station configuration with varying depth. We used the focal mechanism obtained using srfgrd96 program.

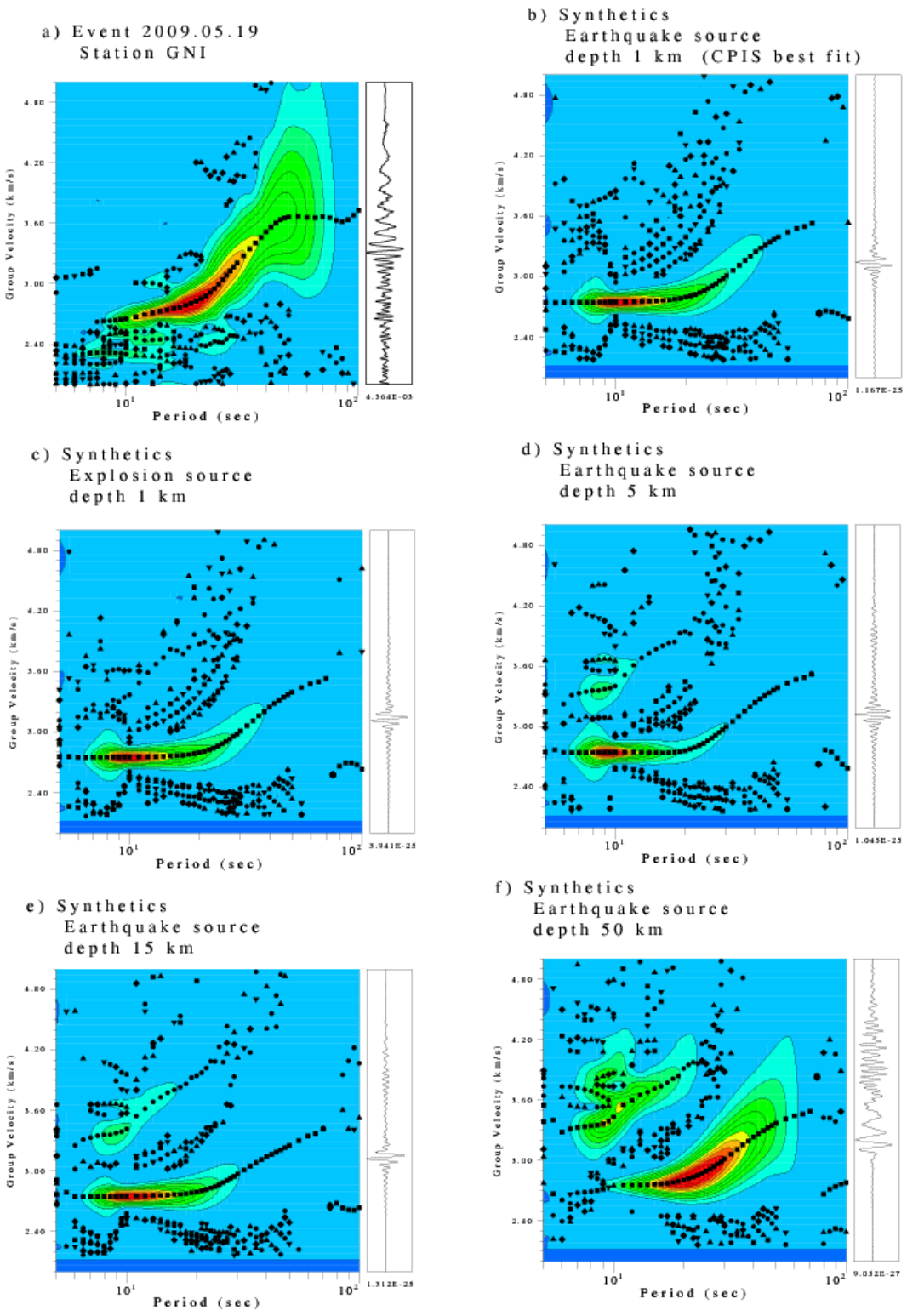

Figure 35. a) Multiple filter analysis for event 2009.05.19 recorded by station GNI; b)-f) synthetics for the same event-station configuration with varying depth. We used the focal mechanism obtained using srfgrd96 program.

Effects of Scattering on $M_s(VMAX)$

In our previous work we observed that the surface wave amplitudes recorded at the stations located to the NW of the Middle Eastern region are reduced with respect to the amplitudes in the NE. Figure 36 shows the results of the multiple filter analysis of the seismic data recorded by stations GNI and KIV. Station KIV is located approximately 500 km NW from station GNI (Figure 27). These stations are separated by the Greater Caucasus mountain range. There is a significant scattering of the Rayleigh waves observed at station KIV compared to GNI. This corresponds to the amplitude reduction, leading to biased (reduced) $M_s(VMAX)$ measured by station KIV with respect to the mean value of $M_s(VMAX)$ averaged between all reporting stations, as shown in Figure 37. Since these two stations are separated by only a short distance, we can assume that the significant amplitude reduction is caused by scattering in the Caucasus Mountain region. This magnitude reduction is important, because it may cause anomalously low M_s:m_b ratios.

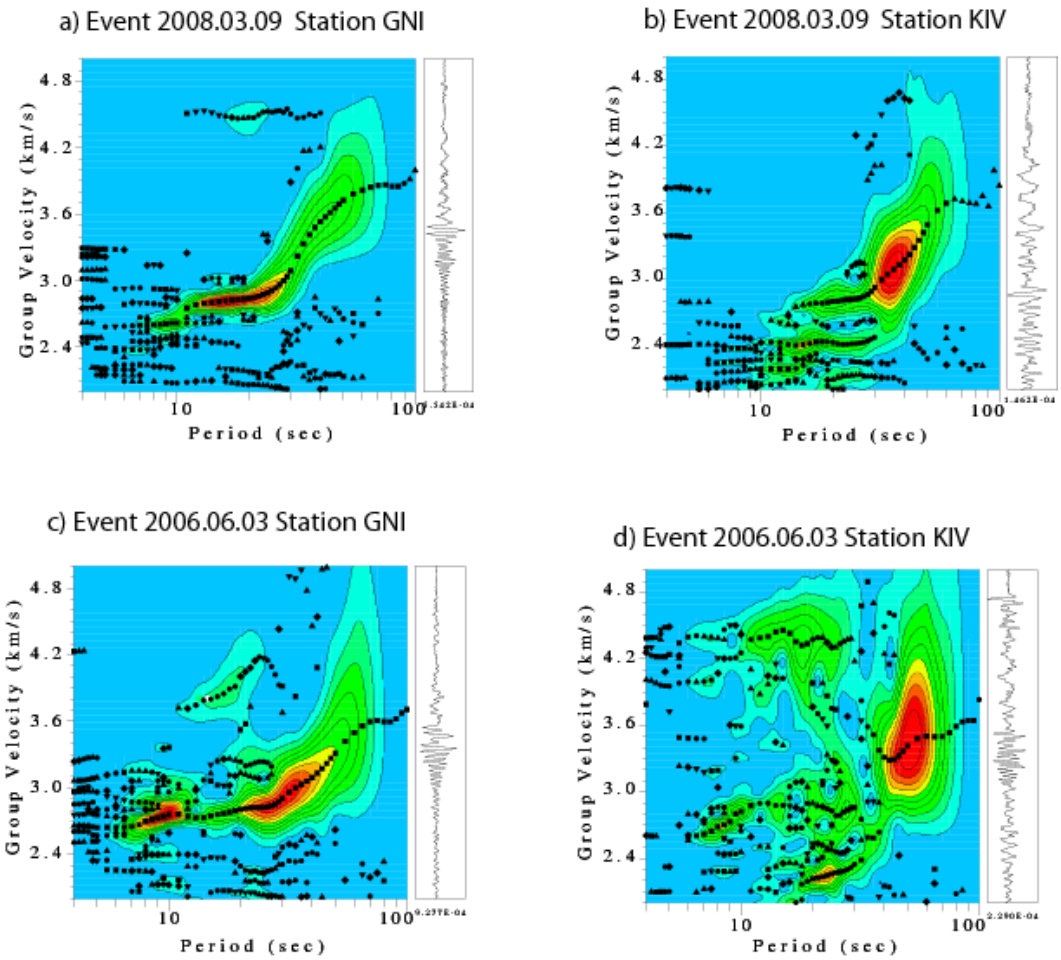

Figure 36. Multiple filter analysis for event 2008.03.09 recorded by a) station GNI and b) station KIV, and event 2006.06.03 recorded by c) station GNI and d) station KIV.

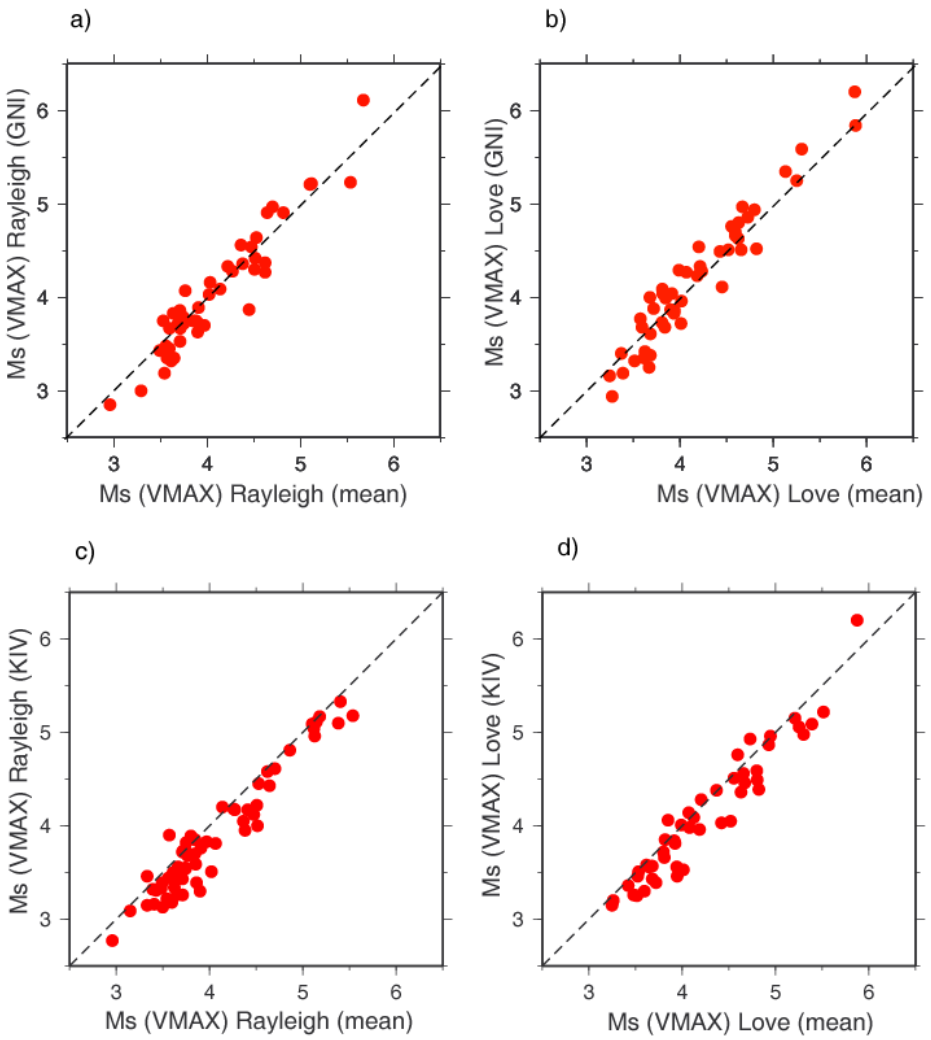

Figure 37. M_s(VMAX) computed for stations GNI and KIV versus the mean values of *Ms*(VMAX): a) station GNI, Rayleigh waves, b) station GNI, Love waves, c) station KIV, Rayleigh waves, d) station KIV, Love waves.

Examples of Event Discrimination

We tested the whether or not the relationship between M_s R and M_s L could be used to discriminate between earthquakes and explosions. It was mentioned earlier that approximately 26% of the earthquakes have M_s R > M_s L, which is also typical for the explosions. We also mentioned that some of these events have low M_s vs m_b. To be classified as an explosion the event should satisfy the following criteria (Murphy et al, 1997):

$$Ms < 1.25\, mb_{IDC} - 2.1 \text{ or} \tag{29}$$

$$Ms < 1.25\, mb_{NEIC} - 2.6 \tag{30}$$

Figure 38 shows m_b vs. $M_s(VMAX)$ for the events of the dataset. Table 11 shows the list of the events which fail at least one of these criteria for either Ms (IDC) or $M_s(VMAX)$. We also provide the data for two nuclear explosions for comparison. There are 8 earthquakes listed in Table 11 (6.7% of the dataset), and 6 of them have M_s R > M_s L. Five of these events are deep, which may account for the reduced surface wave generation. For 5 of these events the depth was verified by using the depth phases. Strangely, one of the explosions was determined to have the depth of 15 km based on the "depth phases."

Additionally we indicated the events which exhibit observable higher modes. These higher modes can be observed due to inefficient radiation of the fundamental modes for deeper events. Five of these events have these phases. I think using these phases may be an additional criterion in determining the event depth and ruling them out as earthquakes.

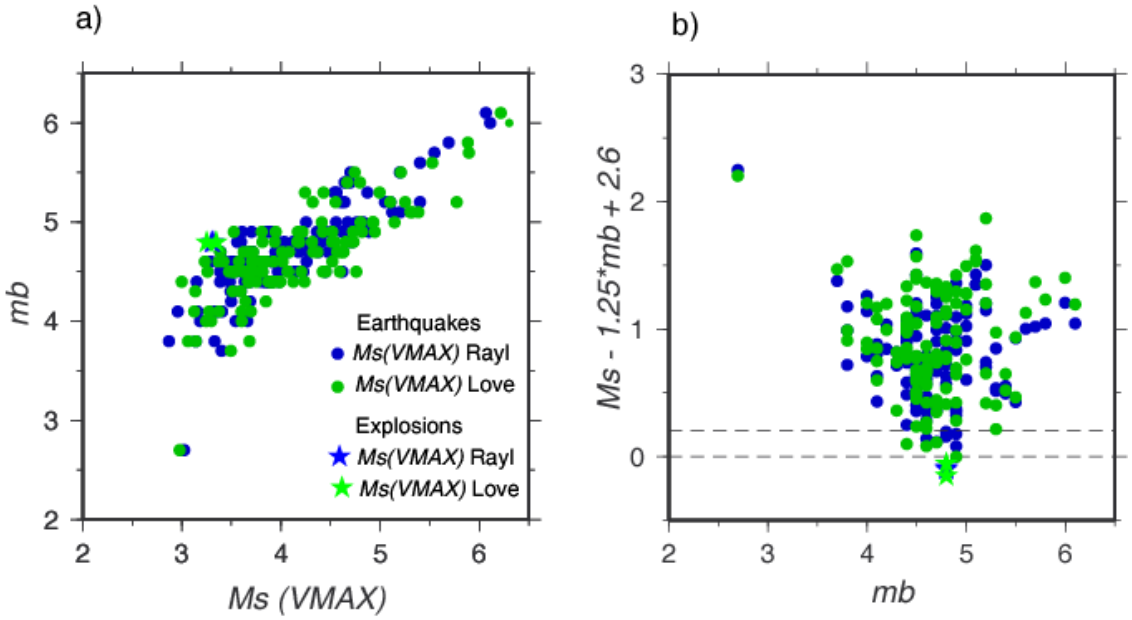

Figure 38. a) Plot of m_b vs. M_s(VMAX) computed for the events of the dataset and two nuclear explosions, b) value $M_s - 1.25m_b+2.6$ (criterion 1) plotted against m_b. All but one earthquake screened according to Murphy et al (1997) criterion. Several more events failed criterion 2.

CONCLUSIONS

In this chapter, we analyzed Rayleigh and Love waves and obtained some additional information to aid with interpretation of the magnitude measurements. We calculated $M_s(VMAX)$ for 120 Middle Eastern events. In addition we computed moment magnitudes *Mw*, depths and focal mechanisms for all the events with Harvard CMT solutions using CPIS software.

Most of the events have M_s *L* greater than M_s *R*; however for some events this is not true. The majority of the events with M_s *R* greater than M_s *L* belong to either (or both) of the two

categories: a) deep events (depth greater than 30 km), and b) thrust or dip-slip events. This observation is interesting because this reverse relationship between M_s R and M_s L is also true for the explosions. Low Love wave magnitudes also correlate with low M_s vs. m_b.

Scattering of the surface waves could be a significant source of bias in magnitude estimation. Significant heterogeneities along the plate boundaries are the most likely causes of such scattering.

The surface wave higher modes can be used for the event screening, because they are mostly observable for deeper events.

REFERENCES

Aki, K., and P.G. Richards, (2002). Quantitative seismology, University Science Books, Sausalito, CA.

Anderson, D.N., D.K. Fagan, M.A. Tinker, G.D. Kraft and K.D. Hutchenson, (2007). A mathematical statistics formulation of the teleseismic explosion identification problem with multiple discriminants. *Bull. Seism. Soc. Am*. **97**, 1730-1741.

Anderson, D. N., H.J. Patton, S.R. Taylor, J.L. Bonner and N.D. Selby, (2013). Sources of Error and the Statistical Formulation of $M_s|mb$ Seismic Event Screening Analysis, *Pure Appl. Geophys,* (submitted).

Berger, J., P. Davis, and G. Ekstrom, (2004). Ambient earth noise: a survey of the Global Seismographic Network, *J. Geophys. Res*. **109**: B11307.

Bhattacharya, S.N., (1983). Higher order accuracy in multiple filter technique, Bull. Seism. Soc. Amer. 73, 1395–1406.

Bonner, J.L., D. Russell, D. Harkrider, D. Reiter, and R. Herrmann, (2006). Development of a Time-Domain, Variable-Period Surface Wave Magnitude Measurement Procedure for Application at Regional and Teleseismic Distances, Part II: Application and M_s —m_b Performance. *Bull. Seism. Soc. Am.* **96***,* 678 – 696.

Bonner, J. L., R. B. Herrmann, D. Harkrider, and M. Pasyanos, (2008). The surface wave magnitude for the 9 October 2006 North Korean nuclear explosion. *Bull. Seism. Soc. Am*., **98**, 2598-2506.

Bonner, J. L., A. Stroujkova, and D. Anderson, (2011). Determination of Love- and Rayleigh-wave magnitudes for earthquakes and explosions. Bull. Seism. Soc. Am. 101. 3096-3104.

Cho, K. H., R. B. Herrmann, C. J. Ammon, and K. Lee, (2007). Imaging the upper crust of the Korean peninsula by surface-wave tomography, *Bull. Seismol. Soc. Am.* **97**, 198-207.

Doloei, J. and R. Roberts, (2003). Crust and uppermost mantle structure of Tehran region from analysis of teleseismic P-waveform receiver functions, *Tectonophysics*, **364**, 115-133.

Evernden, J. F., and W. M. Kohler, (1976). Bias in Estimates of m_b at small magnitudes, *Bull. Seism. Soc. Am.* **66**: 3*,* 1887–1904.

Gutenberg, B., (1945). Amplitudes of surface waves and the magnitudes of shallow earthquakes. *Bull. Seism. Soc. Am.* **35**, 3.

Hatzfeld, D., M. Tatar, K. Priestley, and M. Ghafory-Ashtiany, (2003). Seismological constraints on the crustal structure beneath the Zagros Mountain belt (Iran), *Geophys. J. Int.*, **155**, 403-410.

Herrmann, R.B., (1973). Some aspects of band-pass filtering of surface waves. *Bull. Seismol. Soc. Am*. **63**, 663–671.

Herrmann, R. B., and B. J. Mitchell, (1975). Statistical analysis and interpretation of surface wave anelastic attenuation data for the stable interior of North America, *Bull. Seismol. Soc. Am.* **65**, 1115–1128.

Herrmann, R., and C. Ammon, (2002). Surface waves, receiver functions and crustal structure. In *Computer programs in seismolo*gy.

Herrmann, R. B., (2004). *Computer Programs in Seismology*. St. Louis University.

Herrmann, R. B., L. Malagnini, and I. Munafò, (2011a). Regional moment tensors of the 2009 L'Aquila earthquake sequence, *Bull. Seism. Soc. Am*., **101**, 975-993.

Herrmann, R.B., H. Benz, and C.J. Ammon, (2011b). Monitoring the earthquake source process in North America. *Bull. Seismol. Soc. Am*. **101**, 2609–2625.

Kennett, B.L.N. Engdahl, E.R. & Buland R., (1995). Constraints on seismic velocities in the Earth from travel times, *Geophys J Int*, **122**, 108–124.

Kohl, B., J.R., Murphy, J. Stevens, and T. J. Bennett, (2011). Exploitation of the IMS and other data for a comprehensive advanced analysis of the North Korean nuclear tests, Proceedings of the 2011 Science and Technology Meeting of the CTBTO. 8-10 June 2011. Hofburg Palace, Vienna.

Levshin, A., X. Yang, M. Ritzwoller, M. Barmin, and A. Lowry, (2006). Toward a Rayleigh wave attenuation model for Central Asia. in *Proceedings of the 28th Seismic Research Review: Ground-Based Nuclear Explosion Monitoring Technologies*, LA-UR-06-5471, Vol. 1, pp. 82–92.

Marshall, P.D. and P.W. Basham, (1972). Discrimination between earthquakes and underground explosions employing an improved M_S scale. *Geophys. J. R. Astr. Soc*., **29**, 431-458.

McLaughlin, K.L., (1988). Maximum-likelihood event magnitude estimation with bootstrapping for uncertainty estimation, *Bull. Seism. Soc. Am.* 78: 2*,* 855–862.

Murphy, J. R., B. W. Barker, and M. E. Marshall, (1997). Event screening at the IDC using the M_s/*mb* discriminant. Maxwell Technologies Final Report. 23 p.

Patton, H.J. and S. R. Taylor, (2008). Effects of shock-induced tensile failure on m_b-M_s discrimination: Contrasts between historic nuclear explosions and the North Korean test of 9 October 2006, *Geophys. Res. Letts*, **35**, L14301, 5 PP., 2008. doi:10.1029/2008GL034211.

Press, S.J. and S. Wilson, (1978). Choosing Between Logistic Regression and Discriminant Analysis. *J. Am. Stats. Assoc.,* **73**, 699-705.

Rezapour, M., and R.G. Pearce, (1998). Bias in surface-wave magnitude *M*s due to inadequate distance correction. *Bull. Seism. Soc. Am.,* **88**, 43-61.

Ringdal, F., (1976). Maximum-Likelihood Estimation of Seismic Magnitude, *Bull. Seism. Soc. Am.* 66: 3*,* 789–802.

Ringdal, F., (1986). Study of magnitudes, seismicity, and earthquake detectability using a global network, *Bull. Seism. Soc. Am.* 76*:* 6*,* 1641–1659.

Russell, D.R., (2006). Development of a time-domain, variable-period surface wave magnitude measurement procedure for application at regional and teleseismic distances. Part I—Theory. *Bull. Seism. Soc. Am*. **96**, 665-677.

Selby, N. D., P. D. Marshall, and D. Bowers, (2012). mb:Ms Event Screening Revisited. *Bull. Seism. Soc. Am*., **102**(1). 88-97.

Stevens, J. L. and S. M. Day, (1985). The physical basis of the m_b:M_s and variable frequency magnitude methods for earthquake/explosion discrimination. *J. Geophys. Res*., **90**, 3009-3020.

Stevens, J. L. and K.L. McLaughlin, (2001). Optimization of surface wave identification and measurement, in *Monitoring the Comprehensive Nuclear Test Ban Treaty: Surface Waves*, eds. Levshin, A. and M.H. Ritzwoller, *Pure Appl. Geophys*., **158**, 1547-1582.

Stevens, J., J. Given, G. Baker, and H. Xu, (2006). Development of surface wave dispersion and attenuation maps and improved methods for measuring surface waves. *Proceedings of the 28th Seismic Research Review: Ground-Based Nuclear Explosion Monitoring Technologies.* LA-UR-06-5471, Vol. 1, pp. 273-281.

Stevens, J., J. Given, H. Xu, and G. Baker, (2007). Development of surface wave dispersion and attenuation maps and improved methods for measuring surface waves. *Proceedings of the 29th Seismic Research Review: Ground-Based Nuclear Explosion Monitoring Technologies,* LA_UR-07-5613, Vol. 1, pp. 282-291.

Toksöz, M.N., and H.H. Kehrer, (1972). Tectonic Strain Release by Underground Nuclear Explosions and its Effect on Seismic Discrimination, *Geophys. J. R. Astr. Soc*., **31**, 141-161.

Vaněk, J., A. Zatopek, V. Karnik, Y.V. Riznichenko, E.F. Saverensky, S.L. Solov'ev, and N.V. Shebalin, (1962). Standardization of magnitude scales. *Bull. (Izvest.) Acad. Sci. U.S.S.R., Geophys. Ser.,* **2**, 108.

von Seggern, D., (1977). Amplitude distance relation for 20-Second Rayleigh waves. *Bull. Seismol. Soc. Am.* **67**, 405–411.

von Seggern, D. and D. W. Rivers, (1978). Comments on the use of truncated distribution theory for improved magnitude estimation, *Bull. Seism. Soc. Am.* 6: 1543–1546.

Yacoub, N.K., (1983). "Instantaneous Amplitudes": a new method to measure seismic magnitude, *Bull. Seismol. Soc. Am.* **73**, 1345–1355.

Yacoub, N.K., (1988). Maximum spectral energy for seismic magnitude estimation. Part I: Rayleigh-wave magnitude. Bull. Seism. Soc. Am., **88**, 952-962.

DISTRIBUTION LIST

DTIC/OCP
8725 John J. Kingman Rd, Suite 0944
Ft Belvoir, VA 22060-6218 1 cy

AFRL/RVIL
Kirtland AFB, NM 87117-5776 2 cys

Official Record Copy
AFRL/RVBYE/Robert Raistrick 1 cy